Alma Mater Studiorum · Università di Bologna

FACOLTÀ DI SCIENZE MATEMATICHE, FISICHE E NATURALI
Corso di Laurea Magistrale in Fisica

DYNAMIC INDICATORS OF STABILITY IN NONLINEAR MAPS OF LOW DIMENSIONALITY

Tesi di Laurea in Meccanica Analitica

Relatore:
Chiar.mo Prof.
GIORGIO TURCHETTI

Presentata da:
FARANDA DAVIDE

Correlatori:
Prof. SANDRO VAIENTI
Dott. VALERIO LUCARINI

Sessione I
Anno Accademico 2009/2010

A Luca, Mamma e Papà

Introduction

῞Ων ἃ μὲν κατ᾽ ἀνάγκην ἐστίν
ἃ δὲ ἀπὸ τύχης, ἃ δὲ παρ᾽ ἡμᾶς,
διὰ τὸ τὴν μὲν ἀνάνγκην ἀνυπεύθυνον εἶναι,
τὴν δὲ τύχην ἄστατον ὁρᾶν,
τὸ δὲ παρ᾽ ἡμᾶς ἀδέσποτον

Epicurus, letter to Meneceus 133,6-9

The early philosophers whose investigations heralded the dawn of scientific thought, addressed themselves to the study of natural systems interrelations in a speculative analysis. Their task was not to present a scientific account of natural phenomena introducing principles and physical laws but rather defending their ideas with deductions and philosophical speculations. Nevertheless, the observation of nature suggested them the presence of regular and chaotic motions such that many greek thinkers and writers based their philosophy on the notion of order (κόσμος) and chaos (χάος). Let us cite as example of these paired visions Democritus and Aristotle: the former argued that atoms move about casually and chaotically, the latter believed that things can be causes of one another and have ordered motions as the heavenly element has perpetual circular motion.

Although ancient Greeks understood what is now a basis of dynamical system theory, the thought of Aristotle both with the advent of Christianity influenced the scientific thinking till 19th century. The success of a pure deterministic approach to physics suggested an indiscriminate use

of superposition principle. Thus, the successful formulation of Lagrangian and analytical mechanics moved scientists away from looking at natural phenomena which show chaotic behaviour. The apotheosis of this vision of science was reached in the work of Laplace *Essai philosophique sur les probabilités* in which he theorized an infinite predictability of motions once known the present state of the universe.

In late 19th century, Poincaré became the first person to discover a chaotic deterministic system. This laid the foundations of modern chaos theory with his research on the three-body problem introducing important tool to study dynamical systems such the Recurrence Theorem that will be widely used in this work. Through the past century, this field of study drew the attention of not only physicists but also many natural scientists: they understood that this theory could potentially explain biological or chemical behaviours or help in understanding geophysical systems like atmospheric and oceanic motions. In this reference frame the develop of powerful calculators helped to describe in detail the features of systems with an high number of components. This enhanced our ability to perform reliable weather forecasts and lead to the fortuitous discover of sensitivity to initial conditions by a meteorologist: Edward Norton Lorenz.

In the recent past many scientific works have introduced a great variety of tools useful to characterize every kind of dynamical system. They have been named *dynamic indicators of stability* due to the fundamental role that stability plays in determine chaotic or regular behaviours: unstable equilibria are the starting point of irregular motion. On the other hand, one of the most fascinating challenge in studying such type of systems is to understand and possibly forecast unexpected and extreme events. Famines, powerful tornados, major earthquakes, extreme floods played an important role in human history. Nevertheless, the theory which models their behaviour was formulated only in the past century by Gumbel and perfectioned with the

work of Gnedenko. Surprisingly, Freitas et al. [2009] have demonstrated an intimate linkage between this theory and Poincaré Recurrence theory. This fact fosters the growth of knowledge of this theory.

In this work of thesis we try to give an unified vision of different indicators of dynamic stability. Furthermore, we will attempt to use generalized extreme value distribution as a tool to investigate properties of regular and chaotic maps. The analysis will involve both mathematical maps and physical models. The existence of clear mathematical statement for prototypical maps allow us to work in a strong theoretical framework that we can use to investigate the behaviour of generalized extreme value theory parameters even in stochastically perturbed case. Numerical simulations will accompany analytical results when available.
This work is structured as follows: the first chapters are dedicated to construct a brief theoretical background to subsequent investigations:

- in Chapter 1 we present extreme value theory explaining how to model and measure events which occur with very small probability. An important section is dedicated to the Kolmogorov-Smirnov confidence test that is the hearth of numerical computations.

- in Chapters 2 and 3 it has been inserted a theoretical framework for indicators of stability such as Recurrence and Hitting Time statistics, Fidelity, Correlations decay and Reversibility Error.

The experimental part of this work of thesis is organized as follows:

- Chapter 4 is dedicated to the comparison between Extreme Value Theory and Recurrences. Following the work of Freitas et al. [2009] we describe their main results trying to extend them to the stochastically perturbed case. Furthermore, an analytical and numerical study on observable functions used to link the two theories has been performed.

- in Chapter 5 different mathematical models have been analysed. We choose well known maps presenting how dynamic indicators behave both with deterministic and stochastic perturbations.
- in Chapter 6 we introduce different physical models of low dimensionality using the goodness of fit parameter obtained using generalized extreme value distribution to highlight important properties of systems which show a mixed behaviour.

Positive results in using this kind of indicators may lead to different applications in models with a large number of degrees of freedom. In particular we may think to use them in meteorological or climate models to understand what parameters values cause unstable situation or to support forecast quality control using these indicators as well as ensamble predictions. In this kind of systems, forecasting and understanding extreme events is important for their involvement in human activities but may also help the scientists to put together the pieces of dynamical systems puzzle.

Contents

List of Figures

Chapter 1

Extreme value theory and modeling

The study of extreme events is of great interest in different disciplines. It has been applied successfully to extreme floods [Sveinsson and Boes, 2002], amounts of large insurance losses [Brodin and Kluppelberg, 2006], extreme earthquake, meteorological and climate events [Felici et al., 2006] [Altmann et al., 2006].
The extreme value theory originates to find up methods to model and measure events which occur with very small probability. It deals with the stochastic behaviour of the extremes of independent and identical distributed (hereinafter i.i.d.) variables. The tail of underlying distribution determines the properties of maxima and minima distribution.
Under certain hypothesis we obtain an asymptotically justified probability model and, using the sample data from rare events of a process, it's possible to make rational predictions about the likely levels of future extremes of the process.
There are basicly two approaches to extreme value theory:

- Compute the distribution of a series of maxima (minima) which, under certain conditions, converges to the so-called generalized extreme value (hereinafter GEV) distribution.

- Compute the distribution of excess over a given threshold to model the behaviour of the excess loss once a high threshold (loss) is reached (Pareto distribution).

In this chapter we explain the theoretical basis for the study of extreme events with emphasis on the GEV distribution. We widely point out the methods used for the subsequent numerical analysis and the inference of the GEV parameters from a set of data.

1.1 The three types of extreme value distribution

Extreme value distribution includes the following three families:

- Gumbel cumulative distribution (type 1):

$$\Pr[X \leq x] = \exp\left\{-e^{-(x-\mu)/\sigma}\right\} \quad x \in \mathbb{R} \tag{1.1}$$

- Frechet cumulative distribution (type 2):

$$\begin{cases} 0 & x \leq \mu \\ \Pr[X \leq x] = \exp\left\{-\left(\frac{x-\mu}{\sigma}\right)^{-\xi}\right\} & x > \mu \end{cases} \tag{1.2}$$

- Weibull cumulative distribution (type 3):

$$\begin{cases} \Pr[X \leq x] = \exp\left\{-\left(-\frac{(x-\mu)}{\sigma}\right)^{\xi}\right\} & x < \mu \\ 0 & x \geq \mu \end{cases} \tag{1.3}$$

  where $\mu, \sigma > 0, \xi > 0$ are parameters.

It is possible to represent the three types distributions using a single family of generalized distribution called Generalized Extreme Value distribution:

$$G(x;\mu,\sigma,\xi) = \frac{1}{\sigma}\left[1+\xi\left(\frac{x-\mu}{\sigma}\right)\right]^{-1/\xi-1} \cdot \exp\left\{-\left[1+\xi\left(\frac{x-\mu}{\sigma}\right)\right]^{-1/\xi}\right\} \tag{1.4}$$

which holds for:

$$1+\xi(x-\mu)/\sigma > 0 \tag{1.5}$$

and where:

- $\mu \in \mathbb{R}$ is the location parameter
- $\sigma > 0$ the scale parameter
- $\xi \in \mathbb{R}$ the shape parameter. also called the tail index, indicates the thickness of the tail of the distribution.

The cumulative distribution may be written as:

$$\Pr[X \leq x] = \exp\left\{-\left[1+\xi\left(\frac{x-\mu}{\sigma}\right)\right]^{-1/\xi}\right\} \tag{1.6}$$

When $\xi \to 0$, the distribution G corresponds to a Gumbel type (eq 1.1) . When the index is negative, it corresponds to a Weibull (eq 1.3); when the index is positive, it corresponds to a Frechet (eq 1.2).
The leading idea in extreme value theory is analogous to the one used in central limit theorem but here the shape parameter ξ unifies the possible characterization of the extreme value distribution. The shape parameter is also called tail index and, intuitively, the three distribution types represent three possibilities for the tail decay of the density function (as detailed in section 1.2).

1.1.1 Obtaining the limiting distribution

Let X_1, X_2, X_n be i.i.d. variables with the same probability density function:

$$p_{X_j}(x) = f(x), \qquad j = 1, 2, ...n \tag{1.7}$$

and cumulative distribution:

$$F(x) = \Pr[X \leq x] = \int_{-\infty}^{x} f(x)dt \tag{1.8}$$

Define $M_{X,n} = \max\{X_1, ..., X_n\}$.
For example, X_i can be a set of precipitation observations taken daily in the ith year so that n maxima $M_{X,n}$ may be chosen over a period corresponding to one year assuming that the block sizes are quite large and the maxima in different blocks are independent realisations [Pauli and Coles, 2001]. For any finite value x , the maximum will exceed x as n increases, with $1-[F(x)]^n$ tends to unit if $F(x) < 1$ or to zero if $F(x) = 1$. It is clear that we obtain a degenerate distribution for $[F(x)]^n$ as $n \to \infty$. If it exists, we must find the limiting distribution introducing some sequence of transformed and reduced values such $(a_n M_{x,n} + b_n)$ where a_n and b_n depend on n. Denoting $G(x)$ this reduced distribution, it follows [Fisher and Tippett, 1928] that $G(x)$ must satisfy this equation:

$$[G(x)]^n = G(a_n x + b_n) \tag{1.9}$$

Using condition 1.9 it is possible to obtain Gumbel distribution by taking $a_n = 1$. We report the proof in the case of type 1. Since $a_n = 1$ equation 1.9 becomes:

$$[G(x)]^n = g(x + b_n) \tag{1.10}$$

the latter equation must satisfy equation 1.9 so that:

$$[G(x)]^{n \cdot m} = [G(x + b_n)]^m = G(x + b_n + b_m) \tag{1.11}$$

$$[G(x)]^{n \cdot m} = G(x + b_{n,m}) \tag{1.12}$$

Using the equations 1.11 and 1.12 we can see that:

$$b_{n,m} = b_n + b_m \tag{1.13}$$

so that:

$$b_n = \sigma \log(n), \qquad \text{with } \sigma \text{ a constant} \tag{1.14}$$

Taking logarithms of 1.11 twice we have:

$$\log n + \log\{-\log G(x)\} = \log\{-\log G(x + b_n)\} \tag{1.15}$$

inserting the equation 1.14 in the latter we write:

$$\log n + \log\{-\log G(x)\} = \log\{-\log G(x + \sigma \log n)\} \tag{1.16}$$

Let us introduce:

$$h(x) = \log\{-\log G(x)\} \tag{1.17}$$

then:

$$h(x) = h(0) - \frac{x}{\sigma} \tag{1.18}$$

Now, since $h(x)$ decreases as x increases, σ is positive:

$$-\log G(x) = \exp\left[-\frac{x - \sigma h(0)}{\sigma}\right] \tag{1.19}$$

denoting $\mu = \sigma \log(-\log G(0))$:

$$-\log G(x) = \exp\left(-\frac{x - \mu}{\sigma}\right) \tag{1.20}$$

which demonstrates our statement since it is the logarithm of the type 1 distribution in equation 1.1.

Types 2 and 3 can be obtained by taking $a_n \neq 1$. In this case

$$x = a_n x = b_n \qquad \text{if} \quad x = b_n(1 - a_n)^{-1} \tag{1.21}$$

See De Haan and Ferreira [2006] for a complete proof.

1.1.2 Gnedenko's results

There is a more immediate way to obtain some conditions that can be easily used to establish the linkages between parent and GEV distribution. Here we study the convergence of probabilities of the form $P\{a_n(M_n - b_n) \leq x\}$ which may be rewritten as $P\{M_n \leq u_n\} = F^n(u_n) = \{1 - (1 - F(u_n))\}^n$ where $u_n = u_n(x) = x/a_n + b_n$. Such types of normalized sequences converge to one of the three types of distribution described in equations 1.1-1.3 (where $\mu = 0$ and $\sigma = 1$ [1]) if one of the following necessary and sufficient conditions established by Gnedenko [1943] is satisfied:

Let us define the right endpoint x_F of a distribution function $F(x)$ as:

$$x_F = \sup\{x : F(x) < 1\} \tag{1.22}$$

Theorem (Gnedenko): *Necessary and sufficient conditions for the distribution function F of the random variables of the i.i.d. sequence $\{\xi_n\}$ to belong to each of the three types are:*

- *For the Frechet (type 2) distribution, $x_F = \infty$:*

$$\lim_{t\to\infty} \frac{1 - F(tx)}{1 - F(t)} = x^{-\alpha}, \qquad \alpha > 0, \forall x > 0. \tag{1.23}$$

- *For the Weibull (type 3) distribution, $x_F < \infty$:*

$$\lim_{h\to 0} \frac{1 - F(x_F - xh)}{1 - F(x_F - h)} = x^{\alpha}, \qquad \alpha > 0, \forall x > 0 \tag{1.24}$$

- *For the Gumbel (type 1) distribution, there exists some positive function $G(t)$ such that:*

$$\lim_{t\to X_F} \frac{1 - F(t + xG(t))}{1 - F(t)} = e^{-x}, \qquad \forall x \in \mathbb{R} \tag{1.25}$$

  It may in fact be shown that $\int_0^\infty (1 - F(u))du < \infty$ when a type 1 limit holds, and one appropriate choice of g is given by

$$G(t) = \int_t^{x_F} \frac{1 - F(u)}{1 - F(t)} du, \quad t < x_F$$

[1] We subsequently will show the linkages between μ, σ, a_n and b_n.

Using this conditions is possible to obtain different limiting distribution for maxima and minima corresponding to the same parent distribution. Gnedenko [1943] shown that these conditions are necessary and sufficient. For example if the parent distribution is normal or exponential, it satisfies 1.25 and the limiting distribution is type 1. Condition 1.23 is satisfied by Cauchy parent distribution and 1.24 by a nondegenerate distributions bounded above. Besides the theorem, a corollary is also important to determine the normalizing sequences a_n and b_n:

Corollary (Gnedenko): *The normalizing sequences a_n and b_n in the convergence of normalized maxima $P\{a_n(M_n - b_n) \leq x\} \to G(x)$ may be taken as:*

- *Type 2:* $a_n = \gamma_n^{-1}, \quad b_n = 0;$
- *Type 3:* $a_n = (x_F - \gamma_n)^{-1}, \quad b_n = x_F;$
- *Type 1:* $a_n = [g(\gamma_n)]^{-1}, \quad b_n = \gamma_n;$

with $\gamma_n = F^{-1}(1 - 1/n) = \inf\{x; F(x) \geq 1 - 1/n\}$.

The complete proof of both the theorem and the corollary can be found in Leadbetter et al. [1983]. Another line of development is the characterization of convergence in terms of moments. It is possible to use the mean μ and standard deviation σ of the distribution as scaling constants in place of b_n, and a_n [Pickands III, 1968]. We will use widely these properties in the following chapters.

1.2 Properties of the GEV distribution

We first recall some properties of the GEV distribution omitting the derivation which can be found in Kotz and Nadarajah [2000].

The mean is computed as:

$$\mathbb{E}(X) = \mu - \frac{\sigma}{\xi} + \frac{\sigma}{\xi} g_1$$

while the relation for the variance is given by:

$$Var(X) = \frac{\sigma^2}{\xi^2}(g_2 - g_1^2)$$

The skewness of the GEV distribution is obtained using:

$$Skewness(X) = \frac{g_3 - 3g_1g_2 + 2g_1^3}{(g_2 - g_1^2)^{3/2}}$$

where $g_k = \Gamma(1 - k\xi)$, k=1,2,3 and $\Gamma(t)$ is Gamma function.

Detailing the behaviour of the three different types of GEV distribution obtained with various values of the shape parameter ξ, in the following paragraphs we point out the linkages between the tail decay of the parent distribution and the resulting tail index.

1.2.1 The Gumbel distribution (type 1)

Using equation 1.4, we obtain the Gumbel distribution (equation 1.1) when $\xi \to 0$. The Gumbel pdf has a shape skewed to the left, and a location parameter μ which is equal to the mode but it differs from median and mean [2]. As μ decreases, the pdf is shifted to the left. As σ increases, the pdf spreads out and becomes shallower. Some example is reported in figure 1.1.

[2]Because of the distribution asymmetry about its μ

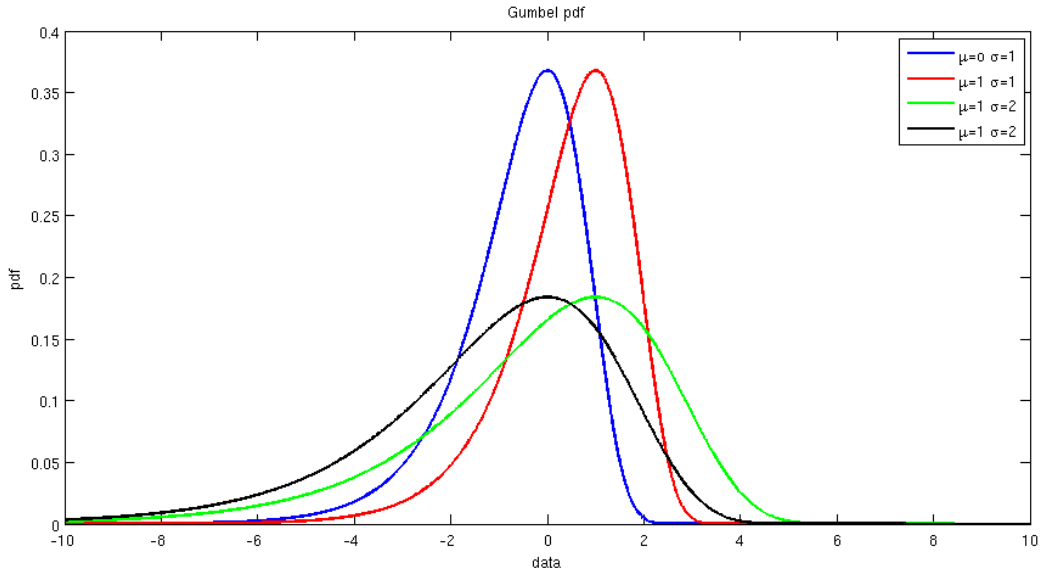

Figure 1.1: Gumbel distribution for different parameters

According to the condition stated in equation 1.25, the Gumbel distribution is likely to be useful if the distribution of the underlying sample data is of the normal, lognormal, gamma or exponential type. Since the data of flood, earthquake occurrences and other natural disaster have this kind of parent distribution, the Gumbel pdf is useful to represent the distribution of maxima related to this extreme events.

1.2.2 The Frechet distribution (type 2)

The Frechet distribution (equation 1.2) is related to a positive shape parameter $\xi > 0$; The parent distribution may be Cauchy, T-Student or any fat-tailed distribution. A fat tailed distribution is so called when the tail decays as a power . We can expect a fit to a Frechet distribution using financial, precipitation or stream-flow data due to the power decay of correlation between subsequent observations.

In this distribution domain, ξ is strictly connected to the maximal order moment. This means that moments of order r greater than ξ are infinite and those less than ξ are finite. In figure 1.2 we present a fit to GEV distribution of maxima computed over fixed length bins using T-student distributed initial data . We can observe, as expected, a positive shape parameter value $\xi \simeq 0.19$.

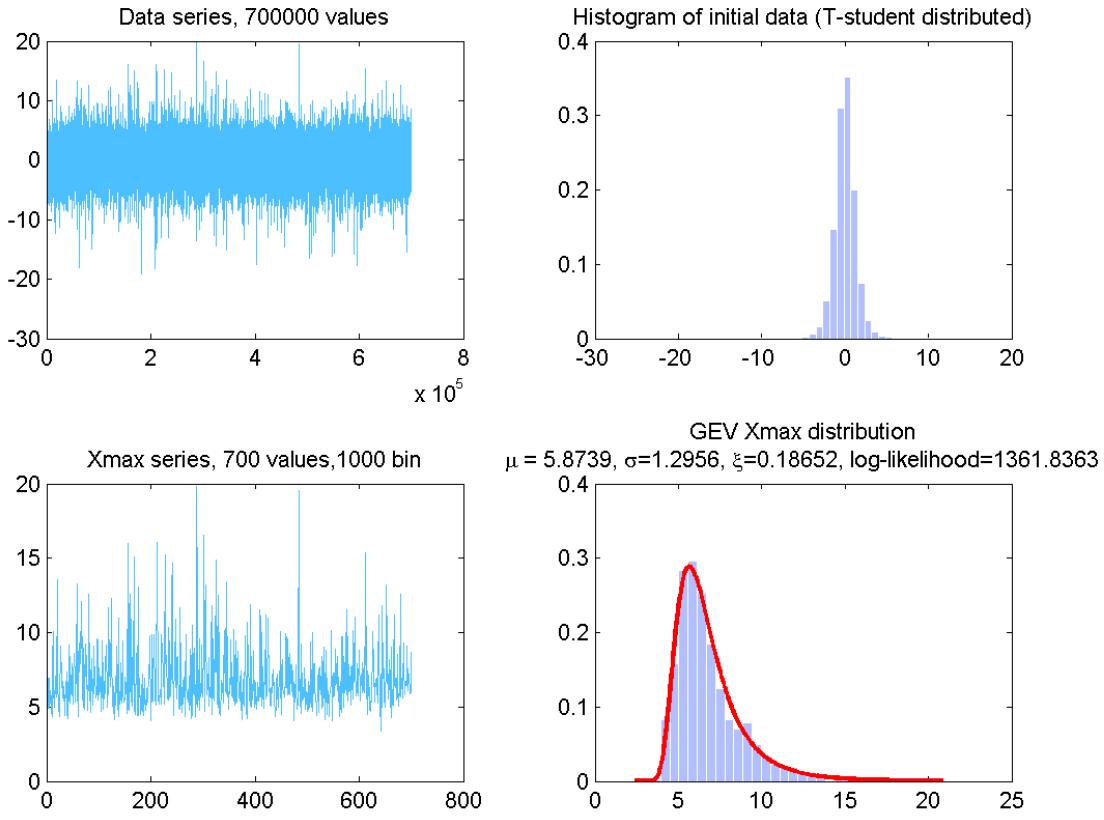

Figure 1.2: GEV fit for a set of maxima with T-student parent distribution.

1.2.3 The Weibull distribution (type 3)

When the tail index is negative ($\xi < 0$) the GEV distribution is a type 3 of Weibull. In this case the parent distribution has a thin tailed distribution with a finite upper endpoint $x_{up} = \mu + \sigma/(-\xi)$. The tail decays with a finite tail index.

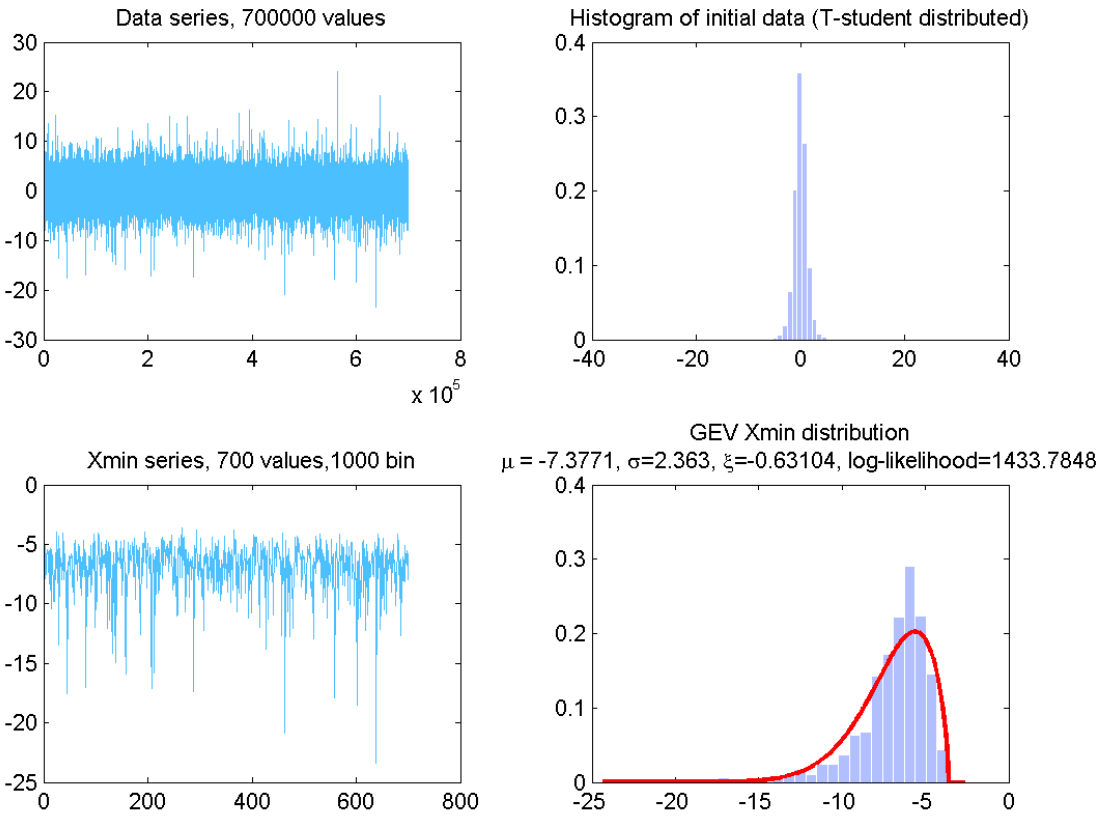

Figure 1.3: GEV fit for a set of minima with T-student parent distribution.

It is also called a "reversed" Weibull distributions pointing out that it was first defined in a specular way with a finite lower endpoint. The Weibull distribution is widely used to fit minima distribution, temperature, wind-speed and sea-level data. In figure 1.3 we present a fit to GEV distribution

of minima computed using the same data reported in figure 1.2. In this case the shape parameter value is negative $\xi \simeq -0.63$. In the following table we summarize the limiting Extreme Value distribution (where $\mu \to 0$ and $\sigma \to 1$) which is obtained starting from a different standardized initial distribution.

Initial Dist.	**Lim. Dist.for Maxima**	**Lim. Dist.for Minima**
Exponential	Gumbel (Type 1)	Weibull (Type 3)
Gamma	Gumbel (Type 1)	Weibull (Type 3)
Normal	Gumbel (Type 1)	Gumbel (Type 1)
Log-normal	Gumbel (Type 1)	Gumbel (Type 1)
Uniform	Weibull (Type 3)	Weibull (Type 3)
Pareto	Frechet (Type 2)	Weibull (Type 3)
Cauchy	Frechet (Type 2)	Frechet (Type 2)

1.3 GEV inference criteria

We present some popular method to obtain GEV distribution parameters. We focus our attention on the maximum likelihood criteria detailed in section 1.3.3 since it has been applied to all our numerical investigation.

1.3.1 Limit of Bayesan Inference procedure

In Bayesan inference the evidence or observations are used to update or to newly infer what is known about underlying parameters or hypotheses. The name "Bayesian" comes from the use of Bayes' theorem in the process. We have to add some additional prior information to our parameters estimation. This approach hides some conceptual problem due to the plausibility of the *a priori* knowledge which is not guaranteed for extremal behaviour. For example it has been shown that the shape parameter, in some hydrological and meteorological application, has a Beta distribution defined on the interval [-0.5, 0.5] [Martins and Stedinger]: in this case, this kind of prior information can be used successfully in a fully Bayesian framework,

leading to the estimation of GEV parameters with some constraint over the tail index.
Generally The Bayesan approach is not suitable for our data since we have no *a priori* information about the parameters affecting the extremal behaviour; in our subsequent numerical investigation only statistical methods are used to infer the limiting distribution.

1.3.2 Method of Probability-Weighted Moments (PWM)

This method was proposed in 1979 by Landwehr and now it is widely used in environmental sciences. It allow to estimate the parameters μ and σ using probability-weighted moment defined as:

$$b_k = \mathbb{E}[X\{1 - F(X)\}^k] \tag{1.26}$$

as b_k unbiased estimator we can use:

$$\hat{b}_k = \frac{1}{n}\sum_{j=1}^{n}\left(\prod_{l=1}^{k}\frac{j-l}{n-l}\right)M_{i,n} \tag{1.27}$$

where $(M_{1,n}....M_{n,n})$ represent the ordered GEV distributed sample so that the i-th ordered maximum is equal to its ith-smallest value.
By making use of the expression b_0 and b_1, equating to respective estimators and solving for the parameters μ and σ, the probability weighted moment are obtained solving the following system of equations:

$$\begin{cases} \hat{b}_0 = \hat{\mu} - \dfrac{\hat{\sigma}}{\hat{\xi}}(1 - \Gamma(1-\hat{\xi})) \\ 2\hat{b}_1 - \hat{b}_0 = \dfrac{\hat{\sigma}}{\hat{\xi}}\Gamma(1-\hat{\xi})(2^{\hat{\xi}} - 1) \\ \dfrac{3\hat{b}_2 - \hat{b}_0}{2\hat{b}_1 - \hat{b}_0} = \dfrac{3^{\hat{\xi}} - 1}{2^{\hat{\xi}} - 1} \end{cases} \tag{1.28}$$

This approach has been criticized because it assumes *a priori* that the GEV shape parameter ξ is smaller than one (this equivalent to specify that the distribution has finite mean) but recently this restriction seems to be removed [Diebolt et al., 2008].

1.3.3 Maximum Likelihood Estimation

As pointed out in section 4.2 we can construct a sequence of maxima (minima) by subdividing the available data X into N bins of equal length L and by extracting the maximum from each bin i: $M_{N,i}$. The block length is a critical parameter to choice fairly between bias and variance in the parametric estimates.
To infer GEV, we choose the maximum likelihood estimator since it shows a great sensitivity to changes of model as detailed in Felici et al. [2006].
It is useful to maximize the log likelihood function:

$$l(\mu, \sigma, \xi) = \prod_{i=1}^{L} \ln(G'(M_{N,i}; \mu, \sigma, \xi)) \tag{1.29}$$

where $G'(x; \mu, \sigma, \xi))$ is the derivative of $G(x; \mu, \sigma, \xi))$. Now, using the equation 1.4, we can rewrite the log likelihood function as:

$$-m \ln(\sigma) - \left(1 + \frac{1}{\xi}\right) \sum_{i=1}^{L} \left\{ \ln\left[1 + \xi\left(\frac{M_{N,i} - \mu}{\sigma}\right)\right] - \left[1 + \xi\left(\frac{M_{N,i} - \mu}{\sigma}\right)\right]^{-\frac{1}{\xi}} \right\} \tag{1.30}$$

if $\xi \neq 0$, and as:

$$-m \ln(\sigma) - \sum_{i=1}^{L} \left\{ \left(\frac{M_{N,i} - \mu}{\sigma}\right) - \exp\left[-\left(\frac{M_{N,i} - \mu}{\sigma}\right)\right] \right\} \tag{1.31}$$

if $\xi = 0$. We can obtain a profile likelihood of μ, ξ or σ by setting the other two parameters to their maximum likelihood estimates $\tilde{\mu}, \tilde{\xi}, \tilde{\sigma}$ in the equation 1.30 or 1.31. For example, to compute the profile likelihood for the parameter ξ, we can construct the graph:

$$(x, y) = (\xi, l(\tilde{\mu}, \tilde{\sigma}, \xi)) \tag{1.32}$$

giving a section of the likelihood surface as viewed from the axis. The intersections of the horizontal line with the profile likelihood graph allow to compute a confidence interval:

$$y = \tilde{\xi} - 0.5 q_{0.95} \tag{1.33}$$

where $q_{0.95}$ is the 95% quantile of the χ^2 distribution with 1 degree of freedom. In our subsequent numerical analysis we have used the Matlab function *gevpdf* and *gevcdf* which return 95% confidence intervals for the parameter estimates.

1.4 Goodness of fit

There exist many methods to check the goodness of fit to GEV distribution. In our numerical investigation we choose the Kolmogorov-Smirnov test because it avoids the discretization of the null hypothesis unlike what happens for the χ^2 test. In the latter test we should group the data and consider a weaker discretized null hypothesis.

1.4.1 The Kolmogorov-Smirnov test

We start with a sample of variable $X_1, ..., X_n$ belonging to some distribution $\mathbb{P}$ and we would like to test the hypothesis that $\mathbb{P}$ is equal to a particular distribution $\mathbb{P}_0$ obtained, for example, by a fit of data. There are two possible hypotheses:

$$H_0 : \mathbb{P} = \mathbb{P}_0 \qquad H_1 : \mathbb{P} \neq \mathbb{P}_0 \tag{1.34}$$

Let us denote, as usual, by $F(x)$ the true underlying cumulative distribution function (hereinafter cdf) of data. While $F(x)$ is defined by equation 1.8, we can also define an *empirical* cdf by:

$$F_n(x) = \mathbb{P}_n(X \leq x) = \frac{1}{n} \sum_{i=1}^{n} I(X_i \leq x) \tag{1.35}$$

that counts the proportion of the data X_i whose value is less than x. The Kolmogorov-Smirnov test uses a law of large numbers result which implies

that:

$$F_n(x) = \frac{1}{n}\sum_{i=1}^{n} I(X_i \leq x) \to \mathbb{P}(X_1 \leq x) = F(x) \tag{1.36}$$

It can be shown that this approximation holds uniformly over all $x \in \mathbb{R}$:

$$\sup_{x\in\mathbb{R}} |F_n(x) - F(x)| \to 0 \tag{1.37}$$

To use the Kolmogorov-Smirnov test, we will need another weaker result which we formulate using the central limit theorem:

$$\sqrt{n}(F_n(x) - F(x)) \to^{dist} N\left(0, F(x)(1 - F(x))\right) \tag{1.38}$$

where N is the Normal distribution, $\to^{dist}$ denotes the convergence in distribution and $F(X)(1 - F(x))$ is the variance of $I(X_1 \leq x)$. This key observation allow us to enunciate the following result:

$$\mathbb{P}(\sqrt(n) \sup_{x\in\mathbb{R}} |F_n(x) - F(x)| \leq t) \to H(t) = 1 - 2\sum_{i=1}^{\infty}(-1)^{i-1}e^{-2i^2t} \tag{1.39}$$

where $H(t)$ is the cdf of Kolmogorov-Smirnov distribution.
We can reformulate the hypotheses 1.34 in terms of cdf:

$$H_0 : F = F_0 \qquad H_1 : F \neq F_0 \tag{1.40}$$

where F_0 is the cdf of $\mathbb{P}_0$.

Let us introduce the statistic:

$$D_n = \sqrt{n} \sup_{x\in\mathbb{R}} |F_n(x) - F_0(x)| \tag{1.41}$$

Using equation 1.34, if the null hypothesis is true, the D_n distribution can be tabulated as it will depend only on n and it is approximated by H if $n \to \infty$. If the null hypothesis fails, F_n will converge but it will not approximate F_0:

$$\sup_{x} |F_n(x) - F_0(x)| > \delta \tag{1.42}$$

with a small $\delta \in \mathbb{R}$. If we now multiply by $\sqrt{n}$:

$$D_n = \sqrt{n} \sup_{x \in \mathbb{R}} |F_n(x) - F_0(x)| > \sqrt{n}\delta \tag{1.43}$$

if H_0 fails then $D_n > \sqrt{n}\delta \to \infty$ as $n \to \infty$.
It is possible to use the following decision rule:

$$\delta = \begin{cases} H_0 : & D_n \leq c \\ H_1 : & D_n > c \end{cases} \tag{1.44}$$

c is a threshold tabulated under H_0. The level of significance α can be related to c by:

$$\alpha = \mathbb{P}(\delta \neq H_0 | H_0) = \mathbb{P}(D_n \geq c | H_0) \tag{1.45}$$

and if n is large the we can use the H distribution to compute c since:

$$\alpha = \mathbb{P}(D_n \geq c | H_0) \approx 1 - H(c) \tag{1.46}$$

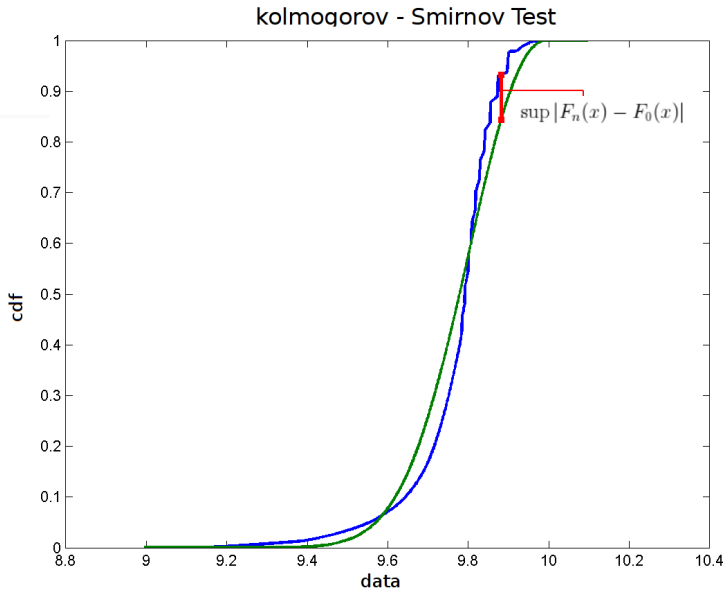

Figure 1.4: Kolmogorov-Smirnov test Example.

To illustrate the idea and how the Kolmogorov-Smirnov test works we present a graphical example. In figure 1.4 are plotted both the empirical and theoretical cumulative distribution. We obtain the parameter D_{max} by calculating the maximum distance between the two cdf. D_{max} is compared with the threshold to decide if the null hypothesis is rejected.

1.5 Limitations and problems using extreme value theory

The first thing to note is that *a priori* we cannot state any assumption about the convergence of the normed maxima to a stable distribution treating tails of empirical distributions. The key observation is that the sample size may be determine a completely different underlying distribution [Green, 1976]. In other words the maxima of random variables governed by the tails of distribution do not have to necessary approach some stable limiting distribution.
Another thing to note is that the selection procedure for the maxima eliminates a part of tail which can be useful to determine accurately the limiting distribution. This problem will be study in detail in the following section introducing the advantages of the Generalized Pareto Distribution.

1.6 The case of dependent variable

Let us define a *mixing sequence* for which the type 1 Gumbel distribution remain valid. In a *mixing sequence*:

1. The various terms in the sequence are weakly dependent when their separation is large:

$$P(X_1 < x, X_2 < x, X_k < x) \to P(X_1 < x, X_2 < x) \cdot P(X_k < x) \quad (1.47)$$

as $k \to \infty$

2. The right tail asymptotic indipendence:

$$P(X_{i+k} \geq r | X_i \geq r) \to 0 \quad \text{as} \quad x \to \infty \quad \text{for every} \quad k \neq 0 \tag{1.48}$$

Note that the limiting distribution of maxima may not coincide with the Gumbel distribution for sequences such that the events $\{X_1 < x_1, ..., X_j < x_j\}$ and $\{X_{j+k} < x_{j+k}, ..., X_n < x_n\}$ are dependent for $k = 1$ and are independent for $k > 1$.
For m-dependent sequences (where the events are independent if separated by m units) the asymptotic Gumbel distribution may be also not valid [Kotz and Nadarajah, 2000].

1.7 Hints to the threshold model: The Generalized Pareto Distribution

We want to characterize the Generalized Pareto Distribution (GPD) which is intimately linked to the GEV distribution. Rewriting the equation 1.4 with $\mu \to 0$ and $\sigma \to 1$, we obtain the expression:

$$G(x, \xi) = \exp(-(1 + \xi x)^{-1/\xi}), \quad -\infty < \xi < +\infty, \quad 1 + \xi x > 0 \tag{1.49}$$

The Gnedenko-Pickands-Balkema-de Haan (hereinafter GPBH) theorem states that the distribution of large events conditioned to be larger than some threshold may be characterized by the GPD.
The GPD is derived from the GEV distribution in equation 1.49 by taking the $G(x, \xi)$ of the largest value given by the equation:

$$H(x/\xi, s) = 1 + \ln(G(x/s, \xi)) = 1 - (1 + \xi x/s)^{-1/\xi} \tag{1.50}$$

showing the link with the Extreme Value Theory.
If the distribution function is unlimited, x_F can be considered to be infinite as in many practical applications. In order to state the GPBH theorem we introduce the excess distribution $F_u(x)$:

$$F_u(x) = P\{X - u < x | X > u\}, \qquad x \geq 0 \tag{1.51}$$

Gnedenko-Pickands-Balkema-de Haan theorem

Let $F(x)$ be a distribution function with excess distribution $F_u(x), u > 0$. Then, for $-\infty < \xi < +\infty$, $F(x) \in D(x, \xi)$ maximum domain of attraction of $G(x, \xi)$ if and only if there exists a positive function $s(u)$ such that:

$$\lim_{u \to x_F} \sup_{0 \leq x \leq x_F - u} |\bar{F}_u(x) - \bar{H}(x/\xi, s(u))| = 0 \tag{1.52}$$

Further on, $\bar{F}(x)$ indicates the complementary cumulative of the distribtuion $F(x)$:

$$\bar{F}(x) = 1 - F(x) \tag{1.53}$$

The importance of the GPBH theorem resides in the statement which is not only valid for the largest value of a data set, as in the case of the Extreme Value Theory, but also to constraint the shape of the tail to the limiting distribution making a full use of all data presents in the tail.
The Extreme Value Theory uses only a part of the parent distribution tail discarding a significant slice of data [Embrechts et al., 1997].

MLE for GPD parameters

Let us denote by N_u the number of observation above a threshold u and as $y_1, ..., y_{N_u}$ the observations such that:

$$u : y_i = x_{j(i)} - u \quad \text{so that } x_{j(i)} > u \tag{1.54}$$

The GPBH theorem yields an approximation to the tail $\bar{F}(x)$ using the Pareto distribution as estimator:

$$\bar{F}(x + u) \simeq \bar{H}(x/\hat{\xi}, \hat{s}) \times (N_u/N) \tag{1.55}$$

As for the GEV distribution we can infer the estimates of the two parameters $\hat{\xi}$, $\hat{s}$ through the Maximum Likelihood Estimation (MLE). Here the log-likelihood l must equals:

$$l = -N_u \ln s - (1 + 1/\xi) \sum_{1}^{N_u} \ln(1 + \xi y_i/s) \tag{1.56}$$

The equation 1.56 is a little bit complicated when $\mu \neq 0$ and $\sigma \neq 0$ and can be maximized numerically. The limit standard deviation can be obtained computing the limit $N \to \infty$, then:

$$\begin{aligned} \sigma_\xi &= (1 + \xi)\sqrt{N_u} \\ \sigma_s &= s\sqrt{2(1 + \xi)/N_u} \end{aligned} \tag{1.57}$$

The q-quantile estimator x_q, which denotes the value of the random variable not overpassed with probability q, can be written as:

$$x_q = u + (\hat{s}/\hat{\xi})(N/N_u(1 - q)^{-\hat{\xi}} - 1) \tag{1.58}$$

While the scale parameter $s = s(u)$ depends on the threshold value u, the shape parameter ξ is, in theory, independent on the threshold value and uniquely determined by the distribution function $F(x)$ of the dataset. For this reason, when possible, it is useful to take a sufficiently high threshold. It is also possible to vary dynamically the threshold, adjusting it when an extreme event overcomes the value of the threshold barrier [Altmann et al., 2006].
The shape parameter ξ is greater than zero when x becomes large. In this case the GPD complementary cumulative approaches a power function:

$$\bar{H}(x/\xi, s) = (\xi x/s)^{-1/\xi} \tag{1.59}$$

and the exponent $1/\xi$ corresponds asymptotically to the exponent of the Pareto law showing that GPD is asymptotically invariant [Pisarenko and Sornette, 2003].

In figure 1.5 is reported the GPD for different shape parameters. Notice that for $\xi < 0$, the GPD has zero probability above an upper limit of $-(1/\xi)$.

For $k \geq 0$, the GPD has no upper limit. Also, the GPD is often used in conjunction with a third, threshold parameter that shifts the lower limit away from zero.

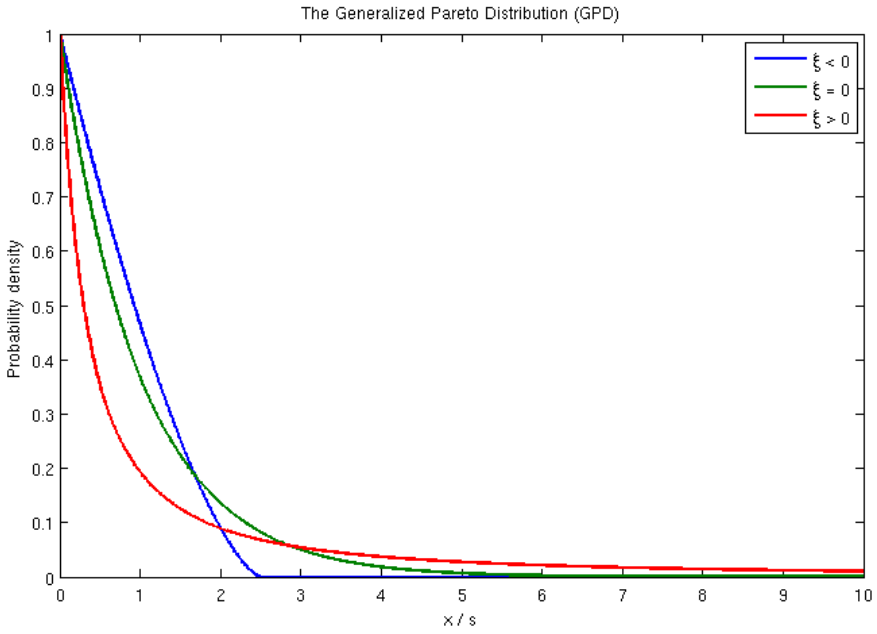

Figure 1.5: Generalized Pareto Distribution examples.

Chapter 2

Poincaré Recurrence statistics

In this chapter we present the basic theory of Return Time Statistics (also known as Poincaré recurrences) showing the well known results obtained for a wide class of dynamical systems. In the past years both strong numerical evidences and theoretical results indicate that this theory is deeply connected with diffusion processes, correlation and fidelity decay not only for mixing dynamical systems but also for integrable maps [Rossi et al., 2005], [Hu et al., 2004], [Artuso, 1999]. Eventually, numerical studies suggest that these results may be connected to understand the behaviour of area-preserving maps in the mixed regions where integrable structures and chaotic components coexist.

2.1 Poincaré Recurrence Theorem

In the late XIX century, Poincaré's memoir on the three body problem was published in the journal *Acta Mathematica*. Poincaré's works has been lauded as milestones in the study of celestial mechanics and dynamics. In his work "Sur le problème des trois corps et les équations de la dynamique" [Poincaré, 1890] he stated that: "*...Dans ce cas, si on laisse de côté certaines trajectoires exceptionnelles, dont la réalisation est infiniment peu*

probable, on peut démontrer que le système repassera une infinité de fois aussi près que l'on voudra de sa position initiale." introducing the basis of return times theory.

Theorem (Poincaré). *Let us consider a standard probability space $(\Omega, \mathcal{F}, \mu)$:*

1. *Ω is a sample space, the set of all possible outcomes.*
2. *$\mathcal{F}$ is a σ-algebra, the collection of all events which characterize groups of outcomes.*
3. *μ is a standard probability measure.*

and let $f : \Omega \to \Omega$ be a measure preserving map:

$$\mu(f^{-1}A) = \mu(A), \qquad \forall A \in \mathcal{F} \tag{2.1}$$

Then, for any $A \in \mathcal{F}$, the set of those points x of A such that $f^n(x) \notin A$ for all $n > 0$ has zero measure, that is almost every point returns infinitely often. i.e

$$\mu\{x \in A : f^n x \in A, \text{ for some } n > 0\} = \mu(A) \tag{2.2}$$

Proof: Let us introduce $A_n = \cup_{k=n}^{\infty} f^{-k}A$ Then, $A \subset A_0$ and $A_i \subset A_j$ when $j \leq i$. Also, $A_i = f^{j-i}A_j$, so that $\mu(A_i) = \mu(A_j)$ for all $i, j \geq 0$, by the f-invariance of μ. Now for any $n > 0$ we have $A - A_n \subset A_0 - A_n$, so that

$$\mu(A - A_n) \leq \mu(A_0 - A_n) = \mu(A_0) - \mu(A_n) = 0.$$

Hence $\mu(A - A_n) = 0$ for all $n > 0$, so that $\mu(A - \cap_{n=1}^{\infty} A_n) = \mu(\cup_{n=1}^{\infty} A - A_n) = 0$. But $A - \cap_{n=1}^{\infty} A_n$ is precisely the set of those $x \in A$ such that for some n and for all $k > n$ we have $f^k(x) \notin A$ [Furstenberg, 1981]. A proof of theorem which follows the original Poincaré formulation can be found in Barrow-Green [1997]. □

2.2 First Visiting Time and Kac's Theorem

In the following we will assume that μ is *ergodic* for f:

$$\nexists A \in \mathcal{F}, 0 < \mu(A) < 1, \text{ such that } \mu(A \Delta f^{-1} A) = 0 \tag{2.3}$$

where $\triangle$ denotes the symmetric difference. This is equivalent to say that μ-almost every point in the whole space visits A; using the ergodicity we can introduce the concept of *visiting time* to a fixed set A of positive measure for μ-almost every point in Ω [Coelho, 2000].
Let us fix $A \in \mathcal{F}$ with $\mu(A) > 0$, we define $\tau : \Omega \to \mathbb{N}$ as:

$$\tau = \inf\{n > 0 : f^n x \in A\} \tag{2.4}$$

first visiting time of A (note that $\tau(x) < \infty$ almost everywhere).
If the set is quite small we have to wait more time in order to observe a return in A. This result is stated formally by the following theorem:

Theorem (Kac). *Let $(\Omega, \mathcal{F}, \mu, f)$ be an ergodic dynamical system and let $A \in \mathcal{F}$ be a set of positive measure, then*

$$\mathbb{E}_A(\tau) = \frac{1}{\mu(A)} \int_A \tau(x) d\mu = \frac{1}{\mu(A)} \tag{2.5}$$

In accordance with this theorem one then looks at the return times which are normalized by the measure of the return set.
To proof both the Kac's Theorem we follow Coelho [2000], Pollicott and Yuri [1998] and Marie [2009].

First we introduce Rokhlin Tower definition :

Rokhlin Tower. In a dynamical system $(\Omega, \mathcal{F}, \mu, f)$ we define Rokhlin Tower a finite family of measurable sets:

$$\Psi = (B, fB, ..., f^{h-1}B) \tag{2.6}$$

where $f^j B$ are two-by-two disjoint sets. The set B represents the tower base, $f^j B$ is a floor and h is the height.

It is possible to partition the set A as follows. Let us define

$$A_i = \{x \in A : \tau(x) = i\} \qquad i \geq 1 \tag{2.7}$$

then:

$$\mu(A) = \mu\left(\bigcup_{i\geq 1} A_i\right). \qquad A = \bigcup_{i=1}^{\infty} A_i \tag{2.8}$$

and we may consider the Rokhlin Tower of height k:

$$(A_k, fA_k, ..., f^{k-1}A_k) \tag{2.9}$$

Eventually, we introduce a lemma which is useful to prove Kac's Theorem:

Rokhlin's Lemmma. *Let $(\Omega, \mathcal{F}, \mu, f)$ be an aperiodic dynamical system. Then $\forall \epsilon > 0, \forall n \in \mathbb{N}, \exists B$ measurable such that:*

- $f^i B, 0 \leq i \leq n$ are two-by-two disjoint
- $\mu(\bigcup_{i=0}^{n-1} f^i B) > 1 - \epsilon$

Proof (Kac's Theorem). μ is ergodic and $\mu(A) > 0$ then:

$$\mu\left(\bigcup_{n\geq 0} f^n A\right) = 1 \tag{2.10}$$

We have seen that A is a disjoint union of A_k and then $\bigcup_{n\geq 0} f^n A$ is composed by the whole $f^j A_k$ in a separate way: on the one hand for the A_k definition, on the other, by the injectivity of T, we know that: $fA_j, f^2 A_j, ..., f^{j-1}A_j$ can't join $fA_k, f^2 A_k, ..., f^{k-1}A_j$ with $k \neq j$, then:

$$\sum_{k=0}^{+\infty} \sum_{j=0}^{k-1} \mu(f^j A_k) = 1 \tag{2.11}$$

and with the invariance measure we obtain:

$$\sum_{k=0}^{+\infty} k\mu(A_k) = 1 \tag{2.12}$$

and

$$\sum_{k=0}^{+\infty} k\mu(A_k) = \int_A \tau(x) d\mu(x) \tag{2.13}$$

which demonstrate Kac's theorem □.

2.3 Return Time Statistics

Kac's theorem suggests that for every set B of positive measure, the expectation value of τ is equal to $1/\mu(B)$. For a wide class of dynamical systems an exponential behaviour of first return times is expected as well as $\mu(B) \to 0$. We are interested in finding out which conditions are suitable in order to obtain this kind of distribution. Recently, many authors have concentrated their attention to solve this problem obtaining specific conditions depending on various definitions of mixing system [Abadi and Galves, 2001]. To show the exponential decay of first return times we have to introduce some useful definitions:

Conditional Measure: *Let $(\Omega, \mathcal{F}, \mu)$ be an ergodic dynamical system. We define conditional measure of the set A:*

$$\mu_A(B) = \frac{\mu(A \cap B)}{\mu(A)} \qquad B \subseteq \Omega \tag{2.14}$$

Weak Convergence: *We say a sequence of distribution functions*

$$F_n \qquad n = 1, 2, ...$$

converges weakly to a function F (which might not be a distribution itself) if F is non-strictly increasing, right continuous and satisfies:

$$\lim_{n\to\infty} F_n(t) = F(t) \tag{2.15}$$

at every point t of continuity of F .

Return times Spectrum: *Let τ_A be the first return time over a set A and $\mathbb{E}(\tau)$ its expectation value, we define Return times Spectrum $\tilde{F}_A(t)$*

$$\tilde{F}_A(t) = \mu_A\left(x \in A : \frac{\tau_A(x)}{\tau_{\mathbb{A}}} \leq t\right) \tag{2.16}$$

Let us consider a neighbourhood sequence $A_K(x)$ of a point $x \in \Omega$ so that $\mu(A_k(x)) \to 0$ as $k \to +\infty$, we define *Limiting Spectrum* or Return Time Statistics $\tilde{F}(t)$:

$$\tilde{F}(t) = \lim_{k\to+\infty} \tilde{F}_{A_k(x)}(t) \tag{2.17}$$

if the limit exists.

2.3.1 Mixing Systems

Here we introduce the notion of strong mixing based on dynamical system and in the subsequent section a mathematical definitions to introduce a more rigorous result.

Strong mixing system: *Let (Ω, f, μ) be a dynamical system, μ an invariant probability measure $\mu(f^{-1}A) = \mu(A)$. It is said to be strongly mixing if $\forall\varphi, \psi \in L^2(\Omega)$:*

$$\lim_{k\to\infty} \int_\Omega \varphi(f^{-k}(x))\psi(x)d\mu = \int_\Omega \varphi(x)d\mu \int_\Omega \psi(x)d\mu \tag{2.18}$$

For the special case when the observables are characteristic functions χ_A and χ_B of sets $A, B \in \Omega$ (these functions have value 1 at points of A (B) and 0 at points of $\Omega - A$ ($\Omega - B$), this means:

$$\lim_{k\to\infty} \int_\Omega \chi_A(f^{-k}(x))\chi_B(x)d\mu = \int_\Omega \chi_A(x)d\mu \int_\Omega \chi_B(x)d\mu \tag{2.19}$$

$$\lim_{k\to\infty} \mu(f^{-k}A \cup B) = \mu(A)\mu(B) \tag{2.20}$$

and in the last passage we have used measure invariance.
Following Arnold, we present a simple physical example of mixing: the Cuba libre: suppose that a glass initially contains 20% rum (the set A) and 80% cola (the set B) in separate regions. After stirring the glass, any region of the glass contains approximately 20% rum. Furthermore, the stirred mixture is in a certain sense inseparable: no matter where one looks, or how small a region one looks at, one will find 80% cola and 20% rum [Arnold and Avez, 1968]. In physics, a dynamical system is said to be mixing if the phase space has a *coarse-graining* structure. Every mixing transformation is ergodic, but there are ergodic transformations which are not mixing.

2.3.2 Heuristic proof for strong mixing systems

Let us consider the set $A_{>t}$. It contains all the points which have a recurrence time greater than $t \cdot \mathbb{E}(\tau_A)$. Calling A_c the complementary set whit respect to the relative measure, it is evident that $\forall x \in A_{>t}$ holds:

$$x \in A_{>T} \Longleftrightarrow f^k(x) \in A_c, \qquad k = \tau_A, \tau_A + 1, ..., t \cdot \mathbb{E}(\tau_{\mathbb{A}}) \tag{2.21}$$

When $\mu(A) \to 0$ then $\tau_A \gg 1$. If we apply the strong mixing condition (equation 2.18) and measure invariance, then:

$$\mu\left(f^{-k}(A_c) \cap f^{-n}(A_c)\right) = \mu(f^{-k}A_c)\mu(A_c) = \mu(A_c)^2 \tag{2.22}$$

which holds for $n \gg 1$. Now we can write:

$$\mu_A(A_{>t}) = \mu\left(f^{-\tau_A}(A_c) \cap f^{-\tau_A-1}(A_c) \cap ... \cap f^{-t\mathbb{E}(\tau_A)}(A_c)\right) \tag{2.23}$$

$$\mu_A(A_{>t}) = \mu\left(A_c\right)^{t\mathbb{E}(\tau_A)-\tau_A} \tag{2.24}$$

It follows that:

$$\mu_A(A_{>t}) = (1-\mu(A))^{t\mathbb{E}(\tau_A)-\tau_A} \tag{2.25}$$

$$\mu_A(A_{>t}) = \exp\left[(t\mathbb{E}(\tau_A)-\tau_A)\log(1-\mu(A))\right] \tag{2.26}$$

Eventually, taking the limit $\mu(A) \to 0$, we obtain:

$$\tilde{F}(t) = \lim_{\mu(A)\to 0} \mu_A\left(A_{>t}\right) = e^{-t} \tag{2.27}$$

2.4 Hitting Time Statistics

We have just introduced the Return Time Statistics $\tilde{F}(t)$ but we may also study the Hitting Time Statistics $F(t)$ that differ by $\tilde{F}(t)$ since τ_A is defined on the whole of Ω and not simply restricted to A:

$$F_A(t) = \mu\left(\frac{\tau_A(x)}{\tau_{\mathbb{A}}} \leq t\right) \tag{2.28}$$

$$F(t) = \lim_{k\to+\infty} F_{A_k(x)}(t) \tag{2.29}$$

To state rigorous results about Hitting Time Statistics, we focus our attention to the class of functions $\mathcal{A}$ and $\tilde{\mathcal{A}}$ which have the following properties [Kupsa and Lacroix, 2005]:

- $\mathcal{A} = \{F : \mathbb{R} \to [0,1], F \equiv 0 \text{ on }]-\infty, 0], F \text{ (non strictly) increasing,}$

  $$\text{continuous, concave on } [0.+\infty[, F(t) \leq t \text{ for } t \geq 0\}$$

- $\tilde{\mathcal{A}} = \{\tilde{F} : \mathbb{R} \to [0,1], F \equiv 0 \text{ on }]-\infty, 0], F \text{ (non strictly) increasing,}$

  $$\text{right-continuous, } \int_0^{+\infty} (1-\tilde{F}(s))ds \leq 1\}$$

2.4.1 Exponential Hitting time statistics

Following the work of Hirata et al. [1999] we introduce their mixing definitions and then proof the exponential spectral decay of recurrence times: We say that $(\Omega, \mathcal{F}, \mu, f)$ is, for all integers $n \geq 1$ and $l \geq 0$,

- γ-*mixing* (or uniform mixing) if

$$\sup_{B \in \mathcal{F}_{\{0,\ldots,n\}}, C \in \mathcal{F}_{\{n \geq 0\}}} \left| \mu(B \cap f^{-(n+l+1)}) - \mu(B)\mu(C) \right| = \gamma(l) \qquad (2.30)$$

- α-*mixing* if

$$\sup_{B \in \mathcal{F}_{\{0,\ldots,n\}}, C \in \mathcal{F}_{\{n \geq 0\}}} \frac{\left| \mu(B \cap f^{-(n+l+1)}) - \mu(B)\mu(C) \right|}{\mu(B)} = \alpha(l) \qquad (2.31)$$

- ϕ-*mixing* if

$$\sup_{B \in \mathcal{F}_{\{0,\ldots,n\}}, C \in \mathcal{F}_{\{n \geq 0\}}} \frac{\left| \mu(B \cap f^{-(n+l+1)}) - \mu(B)\mu(C) \right|}{\mu(B)\mu(C)} = \phi(l) \qquad (2.32)$$

Following Hirata et al. [1999], we state a general implication verified by the preceding types of mixing:

Remark: *ϕ-mixing implies α-mixing which implies uniform mixing:*

$$\gamma(n) \leq \alpha(n) \leq \phi(n) \qquad \forall n \in \mathbb{N}$$

Theorem (Haydn-Lacroix-Vaienti) *Let (Ω, f, μ) be an ergodic system and consider a sequence $\{A_n \in \Omega : n \geq 1\}$ a sequence of positive measure measurable subsets. Then the sequence of functions $\tilde{F}_{A_n}$ converges weakly if*

and only if the functions F_{A_n} converge weakly. Moreover, if the convergence holds, then:

$$F(t) = \int_0^t (1 - \tilde{F}(s))ds, \qquad t \geq 0 \tag{2.33}$$

where $\tilde{F}$ and F are the corresponding limiting (sub-probability) distributions The only previous result in this direction was obtained by Hirata et al. [1999] where it is shown that $\tilde{F}(A_n) \to \tilde{F}$ and $\tilde{F}(t) = 1 - e^{-t}$ for $t \geq 0$ if and only if $F(A_n) - \tilde{F}(A_n) \to 0$ in the supremum norm on the real line. The Haydn-Lacroix-Vaienti Theorem shows that the exponential distribution is the only distribution which can be asymptotic to both return and hitting times, as it is clearly the only fixed point of 2.33. Linking this two theorems one can obtain:

$$F(t) = \int_0^t (1 - \tilde{F}(s))ds = \int_0^t (1 - (1 - e^{-s}))ds = 1 - e^{-t} \tag{2.34}$$

Proof: Let us note:

$$B_k = \{x \in A : \tau_A(x) = k\}$$

$$A_k = \{x \in \Omega : \tau_A(x) = k\}$$

Then, a set of zero measure over Ω can be written as a disjoint union of:

$$\bigcup_{j=0}^{k-1} f^j B_k, \qquad k = 1, 2, ...$$

On the other hand we can write:

$$A_k = \bigcup_{j=0}^{+\infty} f^j B_{k+j}$$

which give considering thatμ is an invariant measure:

$$\mu(A_k) = \sum_{j=k}^{+\infty} \mu(B_k) \tag{2.35}$$

Eventually we can write:

$$F_A(t) = \mu\left(\bigcup_{k=1}^{[t/\mu(A)]} A_k\right) = \sum_{k=1}^{[t/\mu(A)]}$$

F_A is the partition function of a discrete aleatory variable so that it is a simple function : more exactly it is constant over the intervals

$$[k\mu(A), (k+1)\mu(A)[$$

and its value is established by the precedent sum.
It has a jump discontinuity of height $\mu(A_k)$ at the point $k\mu(A)$.
Let us define $\bar{F}_A$ the piecewise linear function which has the same values of F_A for all point $k\mu(A)$, and that is linear over the intervals $[k\mu(A), (k+1)\mu(A)]$. Using equation 2.35, all the jump discontinuities of F_A are decreasing which implies that $\bar{F}_A$ is concave. On the other hand it is continue and increasing and its right derivative for a point $t \in [k\mu(a), (k+1)\mu(A)[$ can be written as:

$$\tilde{F'}_A(t) = \frac{\mu(A_k + 1)}{\mu(A)} \tag{2.36}$$

in the same way, the return

$$\tilde{F}_A(t) = \frac{1}{\mu(A)} \sum_{k=1}^{[t/\mu(A)]} \mu(B_k) \tag{2.37}$$

is constant over $[k\mu(a), (k+1)\mu(A)[$ and has a jump of height $\frac{\mu(B_k)}{\mu(A)}$ in $k\mu(A)$.
$\forall t \geq 0$ we can write:

$$\bar{F'}_A(t) = 1 - \tilde{F}_A(t) \tag{2.38}$$

By the definition of $\bar{F}_A$ we get:

$$||F_A - \bar{F}_A||_\infty \leq \mu(A) \tag{2.39}$$

Let $(A_n)_n$ a sequence of measurable sets so that $\mu(A_n) \to 0$ and $\tilde{F}_{A_n} \Rightarrow \tilde{F}$ (in this case $\tilde{F} \in \tilde{\mathcal{A}}$). Since $\tilde{F}$ is increasing and $\in [0.1]$ then $\tilde{F}_{A_n} \to \tilde{F}$ a.e.

over $[0, +\infty[$. Now, by applying the dominated convergence theorem over $[0, t]$ for $t \geq 0$ and using equation 2.38 we have:

$$\bar{F}_{A_n}(t) = \int_0^t (1 - \tilde{F}_{A_n}(s))ds \to \int_0^t (1 - \tilde{F}(s))ds =: F(t) \tag{2.40}$$

Posing $F(t) = 0$ if $t > 0$, then $\tilde{F} \in \tilde{\mathcal{A}}$ and $F \in \mathcal{A}$. On the other hand, by using equation 2.39, $F_{A_n}(t) \to F(t), \forall t \in \mathbb{R}$. Eventually, if $\tilde{F}_{A_n} \Rightarrow \tilde{F}$ then $F_{A_n} \Rightarrow F$ previously defined.

Corollary *The Hitting times distribution is exponential if and only if the Return times distribution is exponential*

Chapter 3

Reversibility Error, Correlations and Fidelity decay

Important statistical properties of dynamical systems can be inferred also studying the behaviour of correlation and fidelity functions and the Reversibility Error. In this chapter we present the theory used to describe the asymptotic decay of correlations and fidelity for different dynamical systems. This theory is strictly connected to recurrences statistics and extreme value theory as we will show in the next chapters.

The decay of correlations plays a very important role in nonequilibrium statistical mechanics. It is essential in the studies of relaxation to equilibrium. Correlations and autocorrelations functions are explicitly involved in the formulas for transport coefficients, such as heat conductivity, electrical resistance, viscosity, and the diffusion coefficient [Chernov, 2008].

On the other side, classical fidelity is the counterpart of quantum fidelity which is a measure of the stability of quantum motion. The fidelity is a function of the specific perturbation but, usually, the dependence on time shows rather general features [Ruggiero et al., 2006].

3.1 Reversibility Error

It is possible to introduce the reversibility error after n iteration of a map f as:

$$\Delta_n = \text{dist}(f^{-n}(f^n(\vec{x})), \vec{x}) \tag{3.1}$$

Using this definition Marie et al. [2009] have investigated numerically the role of numerical round-off. In a regular region Δ_n is about of the same order of magnitude of the machine precision $10^{-13} - 10^{-16}$ while it is orders of magnitude greater in chaotic regions.
For this reason, by using this indicator it is possible to distinguish chaotic from regular region with a great detail [Franceschelli S., 2007]. In chapter 6 we present some examples of map with different kind of regions depicted using reversibility error.

3.2 Correlations function

Let $(\Omega, \mathcal{F}, \mu, f)$ be a dynamical system and let us denote by f^n the dynamical evolution on the phase space Ω with ergodic measure μ, then, for any choice of $\varphi, \psi \in L^2(\Omega, \mu)$, we want to study:

$$C_{\varphi,\psi}(n) = \int_\Omega \varphi(f^n x)\psi(x)d\mu(x) - \int_\Omega \varphi(x)d\mu(x) \cdot \int_\Omega \psi(x)d\mu(x) \tag{3.2}$$

and we call it correlations function. We will see that sometimes the correlations function $C_{\varphi,\psi}(n)$ decays exponentially with n for suitable φ, ψ, in other cases we will observe a power law decay: we say that correlations:

- *decay exponentially* if $|C_{\varphi,\psi}(n)| < \text{const} \cdot e^{-cn}$ for some $c > 0$.
- *decay polynomially* if $|C_{\varphi,\psi}(n)| < \text{const} \cdot n^{-\alpha}$ for some $\alpha > 0$.

If the relevant invariant measure is unknown, it is necessary to compute time averages instead of phase averages:

$$C_{\varphi,\psi}(n) = \lim_{T\to\infty} \frac{1}{T} \int_0^T \varphi(f^{t+\tau}x_0)\psi(f^{\tau}x_0) - <\varphi> \cdot <\psi> \tag{3.3}$$

One way to obtain analytical results is to consider the Fourier transform of the correlations function:

$$\hat{C}_{\varphi,\psi}(\omega) = \sum_{n\in\mathbb{Z}} e^{in\omega} C_{\varphi,\psi}(n) \tag{3.4}$$

By substituting $e^{in\omega}$ with z in the expression above, we obtain an equation in form of a power series in z. Regarding this series we know the first n coefficients (that is up to the maximum correlation time). Following Artuso [1999] and Baladi [1999] the exponential decay is associated to the analyticity of $\hat{C}_{\varphi,\psi}(\omega)$: if it has a pole in $\omega* = \alpha + \mathrm{i}\beta$, this represents a contribution

$$\exp(-\beta \cdot n + \mathrm{i}\alpha \cdot n)$$

to the correlations function. The analyticity of $\hat{C}_{\varphi,\psi}(\omega)$ regards a strip centred around the real axis: $|\Im\omega| < \eta$ with η not dependent on the observables φ, ψ for same function class.

3.3 Correlations and Recurrences

To show the linkages between correlations decay and Poincaré Recurrences, we follow Young's method for hyperbolic dynamical systems [Young, 1999]. We recall that hyperbolic dynamics is characterized by the presence of expanding and contracting directions for the derivative. This stretching and folding typically gives rise to complicated long-term behaviour in these systems (see Hasselblatt and Katok [2003] for a comprehensive description). We describe the basic idea of Young's method shown in Chernov and Zhang [2005], skipping mathematical and technical details which can be found in the original papers.

Let $f : \Omega \to \Omega$ be an hyperbolic map acting on Ω and μ an absolute continue ergodic measure. We are looking for sufficient conditions under which correlations for the map f decay. Young constructs a set Δ_0 with a hyperbolic structure obtained by intersection of a family of unstable manifolds with a family of stable manifolds similar to an 'horsehoe'. We iterate points $x \in \Delta_0$ using the map f until they make return to Δ_0.
We can now construct a tower, Δ, with base Δ_0, where the induced map f_Δ moves every points one floor up until it hits the ceiling, eventually falling onto the base again. The tower Δ is identified with Ω, and f_Δ with f. Now, we can introduce the first return time defined in equation 2.4 which in this case, for $x \in \Delta$, can be written as:

$$\tau_{\Delta_0}(x) = \inf\{k > 0 : f^k_\Delta(x) \in \Delta_0\} \tag{3.5}$$

that is the first return time of the point X to the base of the tower Δ_0. Since the tower has infinitely many levels, τ is unbounded. As in equations 2.16 and 2.17, we can introduce the Hitting Times statistics:

$$F(x \in \Delta : \tau_{\Delta_0}(x) > n).$$

Young proves both that if the Hitting Time Statistics is exponential (that is exponentially small probability of long returns), then correlations function decays exponentially and that correlations decay polynomially for systems with slower mixing rates:

Theorem (Young) *Let $f : \Omega \to \Omega$ be an hyperbolic map acting on Ω and μ an absolute continue ergodic measure, if*

- *The Hitting Time Statistics shows an exponential decay:*

$$F(x \in \Delta : \tau_{\Delta_0}(x) > n) \leq \text{const} \cdot \theta^n \quad \forall n \geq 1 \tag{3.6}$$

where $\theta < 1$ is a constant, then

$$|C_{\varphi,\psi}(n)| < \text{const} \cdot e^{-cn} \quad \text{for some } n > 0 \tag{3.7}$$

- *The Hitting Time Statistics shows a power law decay:*

$$F(x \in \Delta : \tau_{\Delta_0}(x) > n) \leq \text{const} \cdot n^{-\alpha} \quad \forall n \geq 1 \tag{3.8}$$

where $\alpha > 0$ is a constant, then

$$|C_{\varphi,\psi}(n)| < \text{const} \cdot n^{-\alpha} \tag{3.9}$$

To verify directly the tail bound in specific systems, we have to iterate the map f and construct a Δ_0, an approach that might be quite difficult.

To overpass this problem, we can use another approach, introduced by Chernov and Markarian [2007],which allow us to avoid the computation of Young's tower. Imagine that one can localize, on the Ω manifold, a set $M \subset \Omega$ having a strong hyperbolic behaviour. Consider the hitting time statistics $F : M \to M$, then there exists an horse-hoe $\Delta_O \subset M$ which return times are exponentially bounded under the map f. If we suppose that:

$$F(x \in \Omega : \tau_M(x) > n) \leq \text{const} \cdot n^{-\alpha} \qquad \forall n \geq 1 \tag{3.10}$$

then, equivalentely, we may suppose that:

$$F(x \in M : \tau_M(x) > n) \leq \text{const} \cdot n^{-\alpha-1} \qquad \forall n \geq 1 \tag{3.11}$$

Theorem (Markarian): *Let $f : \Omega \to \Omega$ a non-uniformly hyperbolic map. Suppose $M \subset \Omega$ is a subset such that the Hitting time statistic $F : M \to M$ satisfies equation 3.6 for $\tau_{\Delta_0}(x)$ to a rectangle $\Delta_0 \subset M$. If the return times $\tau_M(x)$ satisfies the bound of equation 3.10 or 3.11, then*

$$|C_{\varphi,\psi}(n)| < \text{const} \cdot (\ln n)^{\alpha+1} n^{-\alpha} \tag{3.12}$$

and this bound differs from Young's by the extra factor $(\ln n)^{\alpha+1}$. A similar argoument can be used to proof the bound for the power law decay.

3.4 Classical Fidelity and Noise Perturbed map

The fidelity was first introduced as a measure of the stability of quantum motion considering the overlap of two states which, starting from the same initial conditions, evolve under two slightly different Hamiltonians H_0 and $H_\epsilon = H_0 + \epsilon V$ where ϵ is a factor smaller than unit [Benenti et al., 2003]. For classic systems, introducing a *classical fidelity* may be also interesting especially for chaotic systems. Following Liverani et al. [2007] we introduce this quantity as:

$$F^{\epsilon}_{\varphi,\psi}(n) = \int_\Omega \varphi(f^n x)\psi(f^n_\epsilon x)d\mu(x) \tag{3.13}$$

where ϵ can be a generic perturbation. On the other hand, fidelity is useful to study the errors: in fact, if we define the error as:

$$\Delta_n(x) = f^n x - f^n_\epsilon x$$

then its Fourier transform is just $F_{\varphi,\psi}(n)$ where $\varphi(x) = e^{ikx}$ and $\psi(x) = e^{-ikx}$.

We can extend both the fidelity and correlations function definitions for a stochastic perturbation [Marie et al., 2009] [Liverani et al., 2007]. Consider a sequence of independent and identically distributed random variables $(\xi_k)_{k\in\mathbb{N}}$ with value in the vector space Ω_ϵ and distribution θ_ϵ. We associate to each $\xi \in \Omega_\epsilon$ a map f_ξ with $f_0 = f$ and the iteration of the map f is replaced by a composition of maps chosen randomly close to it:

$$f^n_\epsilon(x) = (f + \epsilon\xi_n) \circ (f + \epsilon\xi_{n-1}) \circ ... \circ (f + \epsilon\xi_1)(x)$$

To introduce a fidelity definition, following Liverani et al. [2007], we consider a class of maps $\mathcal{M}$ with the following properties:

1. $\mathcal{M}$ admits and *invariant stationary measure* μ_ϵ defined by

$$\lim_{n\to\infty}\int_\Omega\int_{\Omega_\epsilon^{\mathbb{N}}}\prod_i\theta_\epsilon(\xi_i)d\xi_i\varphi(f_\epsilon^n(x))d\mu(x)=\int\varphi d\mu_\epsilon \tag{3.14}$$

   θ_ϵ is chosen ensuring that μ_ϵ is absolutely continuous with respect to μ (that is Lebesgue measure) and furthermore we suppose the stochastic stability:

$$\int_\Omega\varphi d\mu_\epsilon\to\int_\Omega\varphi d\mu\qquad\text{when}\quad\epsilon\to 0.$$

2. The correlations function $C_{\varphi,\psi}(n)$ decays exponentially as detailed in equation 3.7 for the unperturbed map.

3. The correlations function $C_{\varphi,\psi}(n)$ of the perturbed map can be written as

$$|C^\epsilon_{\varphi,\psi}(n)|=\left|\int_\Omega\int_{\Omega_\epsilon^{\mathbb{N}}}\varphi(f_\epsilon^n x)\psi(x)\prod_i\theta(xi_i)d\xi_i d\mu(x)-\int_\Omega\varphi(x)d\mu(x)\cdot\int_\Omega\psi(x)d\mu(x)\right| \tag{3.15}$$

   and we assume an exponential decay:

$$|C^\epsilon_{\varphi,\psi}(n)|\le\text{const}\cdot e^{-cn}\quad\text{for some } n>0.$$

If we now introduce the classical fidelity for a perturbed map as:

$$F^\epsilon_{\varphi,\psi}(n)=\int_\Omega\int_{\Omega_\epsilon^{\mathbb{N}}}\varphi(f_\epsilon^n x)\psi(f^n x)\prod_i\theta(xi_i)d\xi_i d\mu(x) \tag{3.16}$$

then it is possible to proof the following theorem for the fidelity decay [Liverani et al., 2007].

Theorem (Liverani - Marie - Vaienti) *For the class function $\mathcal{M}$ there exists a constant $C_1>0$ such that:*

$$\delta F^\epsilon_{\varphi,\psi}(n)=\left|F^\epsilon_{\varphi,\psi}(n)-\int_\Omega\phi d\mu\int_\Omega\psi d\mu\right|\le C_1\epsilon^{-k}\lambda^{-n}(||\psi||||\varphi||_{\sup}+||\varphi||||\psi||_{\sup}) \tag{3.17}$$

where $||\cdot||$ *is a suitable norm on the space of observables and* $||\cdot||_{\text{sup}}$ *is the supremum norm on continuous functions.*

For chaotic map the decay is more than exponential while for regular maps is exponential.

3.5 Numerical investigation on Correlations and Fidelity decay

Investigations on correlation and fidelity decay may be performed in a number of ways: the method used in this work consists in a Monte Carlo simulations performed simply select a pair of observables and compute correlations function involving a number of N sample points: this leads to a statistical error of the order of $1/\sqrt{N}$. To proof this claim, we briefly recall the basics of Monte Carlo integration:
Consider an integral on the one-dimensional unit interval

$$I[f] = \int_0^1 f(x)dx = \bar{f}$$

Then consider a sequence $(x_n)_{n\in\mathbb{N}}$ sampled from the uniform distribution. Then an empirical approximation to the expectation of the integral is:

$$I_N[f] = \frac{1}{N}\sum_{n=1}^{N} f(x_n)$$

According to the Strong Law of Large Number:

$$\lim_{N\to\infty} I_N[f] \to I[f]$$

Once defined the Monte Carlo integration error as:

$$\epsilon_N[f] = I[f] - I_N[f]$$

the bias is $E[\epsilon_N[f]]$ and the root mean square error is $E[\epsilon_N[f]^2]^{1/2}$. For N large $\epsilon_N[f] \sim \sigma N^{-1/2}\nu$ where ν is a standard normal random variable and:

$$\sigma = \sigma[f] = \left(\int_0^1 (f(x) - I[f])^2 \right)^{1/2}$$

Define $\xi_i = \sigma^1(f(x_i) - \bar{f})$ for x_i uniformly distributed. Then:

$$E[\xi_i] = 0$$

$$E[\xi_i^2] = \int \sigma^{-2}(f(x_i) - \bar{f})^2 dx = 1$$

$$E[\xi_i \xi_j] = 0 \quad \text{if} \quad i \neq j$$

I we now consider the sum:

$$S_N = \frac{1}{N} \sum_1^N \xi_i = \sigma^{-1} \epsilon_N$$

we eventually can calculate its variance:

$$\begin{aligned} E[S_N^2]^{1/2} &= E[N^{-2} \left(\sum_{i=1}^N \xi_i \right)^2]^{1/2} \\ &= N^{-1} \left\{ E\left[\sum_{i=1}^N \xi_i^2 \right] + E\left[\sum_{i=1}^N \sum_{j \neq i} \xi_i \xi_j \right] \right\}^{1/2} \\ &= N^{-1} \left\{ \sum_{i=1}^N 1 + 0 \right\}^{1/2} = N^{-1/2} \end{aligned} \tag{3.18}$$

that is $E[\epsilon_N^2] = \sigma N^{-1/2}$.

In many cases it imposes severe limitations on the maximal time for which correlations and fidelity may be computed. Quite rapidly the signal becomes of the same size of the statistical error data are dramatically spoilt, and one just sees wild fluctuations around that level: for further discussion and references see Artuso [1999].

Chapter 4

Recurrences and EV Theory

In this chapter we explore the link between Extreme Value Laws presented in the first chapter and First Time Statistics, widely described in chapter two, following the recent paper of Freitas et al. [2009]. The main theorem shows a deep connection between the two theories especially for dynamical systems which exhibit an exponential return time statistics. This allow us to explore with both theoretical an numerical arguments Poincaré Recurrence by using Extreme Value Laws and *vice versa*.
This chapter is organized as follows: first we state some results useful to deal with particular dependent variables. The main results obtained by Freitas are presented recalling Lebesgue's Differentiation Theorem which has been used to obtain some evidence about the nature of the observables used in the subsequent numerical investigation. Eventually, we describe the sensitivity numerical studies of some parameters involved in this theory which we have performed to clarify the behaviour of the observables widely studied in the following chapters.

4.1 Preliminaries

4.1.1 Uniform mixing conditions

We have introduced the statistics of maxima $M_n = \max\{X_0, ..., X_{n-1}\}$ for i.i.d variables $X_0, X_1..$ and we have already observed in 1.1.2 that exists a limit distribution under certain conditions.
The same limit laws apply to stationary stochastic processes, under certain conditions on the dependence structure, which allow the reduction to the independent case. Freitas et al. [2009] associate to a given stochastic process $X_0, X_1, ...$ an i.i.d. sequence $Y_0, Y_1, ...$ whose distribution function is the same as that of X_0, and whose partial maximum is defined as:

$$\hat{M}_n = \max\{Y_0, ..., Y_{n-1}\}$$

In the dependent context, the general strategy is to prove that if $X_0, X_1, ..$ satisfies some conditions, then the same limit law for $\hat{M}_n$ applies to M_n with the same normalizing sequences a_n and b_n. See Freitas and Freitas [2008] for the complete proof.

Condition $\mathbf{D_2(u_n)}$: We say that $D_2(u_n)$ holds for the sequence $X_0, X_1, ...$ if for any integers l, t and n

$$|\mu(\{X_0 > u_n\} \cap \{\max\{X_y, ..., X_{t+l-1}\}\}) - \mu(\{X_0 > u_n\})\mu(\{M_l \leq u_n\})| \leq \gamma(n, t)$$

where $\gamma(n, t)$ is non-increasing in t for each n.

Condition $\mathbf{D'(u_n)}$: We say that $D'(u_n)$ holds for the sequence $X_0, X_1, ...$ if

$$\lim_{k\to\infty} \limsup_{n\to\infty} n \sum_{j=1}^{[n/k]} \mu(\{X_0 > u_n\} \cap \{X_j > u_n\}) = 0$$

The main result states that if $D_2(u_n)$ and $D'(u_n)$ hold for the process

$X_0, X_1, ...$, then the following limits exists:

$$\lim_{n\to\infty} \mu(\hat{M}_n \leq u_n) = \lim_{n\to\infty} \mu(M_n \leq u_n) \tag{4.1}$$

4.1.2 Lebesgue's Differentiation Theorem

Theorem (Lebesgue): *Let us consider a Lebesgue integrable real or complex-valued function f on $\mathbb{R}^n$, the indefinite integral is a set function which maps a measurable set A to the Lebesgue integral of $f \cdot \chi_A$, where χ_A denotes the characteristic function of the set A. We can write it as:*

$$\int_A f \, \mathrm{d}\mu_{Leb}$$

with μ_{Leb} the n-dimensional Lebesgue measure.
The derivative of this integral at x is defined to be

$$\lim_{B\to x} \frac{1}{|B|} \int_B f \, \mathrm{d}\mu_{Leb},$$

where $|B|$ denotes the volume (i.e., the Lebesgue measure) of a ball B centred at x, and $B \to x$ means that the diameter of B tends to zero. Then this derivative exists and is equal to $f(x)$ at almost every point $x \in \mathbb{R}^n$.

The points x for which this equality holds are called Lebesgue points. Since functions which are equal almost everywhere have the same integral over any set, this result is the best possible in the sense of recovering the function from integrals [Lebesgue, 1910].

4.2 Freitas' Main Results

Let $(\Omega, \mathcal{F}, \mu, f)$ be a dynamical system where μ is absolute continuous invariant probability measure (that is $\mu(f^{-1}(A)) = \mu(A)$) for all $A \in \Omega$, a d-dimensional Riemannian Manifold . We introduce:

- $B_\delta(\zeta) = \{x \in \Omega : \mathrm{dist}(x, \zeta) < \delta\}$ is the ball of radius δ centered in ζ

- μ_{Leb} is Lebesgue measure on Ω.
- $\rho = \frac{d\mu}{d\mu_{Leb}}$ is a measure density.
- 'dist' a Riemannian metric on Ω.

Consider the stationary stochastic process $X_0, X_1, ...$ which is given by:

$$X_n(x) = g(\text{dist}(f^n x, \zeta)) \qquad \forall n \in \mathbb{N} \tag{4.2}$$

Defining the partial maxima as:

$$M_n = \max\{X_0, ..., X_{n-1}\} \tag{4.3}$$

As in section we are interested in knowing if there are normalizing sequences $\{a_n\}_{n\in\mathbb{N}}$ and $\{b_n\}_{n\in\mathbb{N}}$ such that:

$$\mu(\{x : a_n(M_n - b_n) \leq y\}) = \mu(\{x : M_n \leq u_n\}) \to G(y) \tag{4.4}$$

where $u_n = u_n(x) = x/a_n + b_n$.

4.2.1 Observable functions g_i and normalizing sequences

Following Freitas we now describe the three types of observable functions $g_i, \quad i = 1, 2, 3.$ which are suitable to obtain a GEV distribution for normalized maxima according the Gnedenko's theorem stated in section 1.1.2:

Observation 4.1: *Let ζ be a chosen point in the phase space Ω and consider the function:*

$$g(\text{dist}(x, \zeta)) : \Omega \to \mathbb{R} \tag{4.5}$$

g is such that 0 is a global maximum. $g : V \to W$ is a strictly decreasing bijection and it has one of the following behaviour:

- *Type 1: There exists some positive function* $p : W \to \mathbb{R}$ *such that for all* $y \in R$

$$\lim_{s \to g_1(0)} \frac{g_1^{-1}(s + yp(s))}{g_1^{-1}(s)} = e^{-y} \tag{4.6}$$

- *Type 2:* $g_2(0) = +\infty$ *and there exists* $\beta > 0$ *such that* $\forall y > 0$

$$\lim_{s \to +\infty} \frac{g_2^{-1}(sy)}{g^{-1}(s)} = y^{-\beta} \tag{4.7}$$

- *Type 3:* $g_3(0) = D < +\infty$ *and there exists* $\gamma > 0$ *such that for all* $y > 0$

$$\lim_{s \to 0} \frac{g_3^{-1}(D - sy)}{g_3^{-1}(D - s)} = y^{\gamma} \tag{4.8}$$

g_i conditions are just translations in terms of the shape of g^{-1} of the conditions on the tail of F, since the distribution function F is given by:

$$F(u) = \mu(X_0 \leq u)$$

Note that in this case the dynamic of the system is not introduced in F definition.

$$1 - F(u) = 1 - \mu(X_0 \leq u) \tag{4.9}$$

It follows from X_0 definition that:

$$1 - F(u) = 1 - \mu(g(\text{dist}(x, \zeta) \leq u)) \tag{4.10}$$

using Lebesgue Differentiation Theorem:

$$1 - F(u) = 1 - \mu(\text{dist}(x, \zeta) \geq g^{-1}(u)) \tag{4.11}$$

If we observe that:

$$\mu(\text{dist}(x, \zeta) \geq g^{-1}(u)) = 1 - \rho(\zeta)|B_{g^{-1}(u)}(\zeta)|$$

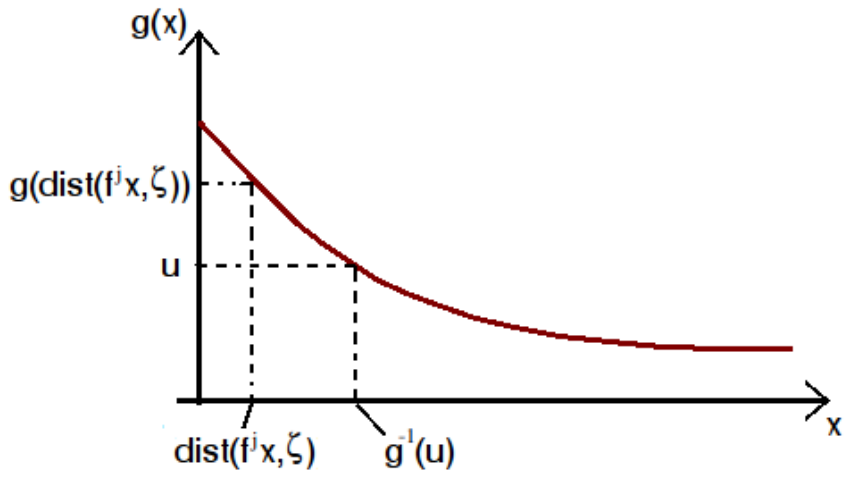

Figure 4.1: g_i behaviour example.

Then we obtain:

$$1 - F(u) \sim \rho(\zeta)|B_{g^{-1}(u)}(\zeta)|$$

From the figure 4.2.1 is also clear that:

$$\text{dist}(f^j x, \zeta) \leq g^{-1}(u) \tag{4.12}$$

Once stated this conditions, it is also possible to apply the corollary in section 1.1.2 in order to obtain the normalizing sequences a_n e b_n:

Observation 4.2: *Let* $\{\delta_n\}_{n\in\mathbb{N}}$ *be such that* $\delta_n \to 0$ *if* $n \to \infty$, *for each* $\zeta \in \Omega$ *and define* $k \in]0, \infty[$ *such that* $|B_{\delta_n}(\zeta)| \sim k \cdot \delta_n^d$, *then:*

- *Type* g_1: $y \in \mathbb{R}$ $\quad u_n = g_1((k\rho(\zeta)n)^{-1/d}) + p(g_1((k\rho(\zeta)n)^{-1/d}))\frac{y}{d}$
- *Type* g_2: $y > 0$ $\quad u_n = g_2((k\rho(\zeta)n)^{-1/d})y$
- *Type* g_3: $y < 0$ $\quad u_n = D - (D - g_3((k\rho(\zeta)n)^{-1/d}))(-y)$

4.2.2 Freitas' Theorem

We are now ready to state the main result obtained by Freitas which links extreme value laws with the hitting time statistics widely presented in section 2.4.

Theorem (Freitas): *Let $(\Omega, \mathcal{F}, \mu, f)$ be a dynamical system where μ is an absolute continue invariant probability measure, and consider $\zeta \in \Omega$ for which Lebesgue's Differentiation Theorem holds.*

- *If we have an exponential Hitting Time Statistics $F(t) = e^{-t}$ (defined in equation 2.29) to balls centred on $\zeta \in \Omega$, then we have an Extreme Value Law for M_n which applies to the observables g_i (described in Observation 4.1) achieving a maximum at ζ.*
- *If we have an exponential Hitting Time Statistics to balls at $\zeta \in \Omega$, then we have an Extreme Value Law for M_n which coincides with that of $\hat{M}_n$ (meaning that equation 4.1 holds). In particular, this Extreme Value Law must be one of the 3 classical types described in equation 1.1 for observables g_1, in equation 1.2 for observables g_2 and in equation 1.3 for observables g_3 where, in all the cases considered, $\mu \to 0$ and $\sigma \to 1$ since normalizing sequences a_n and b_n are used.*

Proof: We describe the part of the proof which demonstrate the theorem for the observable class g_1. The complete proof can be found in Freitas et al. [2009]. Let us note g_i simply g.

- ***First Part:*** For n sufficiently large we have:

$$\{x : M_n(x) \leq u_n\} = \bigcap_{j=0}^{n-1} \{x : g(\text{dist}(f^j x, \zeta)) \leq u_n\} \tag{4.13}$$

  We now apply the Lebesgue Differentiation Theorem:

$$\bigcap_{j=0}^{n-1}\{x : g(\text{dist}(f^j x, \zeta)) \leq u_n\} = \bigcap_{j=0}^{n-1}\{x : \text{dist}(f^j x, \zeta) \geq g^{-1}(u_n)\} \tag{4.14}$$

note the change in the inequality sign. The last equation allow us to introduce the hitting time statistics over the ball $B_{g^{-1}(u_n)}$:

$$\bigcap_{j=0}^{n-1}\{x : \text{dist}(f^j x, \zeta) \geq g^{-1}(u_n)\} = \{x : \tau_{B_{g^{-1}(u_n)}}(x) \geq n\} \tag{4.15}$$

Equation 4.6 and Observation 4.2 allow us to write:

$$\begin{aligned} g^{-1}(u_n) &= g^{-1}\left[g_1((k\rho(\zeta)n)^{-1/d}) + p(g_1((k\rho(\zeta)n)^{-1/d}))\frac{y}{d}\right] \\ &\sim g^{-1}\left[g_1((k\rho(\zeta)n)^{-1/d})\right] e^{-y/d} = \left(\frac{e^{-y}}{k\rho(\zeta)n}\right)^{1/d} \end{aligned} \tag{4.16}$$

Thus:

$$g^{-1}(u_n) \sim \left(\frac{e^{-y}}{k\rho(\zeta)n}\right)^{1/d} \tag{4.17}$$

As said before, since Lebesgue's Differentiation Theorem holds for $\zeta \in \Omega$, we have $\frac{\mu(B_\delta(\zeta)}{|B_\delta(\zeta)|} \to \rho(\zeta)$ as $\delta \to 0$. Consequently, since it is obvious that $g^{-1}(u_n) \to 0$ as $n \to \infty$, then:

$$\mu(B_{g^{-1}u_n)}(\zeta)) \sim \rho(\zeta)|B_{g^{-1}(u_n)}(\zeta)| \sim \rho(\zeta)k(g^{-1}(u_n))^d \tag{4.18}$$

and the last passage is clear by using the relation 4.12.

$$\rho(\zeta)k(g^{-1}(u_n))^d = \rho(\zeta)k\frac{e^{-y}}{k\rho(\zeta)n} = \frac{e^{-y}}{n} \tag{4.19}$$

We can now express n as:

$$n \sim \frac{e^{-y}}{\mu(B_{g^{-1}(u_n)(\zeta)})} \tag{4.20}$$

Now, by substituting 4.20 in the equation 4.15, taking the limit, we have:

$$\lim_{n\to\infty} \mu\left(\left\{x : \tau_{B_{g^{-1}(u_n)}}(x) \geq \frac{e^{-y}}{\mu(B_{g^{-1}(u_n)(\zeta)})}\right\}\right) = F(e^{-y}) = e^{-e^{-y}} \tag{4.21}$$

Eventually it is possible to write:

$$\lim_{n\to\infty} \mu(\{x : M_n(x) \leq u_n\}) = e^{-e^{-y}} \tag{4.22}$$

which is the equation 1.1 with $\mu = 0$ and $\sigma = 0$ obtained using the normalizing sequences as stated by Gnedenko (see section 1.1.2).

- ***Second Part:*** We use the exponential Hitting Time Statistics hypothesis

$$F(t) = e^{-t} \tag{4.23}$$

to proof the second part. It follows by equation 4.22 and 4.1 that also:

$$\lim_{n\to\infty} \mu(\{x : \hat{M}_n(x) \leq u_n\}) = e^{-e^{-y}} \tag{4.24}$$

which means that the Extreme Value Laws applies to M_n (rather than $\hat{M}_n$). In the case of observable g_1 which we have considered this is true $\forall y \in \mathbb{R}$.

4.3 Noise perturbed case

Let ξ be an aleatory variable with a uniform distribution, then we are interested in studying:

$$f_{\vec{\xi}}^{n}x = f_{\xi_n} \circ ... \circ f_{\xi_2} \circ f_{\xi_1}$$

We introduce:

$$\begin{aligned} \bar{X}_0(x) &= g(\text{dist}(x, \zeta)) \\ \bar{X}_1(x) &= g(\text{dist}(f_{\xi_1}x, \zeta)) \\ \bar{X}_2(x) &= g(\text{dist}((f_{\xi_2} \circ f_{\xi_1})x, \zeta)) \\ &\vdots \end{aligned} \tag{4.25}$$

Are these variables independent? If we suppose that uniform mixing conditions stated in 4.1.1 are valid even in this case, then we can introduce an analogue of Birkhoff's theorem:

$$\lim_{N\to\infty} \frac{1}{N} \sum_{n=0}^{N-1} \varphi(f_{\vec{\xi}}^{n}(x)) = \int \varphi d\mu_\epsilon \tag{4.26}$$

Then $\bar{X}_n(x)$ are independent for μ_ϵ a.e. in respect to the initial state and for almost all the realisations. Note that in this case μ_ϵ is the stationary measure defined in equation 3.14. We have to study the following statistics:

$$\bar{F}_\epsilon(u) = \mu_\epsilon(X_0 \leq u) = \mu_\epsilon(g(\text{dist}(x, \zeta) \leq u) = \int_{\{X_0 \leq u\}} d\mu_\epsilon$$

There are two possibilities to investigate the behaviour of $\bar{F}$:

1. Studying the stationary measure μ_ϵ, finding the density $\rho_\epsilon = \frac{d\mu_\epsilon}{d\mu_{Leb}}$ and then calculate the expression of u_n in order to obtain the statistics.

2. Using the results of Pickands III [1968] (cited in section 1.1.2) according to which the mean and standard deviation of the distribution can be taken as scaling constants in place of b_n, and a_n. In this case we have to compute the following Stieltjes integrals:

$$\begin{aligned} < u > &= \int u dF(u) \\ Var(u) &= < u^2 > - < u >^2 \end{aligned}$$

4.4 Properties of observable functions g_i

We want investigate the observable functions nature by studying them numerically using the Arnold's cat map which is suitable to obtain fair results as it satisfies mixing conditions as detailed in section 5.4.
According to conditions 4.6, 4.7 and 4.8 the following are proper observables:

$$g_1(x) = -\log(\text{dist}(x, \zeta)) \tag{4.27}$$

$$g_2(x) = \text{dist}(x, \zeta)^{-1/\alpha} \tag{4.28}$$

$$g_3(x) = C - \text{dist}(x, \zeta)^{1/\alpha} \tag{4.29}$$

where C is a constant and $\alpha > 0 \in \mathbb{R}$.

4.4.1 Methodological notes and informatic tools

All the numerical analysis contained in this work have been performed using self-write MATLAB and C++ code. The results have been presented by using MATLAB Statistics Toolbox function such as *gevfit* and *gevcdf*. These functions returns maximum likelihood estimates of the parameters for the generalized extreme value (GEV) distribution and 95% confidence intervals for the parameter estimates [Martinez and Martinez, 2002].
We have also tried to use ROOT, developed by CERN, using the Maximum Likelihood criterion [Brun et al., 1997]. Even if the ROOT fit functions works well in many cases, we have found different situations in which MATLAB fit successfully the dataset while ROOT estimation of parameters doesn't converge. This is the main reason why we have decided to prefer MATLAB statistics toolbox to perform the analysis and C++ code to quickly iterate the maps.

In this work different pseudo-random number generators have been employed. In MATLAB it has been used the default function *rand* while in C++ code our choice has fallen on Mersenne Twister (MT) generator since it is faster than *random* or *rand* functions and has a long period of $2^{19937}-1$ [Matsumoto and Nishimura, 1998].
The whole numerical work has produced thousands of GB which have requested the use of a dozen processors to generate and analyse the data.

4.4.2 Relations between EV and GEV distribution for the observable functions g_i

Freitas et al. [2009] have introduced normalizing sequences a_n and b_n in order to proof the convergence of normalized maxima to Extreme Value (EV) distribution (that is GEV distribution where $\mu = 0$ and $\sigma = 1$.). Since in the following numerical studies we fit our data to Generalized Extreme Value Distribution, it is necessary to explain what is the linkage between a_n, b_n, μ and σ.
To accomplish this task we present a case of study which involves the computation of a_n and b_n for $g_1 = -\log(\text{dist}(x,\zeta))$ observable function of a mixing map (Arnold's cat map detailed in section 5.4). Once fitted the data to GEV distribution varying the number N of maxima, we look at μ and σ behaviour with $n \to \infty$.
By the equation 4.9 we know that:

$$\begin{aligned} 1 - F(u) &= 1 - \mu(g(\text{dist}(x,\zeta)) \leq u) \\ &= 1 - \mu(-\log(\text{dist}(x,\zeta)) \leq u) \\ &= 1 - \mu(\text{dist}(x,\zeta) \geq e^{-u}) \\ &= \mu(B_{e^{-u}}(\zeta)) = \Omega_d e^{-ud} \end{aligned} \tag{4.30}$$

where d is the dimension of the space and Ω_d is a constant. To use Gnedenko condition 1.25 it is necessary to calculate u_F

$$u_F = \sup\{u; F(u) < 1\}$$

in this case $u_F = +\infty$. In fact:

$$F(u) = 1 - \Omega_d e^{-ud} < 1$$

then $e^{-ud}\Omega_d > 0$ so that $u \in \mathbb{R}$.
Using Gnedenko equation 1.25 we can calculate $G(t)$ as follows:

$$G(t) = \int_t^\infty \frac{1 - F(u)}{1 - F(t)} du = \int_t^\infty \frac{e^{-ud}}{e^{-td}} du = \frac{1}{d} \int_{td}^\infty \frac{e^{-v}}{e^{-td}} dv = \frac{1}{d} \tag{4.31}$$

then the limit condition 1.25 is easily verified.
According Leadbetter et al. [1983] proof of Gnedenko theorem we can study both a_n and b_n or γ_n convergence as:

$$\lim_{n\to\infty} n(1 - F\{\gamma_n + xG(\gamma_n)\}) = e^{-x}$$

$$\lim_{n\to\infty} n\Omega_d e^{-d}(\gamma_n + xG(\gamma_n)) = e^{-x}$$

then:

$$\gamma_n \simeq \frac{\log(n\Omega_d)}{d}$$

Using Gnedenko Corollary in section 1.1.2 we can obtain a_n and b_n by using γ_n:

$$a_n = d \qquad b_n = -\frac{1}{d}\log(n) + \frac{\log(\Omega_d)}{d}$$

In Arnold's cat map $d = 2$, we have to verify that:

$$\sigma = \frac{1}{a_n} = \frac{1}{d} = \frac{1}{2} \tag{4.32}$$

$$\mu = b_n = C - 0.5\log(n) \tag{4.33}$$

Looking at figure 4.2 these relations seem to be verified. σ is almost constant around a value of 0.5 and μ has a logarithmic behaviour with n. A linear fit give the following decay:

$$\mu = 9.133 - 0.504 \log(n) \qquad r^2 = 0.99$$

where r is the correlation parameter. These results justifies the use of GEV instead of EV distribution with the normalizing sequences substituted by the parameters μ and σ obtained by the fit function.

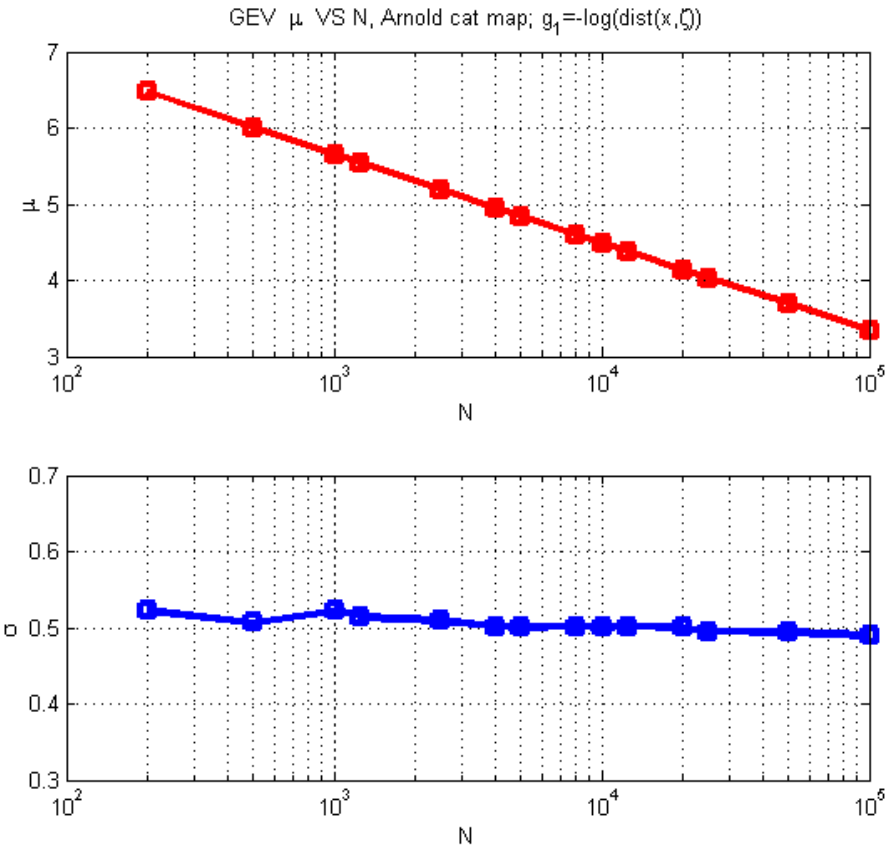

Figure 4.2: GEV μ and σ parameter VS n for g_1 observable, Arnold's cat Map.

4.4.3 Sensitivity studies of α parameter

The first analysis we have performed regards a sensitivity study about α parameter in order to evaluate which is the response of the fit function and which α value is eligible to our further analysis.
The map used was a hyperbolic toral automorphism known as Arnold's cat map (see also section 5.4). For each α value we have computed the g_2 and g_3 observable series for a total of 10^4 maxima each chosen over 10^4 iteration of the map.
In figure 4.3 we can observe the behaviour of ξ tail parameter in respect to α. Recalling that ξ is expected to be positive in this case, we see that ξ reaches very quickly a negative asymptotic value $\xi_\infty^{(g_2)} \simeq -0.008$. This is unexpected from a theoretical point of view but we have to note that the uncertainty in the estimation of ξ parameter is of order 10^{-2} so that even ξ positive values are allowed. It is also interesting to note that the behaviour for the g_3 observable is similar and that $\xi_\infty^{(g_3)} \simeq \xi_\infty^{(g_2)} \simeq -0.008$. Eventually we can imagine that the ξ estimator is biased although the uncertainty justifies also positive value of $\xi_\infty^{(g_2)}$. To avoid this problem, in order to obtain clear positive ξ values for g_2 observables and negative for g_3, we will set $\alpha = 3$ for our subsequent investigations.
Besides ξ we have investigated the behaviour of μ and σ parameters. In figure 4.4 it is possible to observe a rapid decay to an asymptotic μ_∞ value for g_2 and g_3 observables. The uncertainty over μ estimation is of order 10^{-2} for $\alpha \simeq 10$ and of order 10^{-4} when $\alpha \simeq 10^3 - 10^4$.
The behaviour of σ parameter is interesting since it shows a linear decay when plotted against α in a log-log scale as shown in figure 4.5. A linear interpolation of data gives the following results:

$$\log(\sigma^{(g_2)}) = -1.006 \log(\alpha) - 0.612 \qquad r^2 = 0.99$$

$$\log(\sigma^{(g_3)}) = -0.995 \log(\alpha) - 0.711 \qquad r^2 = 0.99$$

where r is the correlation parameter.

Note that all the fits shown in figure 4.3-4.5 pass Kolmogorov Smirnov test described in section 1.4.1 with the maximum confidence level even the test parameter D increases as α increases.

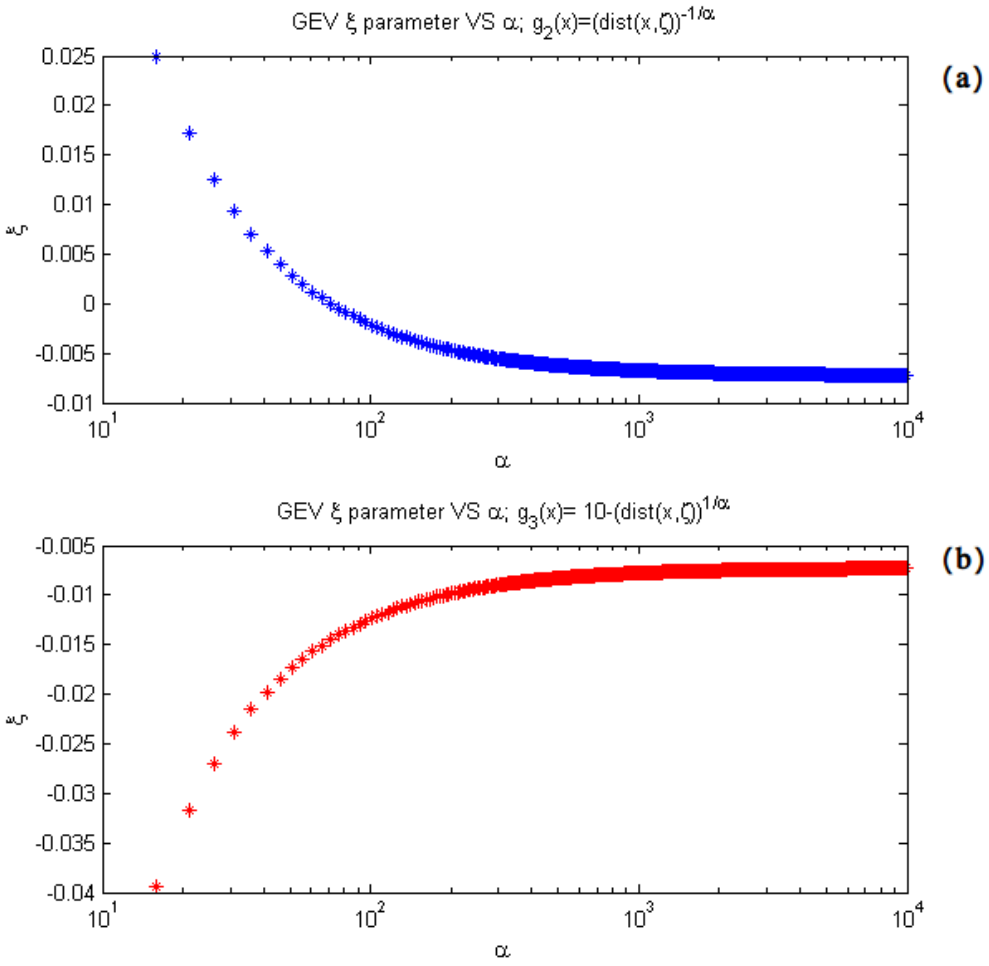

Figure 4.3: GEV ξ parameter VS α for g_2 observable (a) and g_3 observable (b), Arnold's cat Map.

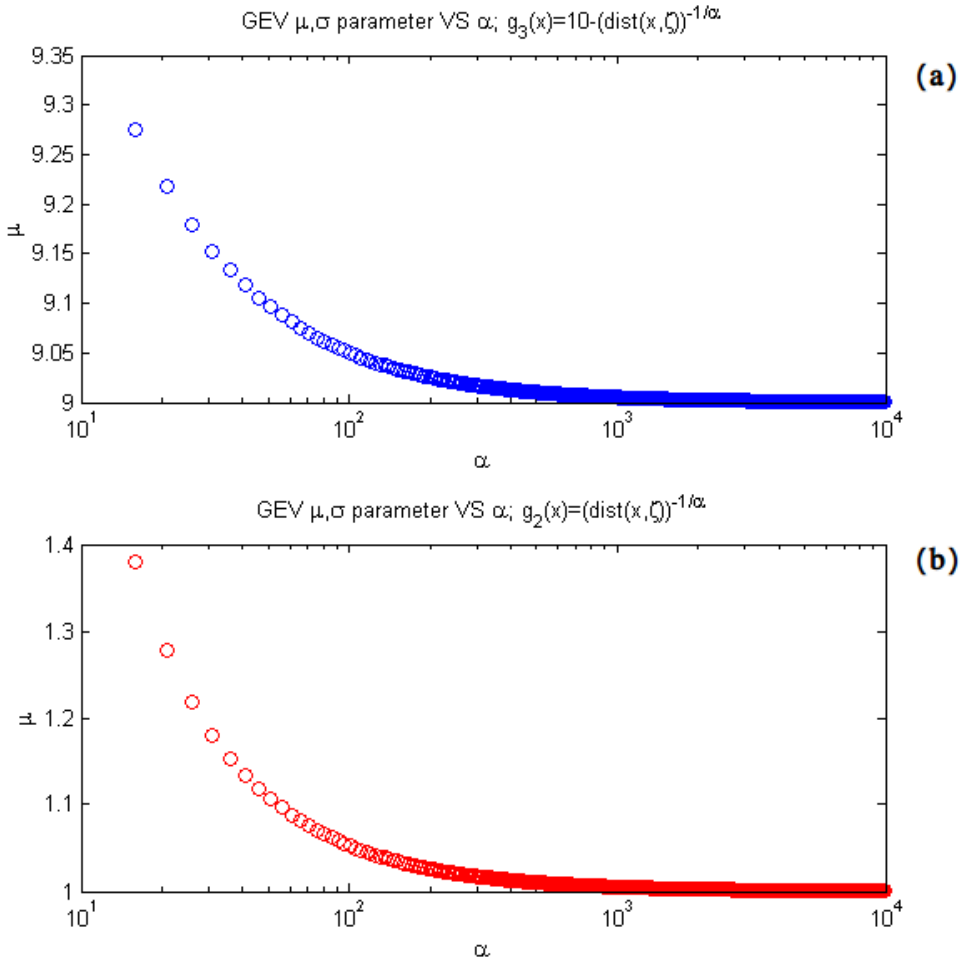

Figure 4.4: GEV μ parameter VS α for g_2 observable (a) and g_3 observable (b), Arnold's cat Map.

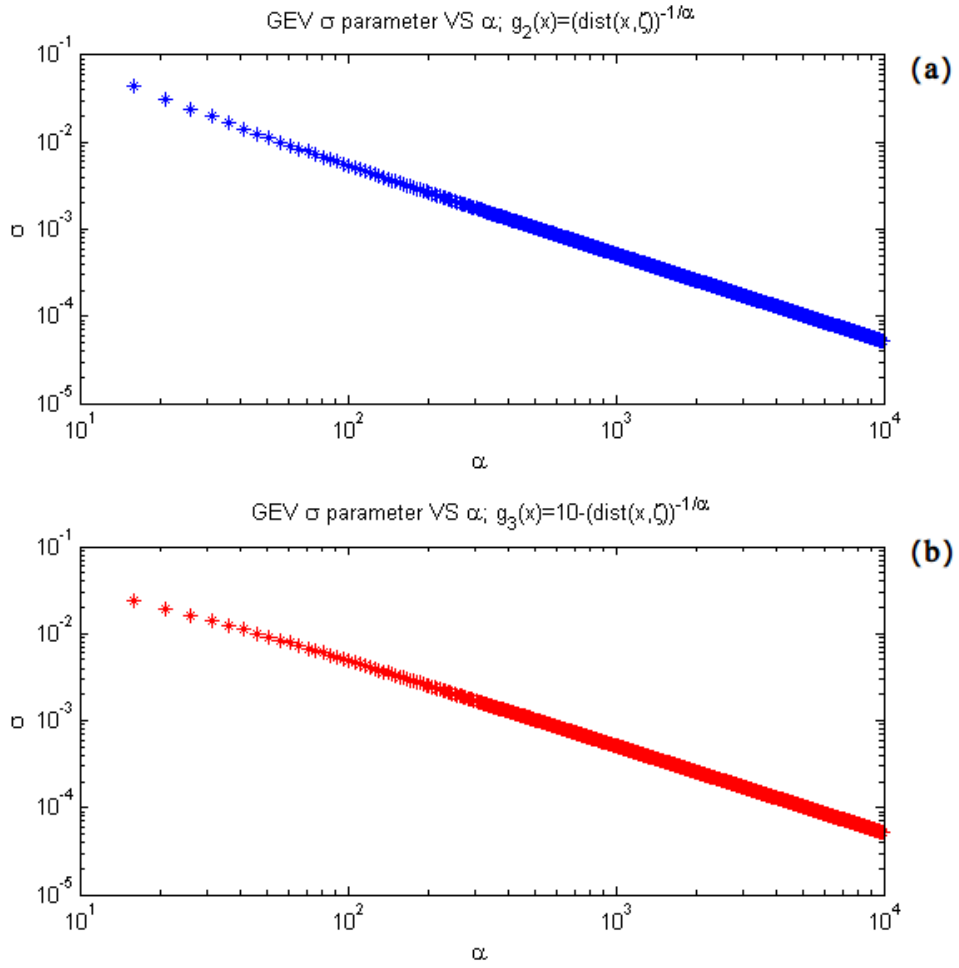

Figure 4.5: GEV σ parameter VS α for g_2 observable (a) and g_3 observable (b), Arnold's cat Map.

Chapter 5

Mathematical models

In this chapter we apply different indicators of dynamic stability to mathematically simple prototype maps which show interesting properties of stability, chaoticity or mixing. The existence of clear mathematical statement for these maps allow us to work in a strong theoretical framework that we can use to investigate the behaviour of GEV parameters even in stochastically perturbed maps.
We show that in case the Lebesgue measure is the same of stationary measure for a perturbed map we expect no difference in GEV parameters among the different noise amplitudes and if compared to the deterministic map.
When this condition is not verified a quite different behaviour is achieved: this is the case of Shear Flow Perturbed Map.
Through the chapter we present many dynamic indicators of stability explaining what can be expected theoretically and what are the difficulties in their numerical computation. The use of all indicators give us a theoretical environment to begin the study of physical systems. This topic will be pursued in the next chapter.

5.1 Irrational Rotations

The name originates from the fact that this map comes from a rotation by an angle of ω on a circle after identifying that circle with the interval $[0, 1]$ where the boundary points are identified. The map, in its unperturbed version, can be written as:

$$x_{n+1} = x_n + \omega \mod 1 \tag{5.1}$$

If we introduce both deterministic and stochastic perturbations, then:

$$x_{n+1} = x_n + \omega + \eta\omega + \epsilon\xi_n \mod 1 \tag{5.2}$$

where η is a small parameter representing a deterministic perturbation, ϵ represents the noise amplitude, and $\xi \in [-1, 1]$ is a random variable with uniform distribution.

5.1.1 Orbit Divergence

Let us consider two orbits:

$$\begin{cases} x_{n+1} &= f^n(x_0) \\ \bar{x}_{n+1} &= f^n(x_0 + \delta x_0) \end{cases} \tag{5.3}$$

where δx_0 is a small quantity. Then, the orbit divergence is defined as:

$$\mathbb{D}x_{n+1} = \bar{x}_{n+1} - x_{n+1} \tag{5.4}$$

We can introduce a stochastic perturbation:

$$\begin{cases} x_{n+1} &= f^n(x_0) \\ \bar{x}_{n+1} &= f_\epsilon^n(x_0) \end{cases} \tag{5.5}$$

Then the divergence is in a statistical sense:

$$\mathbb{D}x_{n+1} =< (x_{n+1} - < \bar{x}_{n+1} >)^2 >^{1/2} \tag{5.6}$$

Let us compute orbits divergence in case of perturbed or unperturbed map. We consider the following cases:

- $\eta = \epsilon = 0$. It follows that:

  $$x_{n+1} = x_0 + n\omega \mod 1$$

  so that

  $$\mathbb{D}x_{n+1} = \delta x_0 \mod 1$$

  and there is not orbit divergence.

- $\eta \neq 0, \epsilon = 0$ As before:

  $$\begin{cases} x_{n+1} &= x_0 + n\omega \mod 1 \\ \bar{x}_{n+1} &= x_o + \delta x_0 + n\omega + n\eta\omega \mod 1 \end{cases} \tag{5.7}$$

  In this case we obtain a divergence proportional to n:

  $$\mathbb{D}x_{n+1} = n\eta\omega + \delta x_0 \mod 1$$

- $\eta = 0, \epsilon \neq 0$ In this case we define:

  $$\begin{cases} x_{n+1} &= x_0 + n\omega \mod 1 \\ \bar{x}_{n+1} &= x_o + n\omega + \epsilon \sum_{j=0}^{n} \xi_j \mod 1 \end{cases} \tag{5.8}$$

  We use the definition 5.6, then:

  $$\mathbb{D}x_{n+1} =< \epsilon^2(\xi_0 + \cdots + \xi_n)^2 >^{1/2} \qquad \mod 1$$

$$\mathbb{D}x_{n+1} =< \epsilon^2 \sum_{i,j=0}^{n} < \xi_i \xi_j >>^{1/2} \qquad \text{mod } 1$$

$$\mathbb{D}x_{n+1} =< \epsilon^2 \sum_{i,j=0}^{n} \delta_{ij} >^{1/2} \qquad \text{mod } 1$$

$$\mathbb{D}x_{n+1} = \epsilon(n+1)^{1/2} \qquad \text{mod } 1$$

with a divergence proportional to the square root of n that is typical of a diffusion process.

5.1.2 Correlations decay

Correlations decay detailed in section 3.3 can be computed both analytically and numerically for $qx \mod 1$. The analytical result can be obtained using Fourier theory as detailed in Turchetti et al. [2010].

Considering a pure irrational rotation without perturbation we observe no correlations decay:

$$c_n = \sum_{k,k'} \phi_k \phi^*_{k'} \int_0^1 e^{2\pi i k(x+n\omega)} e^{-2\pi i k' x} dx \tag{5.9}$$

the integral vanishes if $k \neq k'$, so that:

$$c_n = \sum_{k} \phi_k \phi^*_k e^{2\pi i k n \omega} \tag{5.10}$$

if $|\phi_k| \leq C/|k|$, then we observe only an oscillating behaviour with no correlations decay.

5.1.3 Fidelity decay

We have introduced Classical Fidelity in equation 3.16 and fidelity decay has been noted as $\delta F^{\epsilon}_{\varphi,\psi}(n)$ in equation 3.17.

In case of irrational rotations we write Fidelity as:

$$F^{\epsilon}_{\phi,\psi}(n) = \int_0^1 \left(\int_{-1}^1 \cdots \int_{-1}^1 \phi\left(x + n\omega\right) \psi\left(x + n\omega + \epsilon \sum_{j=0}^{n} \xi_j \right) \frac{d\xi_0}{2} \cdots \frac{d\xi_n}{2} \right) dx$$

Let $\phi(x+1) = \phi(x)$ be periodic of period 1. Using Fourier theory as in the decay of correlations:

$$F^{\epsilon}_{\phi,\phi}(n) = \phi_0^2 + \sum_{k\neq 0} |\phi_k|^2 \int_{-1}^1 \cdots \int_{-1}^1 \exp\left(2\pi i k \epsilon \sum_{j=0}^{n} \xi_j \right) \frac{d\xi_0}{2} \cdots \frac{d\xi_n}{2}$$

If we perform the integrals over noise, then:

$$F^{\epsilon}_{\phi,\phi}(n) = \phi_0^2 + \sum_{k\neq 0} |\phi_k|^2 \left(\frac{\sin(2\pi k\epsilon)}{2\pi k\epsilon} \right)^{n+1}$$

Let us choose $\phi(x) = \cos(2\pi x)$ then $\phi_{\pm 1} = 1/2$ and $\phi_k = 0$ otherwise. Then:

$$\delta F^{\epsilon}_{\phi,\phi}(n) = \frac{1}{2} \left(\frac{\sin(2\pi k\epsilon)}{2\pi k\epsilon} \right)^{n+1} \tag{5.11}$$

The following relations hold:

$$\lim_{n\to\infty} F^{\epsilon}_{\phi,\phi}(n) = 0$$

$$F^{\epsilon}_{\phi,\phi}(0) = 1/2$$

If $\alpha << 1$ then:

$$\left(\frac{\sin(\alpha)}{\alpha} \right)^n = \exp\left(n \log\ \left(\frac{\sin(\alpha)}{\alpha} \right) \right) = \exp\left(n \log\left(1 - \frac{\alpha^2}{3} + ... \right) \right)$$

$$\left(\frac{\sin(\alpha)}{\alpha} \right)^n = \exp\left(-\frac{n\alpha^2}{3} \right)$$

furthermore, with $\alpha^2 n << 1$:

$$\left(\frac{\sin(\alpha)}{\alpha} \right)^n \simeq 1 - \frac{n\alpha^2}{3}$$

Eventually, if $\alpha >> 1$:

$$\left(\frac{\sin(\alpha)}{\alpha}\right)^n \leq \alpha^{-n} = \exp(-n \log \alpha)$$

and in this case the fidelity decay is almost exponential.

In figure 5.1 it is possible to observe what we have just analytically described. The computation has been performed using a Monte Carlo method starting with 10^6 random initial points within the torus $[0, 1]$. For $\epsilon = 0.1$ the decay is exponential while small ϵ values show slower decay behaviours.

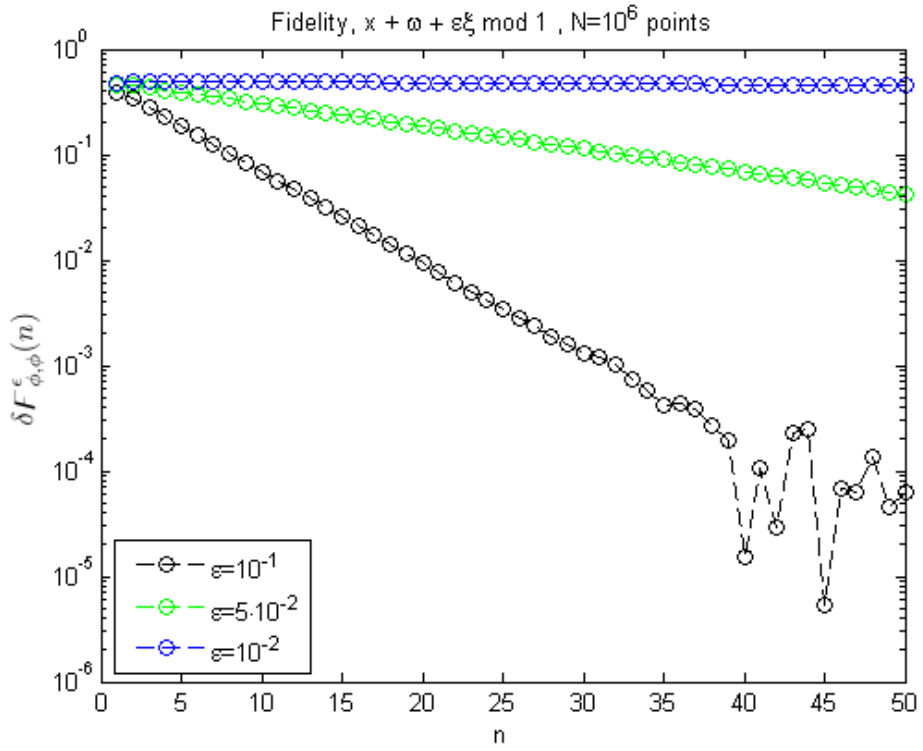

Figure 5.1: Fidelity for different ϵ, Irrational rotations perturbed map

5.1.4 Return time statistics

The existence of at most three different return times for irrational rotations on the circle was proved by Slater about forty years ago. However, the proof of the existence of a limit law, provided the shrinking subsets of the circle are chosen in a descending chain of re-normalisation intervals, is a recent result. Coelho and De Faria [1996] were able to find the limit distribution of first entry times when the rotation number is taken as an arbitrary irrational number whereas a simple proof concerning the limit statistics of first return times and restricted to a particular class of quadratic irrationals was independently given by Buric et al. [2005].

5.2 Skew Map

This integrable map was widely studied by Hu et al. [2004] and Rossi et al. [2005] to show an algebraic decay of return time spectrum and introduce the concept of *local mixing*.
The map may be written as:

$$\begin{cases} x_{n+1} &= x_n + y_n \mod 1 \\ y_{n+1} &= y_n \end{cases} \tag{5.12}$$

The concept of local mixing over a domain is intuitively understandable looking at figure 5.2, the stretched form of domain justifies the other name given to this map that is *shear flow*. It can be formalized following Hu et al. [2004] as follows:
Let μ_L be the Lebesgue measure and take a cylinder $C_\epsilon = \mathbb{T} \times [0, l_{side}]$ where we define the measure $\mu_{l_{side}}$

$$\mu_{l_{side}}(A) = \frac{\mu_L(A)}{\mu_L(C_{l_{side}})} = \frac{\mu_L(A)}{l_{side}} \qquad A \subseteq C_{l_{side}}$$

The set $C_{l_{side}}$ is invariant with respect to system 5.12 and $\mu_{l_{side}}$ is its invariant measure.

Now we are ready to introduce the definition of local mixing which is proved in Hu et al. [2004].

Proposition: *Given the dynamical system 5.12 over the cylinder* $C_{l_{side}}$ *and with measure* $\mu_{l_{side}}$ *and the square* $A_{l_{side}} = [0, l_{side}] \times [0, l_{side}]$ *the following property holds:*

$$\mu_\epsilon(A_{l_{side}} \cap R^n(A_{l_{side}})) - \mu^2_{l_{side}}(A_{l_{side}}) = \mathcal{O}\left(\frac{1}{n}\right). \tag{5.13}$$

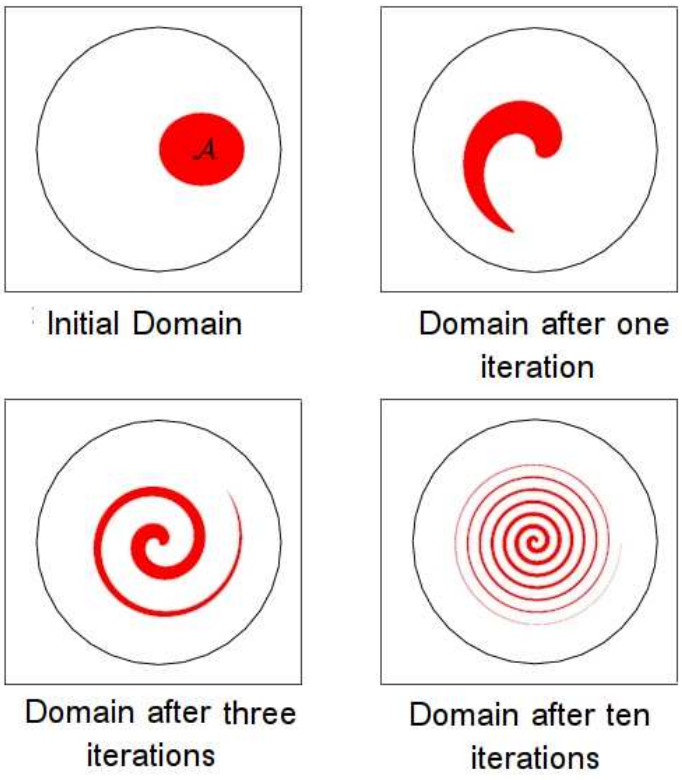

Figure 5.2: Skew map, representation after some iterations

5.2.1 Orbit Divergence

Proceeding in the way shown in section 5.1.1, we compute the divergence in different cases:

- First we consider the unperturbed map:

$$\begin{cases} \bar{x}_{n+1} &= x_0 + \delta x_0 + n(y_0 + \delta y_0) \mod 1 \\ \bar{y}_{n+1} &= y_0 + \delta y_0 \end{cases} \tag{5.14}$$

  Since we are in two dimensions:

$$\mathbb{D}\vec{x}_{n+1} = \sqrt{(\bar{x}_{n+1} - x_{n+1})^2 + (\bar{y}_{n+1} + y_{n+1})^2} \tag{5.15}$$

$$\mathbb{D}\vec{x}_{n+1} = \sqrt{(\delta x_0 + n\delta y_0)^2 + (\delta y_0)^2} \tag{5.16}$$

$$\mathbb{D}\vec{x}_{n+1} \simeq n\delta y_0 \tag{5.17}$$

  and we obtain a similar result, except a factor $(1 + \eta)$, considering a deterministic perturbation such ηy_n

- Let us consider a stochastically perturbed version of the Skew map:

$$\begin{cases} \bar{x}_{n+1} = x_0 + ny_0 + \epsilon \sum_{j=0}^{n} \xi_j \\ \bar{y}_{n+1} = y_0 \end{cases} \tag{5.18}$$

  Using the definition 5.6, then we obtain the same decay that holds for perturbed irrational rotations map:

$$\mathbb{D}\vec{x}_{n+1} =< \epsilon^2 \sum_{i,j=0}^{n} < \xi_i \xi_j >>^{1/2}$$

$$\mathbb{D}\vec{x}_{n+1} =< \epsilon^2 \sum_{i,j=0}^{n} \delta_{ij} >^{1/2}$$

$$\mathbb{D}\vec{x}_{n+1} = \epsilon(n+1)^{1/2}$$

- We can perturb the angular variable y obtaining a different result:

$$\begin{cases} \bar{x}_{n+1} = x_0 + ny_0 + \epsilon \sum_{j=0}^{n} \xi_j (n-j) \\ \bar{y}_{n+1} = y_0 + \epsilon \sum_{j=0}^{n} \xi_j \end{cases} \tag{5.19}$$

Let us divide into two parts:

$$\mathbb{D}y_{n+1} = \epsilon(n+1)^{1/2}$$

as shown in the precedent computation. It is more interesting $\mathbb{D}x_{n+1}$, in fact:

$$\mathbb{D}y_{n+1} =< \epsilon^2 \sum_{j,l=0}^{n} < (n-j)\xi_j(n-l)\xi_l >>^{1/2}$$

but $j = l$, so that:

$$\mathbb{D}x_{n+1} =< \epsilon^2 \sum_{i,j=0}^{n} (n-l)^2 >^{1/2}$$

$$\mathbb{D}x_{n+1} \simeq \frac{\epsilon}{3}(n+1)^{3/2}$$

this kind of diffusion is typical for angular variables. The same kind of results hold in the continuous case

5.2.2 Correlations decay

For the shear-flow map in absence of noise, the correlation function may be written as:

$$c_n = \int \Phi(x)\Phi(x+ny))d\mu(x,y) \tag{5.20}$$

where $\Phi(x)$ is a generic observable. The map is here defined over $\mathbb{T} \times [0, \eta]$ so that $d\mu = dx \cdot dy/\eta$.

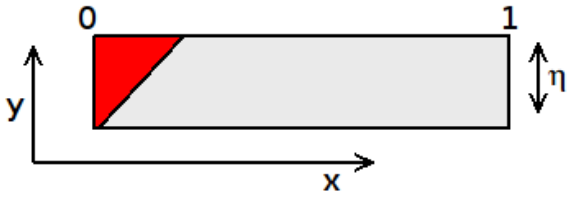

We can obtain the correlation spectral decay $C_\phi(n) = |c_n - c_0|$ using Fourier theory as in the precedent cases:

$$\begin{aligned} c_n &= \sum_{k,k'} \phi_k \phi^*_{k'} \int_0^\eta \int_0^1 \frac{1}{\eta} e^{2\pi i k(x+ny)} e^{-2\pi i k' x} dx dy \\ &= \sum_k \phi_k \phi^*_k \frac{1}{\eta} \int_0^\eta e^{2\pi i k n y} dy \\ &= \phi_0 \phi^*_0 + \sum_{k\neq 0} \frac{e^{2\pi i k \eta n} - 1}{2\pi i k n} \phi_k \phi^*_k \\ &= \phi_0 \phi^*_0 + \frac{1}{n} \sum_{k\neq 0} e^{\pi i k \eta} \frac{\sin(\pi k \eta n)}{\pi k \eta} \phi_k \phi^*_k \end{aligned} \tag{5.21}$$

if $|\phi_k| \leq C/|k|$, then:

$$C_\phi(n) = |c_n - \phi_0^2| \leq 2C^2 \sum_{k=1}^{\infty} S(k\eta n) \cdot \frac{1}{k^2} \tag{5.22}$$

The next task is to estimate decay analysing the structure of $S(x)$.

$$|S(x)| = \left| \frac{sin(2\pi x)}{2\pi x} \right| \leq \begin{cases} \exp\left(-x^2 \log(2\pi)\right) & |x| < 1 \\ \dfrac{1}{2\pi |x|} & |x| \geq 1 \end{cases} \tag{5.23}$$

we obtain:

$$\begin{aligned}\sum_{k=1}^{\infty}\frac{1}{k^2}S(k\eta n) &\leq \sum_{k=1}^{1/\eta}\frac{1}{k^2}\exp\left(-\frac{k^2}{4}\eta^2 n^2\log(2\pi)\right)+\frac{1}{n}\sum_{k=1/\eta}^{\infty}\frac{1}{\pi k\eta}\cdot\frac{1}{k^2}\leq\\ &\leq\int_1^{\infty}\exp\left(-\frac{k^2}{4}\eta^2 n^2\log(2\pi)\right)dk^2+\frac{1}{n}\cdot\frac{1}{\pi\eta}\int_{1/\eta}^{\infty}\frac{dk}{k^3}=\\ &=\frac{\exp\left(-\eta^2\frac{n^2}{4}\log(2\pi)\right)}{\eta^2\frac{n^2}{4}\log(2\pi)}+\frac{1}{n}\cdot\frac{1}{\pi\eta}\frac{\eta^2}{2}=\\ &=\frac{\eta}{2\pi n}+\frac{\exp\left(-\eta^2\frac{n^2}{4}\log(2\pi)\right)}{\eta^2\frac{n^2}{4}\log(2\pi)}\end{aligned} \tag{5.24}$$

which shows an asymptotic power-law decay for the correlation spectrum in a shear-flow map.

Correlation decay - noise added only to x variable

By adding noise only to x variable, as in equations 5.18, the correlation decay spectrum can be observed only if $\Phi = \Phi(x)$. Otherwise, if the observable is of the type $\Psi = \Psi(x, y)$ and, for example, factorizable as $\Psi = \varphi(x) \cdot \chi(y)$, the decay cannot be observed.
In fact, supposing φ as constant , we obtain the following contradiction:

$$c_n = \int \chi^2(y)dy \neq \left(\int \chi(y)dy\right)^2 \tag{5.25}$$

Again, using Fourier series decomposition, we rewrite:

$$c_n = \sum_{k,k'}\phi_{k'}\phi_k^*\int_{-1}^{1}\int_{-1}^{1}\int_{0}^{1}\exp\left(2\pi ikx\right)\exp\left(-2\pi ik\left(x+n\omega+\epsilon\sum_{j=0}^{n-1}\xi_j\right)\right)dx\frac{d\vec{\xi_n}}{2^n} \tag{5.26}$$

and proceeding as before:

$$c_n = \sum_k |\phi_k|^2 e^{-2\pi ik\omega}\mathcal{S}^n(k\epsilon) \tag{5.27}$$

$$|S(x)| = \left|\frac{sin(2\pi x)}{2\pi x}\right| \leq \begin{cases} \exp\left(-x^2 \log(2\pi)\right) & |x| < 1 \\ \dfrac{1}{2\pi|x|} & |x| \geq 1 \end{cases} \tag{5.28}$$

supposing $|\phi_k| \leq C/|k|$, we write:

$$\begin{aligned} C_\phi(n) &\leq 2C \sum_{k=1}^{1/\epsilon} \frac{1}{k^2} \exp\left(-nk^2\epsilon^2 \log(2\pi)\right) + \frac{2C}{(2\pi)^n} \sum_{k=1/\epsilon}^{\infty} \frac{1}{k^2} \cdot \frac{1}{(k\epsilon)^n} \leq \\ &\leq 2C \exp\left(-\epsilon^2 n \log(2\pi)\right) \sum_{k=1}^{1/\epsilon} \frac{1}{k^2} + \frac{2C}{(2\pi)^n} \epsilon \sum_{k=1/\epsilon}^{\infty} \frac{\epsilon}{(k\epsilon)^{n+2}} \leq \\ &\leq 2C \exp\left(-\epsilon^2 n \log(2\pi)\right) \left(1 + \int_1^{1/\epsilon} \frac{dk}{k^2}\right) + \frac{2C\epsilon}{(2\pi)^n} \left(\epsilon + \int_{1/\epsilon}^{\infty} \epsilon \frac{dk}{(k\epsilon)^{n+2}}\right) = \\ &= 2C \exp\left(-\epsilon^2 n \log(2\pi)\right)(2-\epsilon) + \frac{2C\epsilon}{(2\pi)^n} \left(\epsilon + \frac{1}{n+1}\right) \leq \\ &\leq 4C \exp\left(-\epsilon^2 n\right) \end{aligned} \tag{5.29}$$

Equation 5.29 shows the exponential decay of correlations in the case of random noise added only to x variable.

Correlation decay - noise added to y variable

We now consider the map 5.19 expecting some difference in correlations decay when noise is added to angular variable as in this case. The correlation function may be written as:

$$c_n = \int_0^1 dx \int_0^\eta \frac{dy}{\eta} \int_{-1}^1 \frac{d\xi_1}{2} \ldots \int_{-1}^1 \frac{d\xi_{n-1}}{2} \phi(x)\phi\left(x + ny + \epsilon \sum_{k=1}^{n-1} (n-k)\xi_k\right) \tag{5.30}$$

$$c_n = \phi_0^2 + \sum_{k\neq 0} \phi_k \phi_k^* \int_0^1 \exp(2\pi i k n y) \frac{dy}{\eta} \cdot \frac{1}{2} \int_{-1}^1 \exp(2\pi i k \epsilon (n-1)\xi_1) d\xi_1 \cdot \\ \cdot \frac{1}{2} \int_{-1}^1 \exp(2\pi i k \epsilon (n-2)\xi_2) d\xi_2 \cdots \frac{1}{2} \int_{-1}^1 \exp(2\pi i k \epsilon \xi_{n-1}) d\xi_{n-1} \tag{5.31}$$

$$c_n = \phi_0^2 + \sum_{k\neq 0} \phi_k \phi_k^* \exp(\pi i k \epsilon) S(\eta(k/2)n) \cdot S(k\epsilon(n-1)) \cdot S(k\epsilon(n-2)) \cdots S(k\epsilon) \tag{5.32}$$

We note an initial power lay decay followed by an asymptotic exponential decay, as shown In the following proof.

Suppose that $k \leq k_{max}$ with $|\phi_n| \leq C/|k|$, if $k_{max}\epsilon n << 1$, then:

$$\prod_{j=1}^{n-1} |S(k\epsilon j)| \leq \exp\left(-\log(2\pi) k^2 \epsilon^2 \sum_{j=1}^{n} j^2 \right) \leq \exp\left(-k^2 \epsilon^2 n^3 \frac{\log(2\pi)}{3} \right) \tag{5.33}$$

if $n^3 k_{max}^2 \epsilon^2 << 1$ the product of $S(k\epsilon j)$ is about of order 1 while $S(\pi k \eta n)$ decay as $1/n$.

If, instead, $n\epsilon >> 1$ the we have:

$$\begin{aligned} \prod_{j=1}^{n-1} |S(k\epsilon j)| &\leq \prod_{j=n/2}^{n} \frac{1}{2\pi k \epsilon j} = \frac{1}{2\pi k \epsilon} \frac{n}{2} \exp\left(\sum_{n/2}^{n} \log j \right) = \\ &= \frac{1}{(2\pi\epsilon)^{n/2}} \exp\left(n\log(n) - n - \frac{n}{2}\log\left(\frac{n}{2}\right) + \frac{n}{2} \right) = \\ &= \frac{1}{(2\pi\epsilon)^{n/2}} \exp\left[\frac{n}{2} (\log 2n - 1) \right] \end{aligned} \tag{5.34}$$

The product of $S(k\epsilon j)$ is about of order 1 and the decay is given by the first term:

$$C_\phi(n)) = |c_n - \phi_0^2| \leq \frac{\eta}{\pi} \cdot \frac{1}{n}$$

To observe the exponential decay we have to consider the region in which $k_{max}\epsilon\bar{n} >> 1$ and $n > \bar{n} > 1$.
Assume $\bar{n} = n/2$ we eventually obtain:

$$\begin{aligned} \prod_{j=1}^{n-1} |S(k\epsilon j)| \leq \prod_{j=n/2}^{n} \frac{1}{2\pi\epsilon jk} = \frac{1}{(2\pi\epsilon k)^{n/2}} \exp\left(\sum_{j=1}^{n/2} \log(j)\right) = \\ = \frac{1}{(2\pi\epsilon k)^{n/2}} \exp\left(\frac{n}{2}(\log 2n - 1)\right) = \frac{1}{(4\pi\epsilon nk)^{n/2}} \end{aligned} \tag{5.35}$$

from which we obtain:

$$\sum_{k=1}^{k_{max}} \frac{1}{k^2} \cdot \frac{1}{k^{n/2}} \leq \int_1^\infty \frac{dk}{k^{2+n/2}} = \frac{1}{1+n/2} \leq \frac{2}{n} \tag{5.36}$$

Then:

$$C_\phi(n) = |c_n - \phi_0^2| \leq \frac{2c^2}{n} \cdot \frac{1}{(4\pi\epsilon n)^{n/2}} \tag{5.37}$$

and the decay is more than exponential, that is $\exp\left(-\frac{n}{2}\log n\right)$.

5.2.3 Fidelity decay

Fidelity decay in Skew map follows the general framework described for correlations except some oscillating factor. In the case of noise added only to x variable, we observe an exponential decay of fidelity as for the perturbed case of irrational rotations. It is possible to compute numerically δF_ϵ for various noise values. In figure 5.3 this task has been done using a Monte Carlo. The behaviour shown in figure reproduces analytical results. We verify a super-exponential decay in the case of noise added on the angular variable y as shown in figure 5.4.

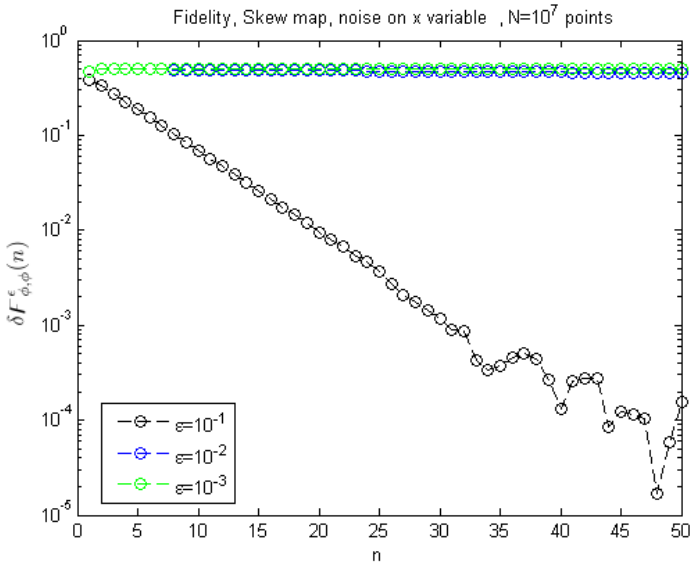

Figure 5.3: Fidelity for different ϵ, Shear Flow map, noise added to x variable

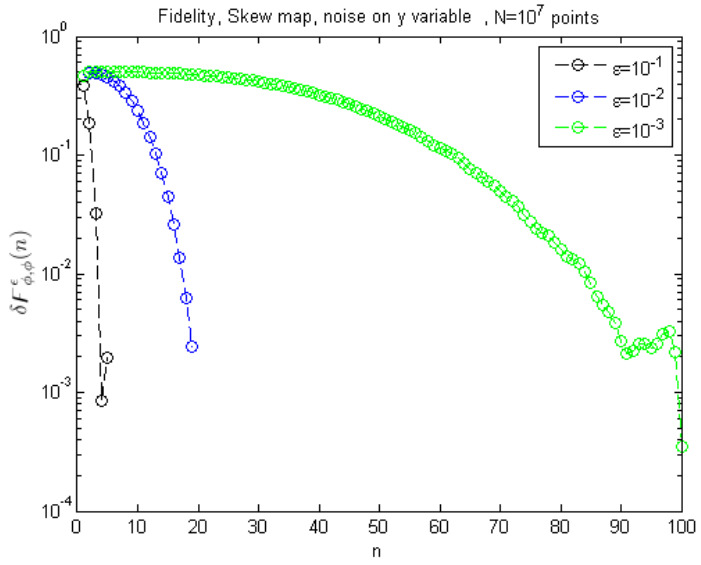

Figure 5.4: Fidelity for different ϵ, Shear Flow map, noise added to y variable

5.2.4 Return time Statistics

The power law decay of return time spectrum has been proved by Hu et al. [2004] analytically with a geometric construction and investigated numerically obtaining the same result. We report their main result:

Proposition Given the cylinder $C = \mathbb{T} \times [0, l_{side}]$ (where $\mathbb{T}$ represents a one-dimensional torus) and the set $A = [0, l_{side}] \times [0, l_{side}] \subset C$ the spectrum $F_{l_{side}}$ of the return times in A is given by

$$F_{l_{side}}(t) = \begin{cases} 1 & \text{if} \quad 0 \leq t < t_1 \\ \\ \dfrac{1}{2} & \text{if} \quad t \in [t_n, t_{n+1}[, t_n < t_{\bar{n}} \\ \\ \dfrac{1}{2}\left[1 - \dfrac{(t_n - 1 + \epsilon)^2}{t_n\,\epsilon}\right] & \text{if} \quad t \in [t_n, t_{n+1}[, t_n = t_{\bar{n}} \\ \\ \dfrac{(1 - l_{side})^2}{2t_n(t_n - l_{side})} & \text{if} \quad t \in [t_n, t_{n+1}[, t_n > t_{\bar{n}} \end{cases} \tag{5.38}$$

where $\bar{n} = \lfloor 1/l_{side} \rfloor$ and $t_n = n \cdot l_{side}$. The asymptotic decay is proportional to $1/t^2$.

It is interesting analyse numerically the Return Time Statistics for a noise perturbed Skew map. To accomplish this task we have choose the map of equation 5.18. Then we followed the orbit of 10^4 points starting in a square centred in $x_c = 0.3, y_c = 0.6$ and $l_{side} = 0.01$. For each orbit we have registered the number of iteration that causes a return into the initial square. In this way we have constructed return time statistics that now are reported in figure 5.5. The time on x axis is normalized as: $t = n \cdot l_{side}^2$.

For small ϵ values a power law decay is obtained. If $\epsilon = 10^{-7}$ the spectrum decays as $1/t^2$, while for intermediate values of noise ($\epsilon = 10^{-4} - 10^{-5}$) Return time statistics follows $1/t^2$ and then $1/\sqrt{t}$ power law decay. When the noise amplitude $\epsilon > 10^{-3}$ the decay is exponential after an initial plateau.

This behaviour presents again assonances with the correlation and fidelity behaviour where a power law decay is observed in deterministic map while the presence of noise involves in an exponential behaviour.

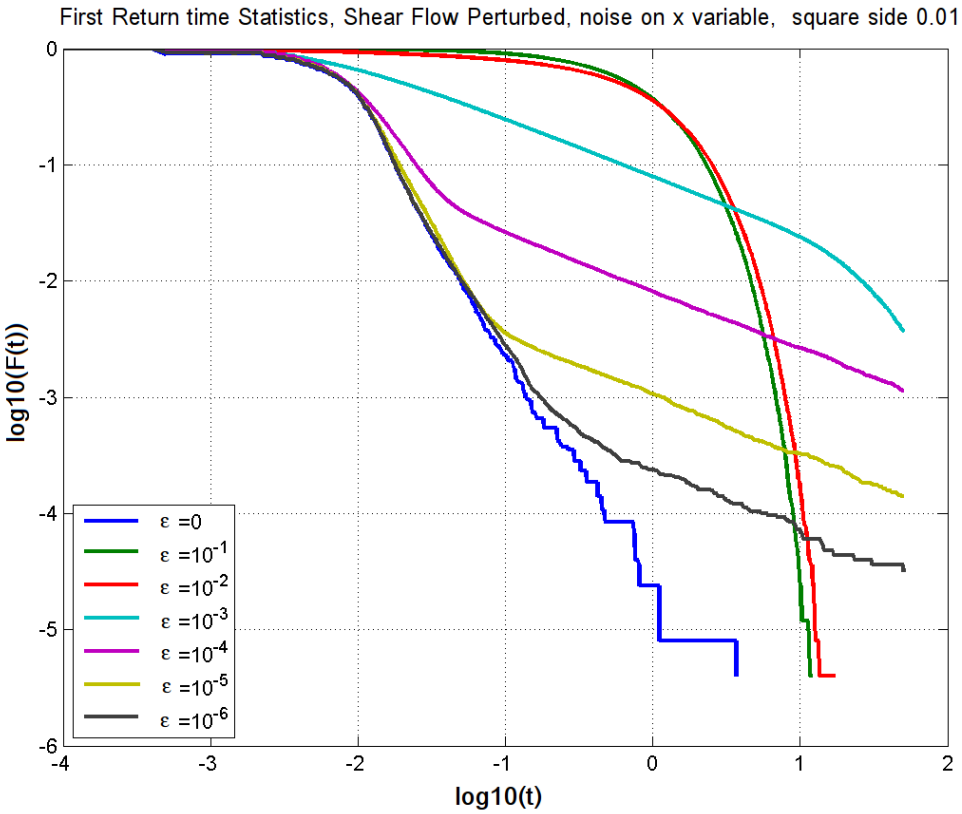

Figure 5.5: Recurrence Statistics for different ϵ, Shear Flow map

5.2.5 Extreme value distribution for unperturbed and perturbed map

Freitas' Theorem in section 4.2.2 tell us that Skew Map is not suitable to obtain a reliable fit of GEV distribution. In fact, it follows that local mixing is not enough to satisfy conditions necessary to obtain one of the three type distribution of maxima.

The situation is different if we introduce noise, for example on x variable as done for Recurrences. For each different ϵ value, we have performed 10^4 realisations of the map in equation 5.18, starting from the same initial point $\zeta_x = \zeta_y = 0.3 + \pi/10$. we have used the block of maxima approach in order to obtain a fit to GEV distribution. For each time step we compute the distance from the initial point as

$$d((x,y),(\zeta_x,\zeta_y)) = \sqrt{\min\{|x-\zeta_x|, 1-|x-\zeta_x|\}^2 + \min\{|y-\zeta_y|, 1-|y-\zeta_y|\}^2} \tag{5.39}$$

Then, once divided distance series in 10^4 bin each containing $3 \cdot 10^5$ iterations of the map, we compute the minimum distance for each bin and then calculate the observable functions g_1, g_2, g_3. Eventually we fit 10^4 g_i data to the GEV distribution using maximum likelihood estimation of parameters. The GEV parameters obtained show a normal distribution (KS test for normal distribution passed at confidence level 0.20). These results are presented in figures 5.6-5.8:
In the deterministic case we are unable to fit data to GEV distribution. For small ϵ we recall that Return Time Statistics show a power-law spectral decay. For this reason we expect no reliable fits for our perturbed data. This is verified in all the cases considered and noted in figure with a dotted line: the Kolmogorov-Smirnov test is not accomplished if $\epsilon < 10^{-3}$ and the normal fit show substantially a great spread of parameters value. On the other hand if $\epsilon > 10^{-3}$ we obtain reliable fit to GEV distribution and the spread of parameters value are contained in small intervals. Note that the bin length ($3 \cdot 10^5$ data for each bin) is greater than the one used for the subsequent cases of mixing maps. This is necessary since the Recurrence Statistics is exponential only after an initial plateau.
In figure 5.6 we may also note how for g_1 observable, even for $\epsilon > 10^{-3}$ the fit parameter ξ is negative and not distributed around zero as expected from theory. We have to say that in all cases considered the KS test is not passed at maximum confidence level and this affects the value of considered parameters.

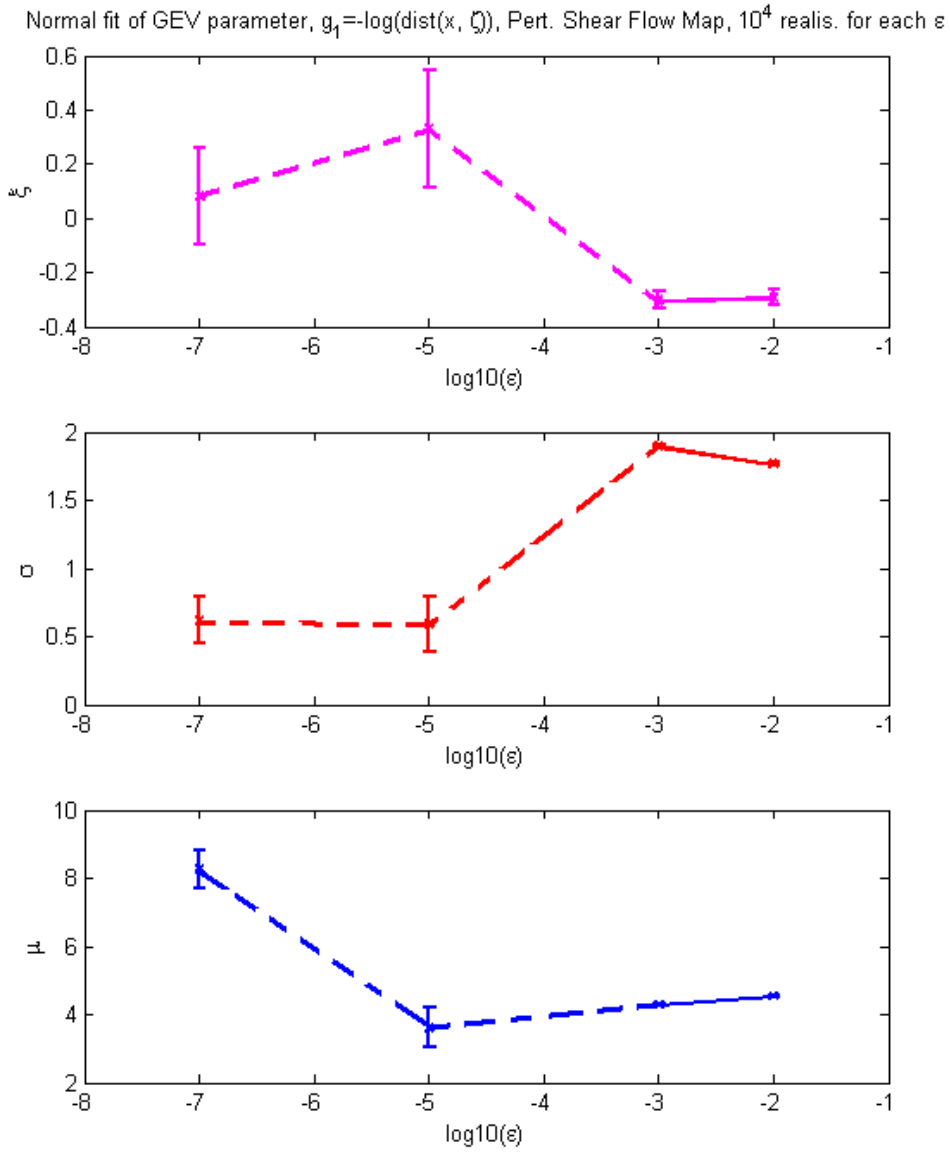

Figure 5.6: Normal fit mean and standard deviation of GEV parameter for 10^4 realisations of Shear Flow Perturbed Map VS (noise on x) ϵ; g_1 observable

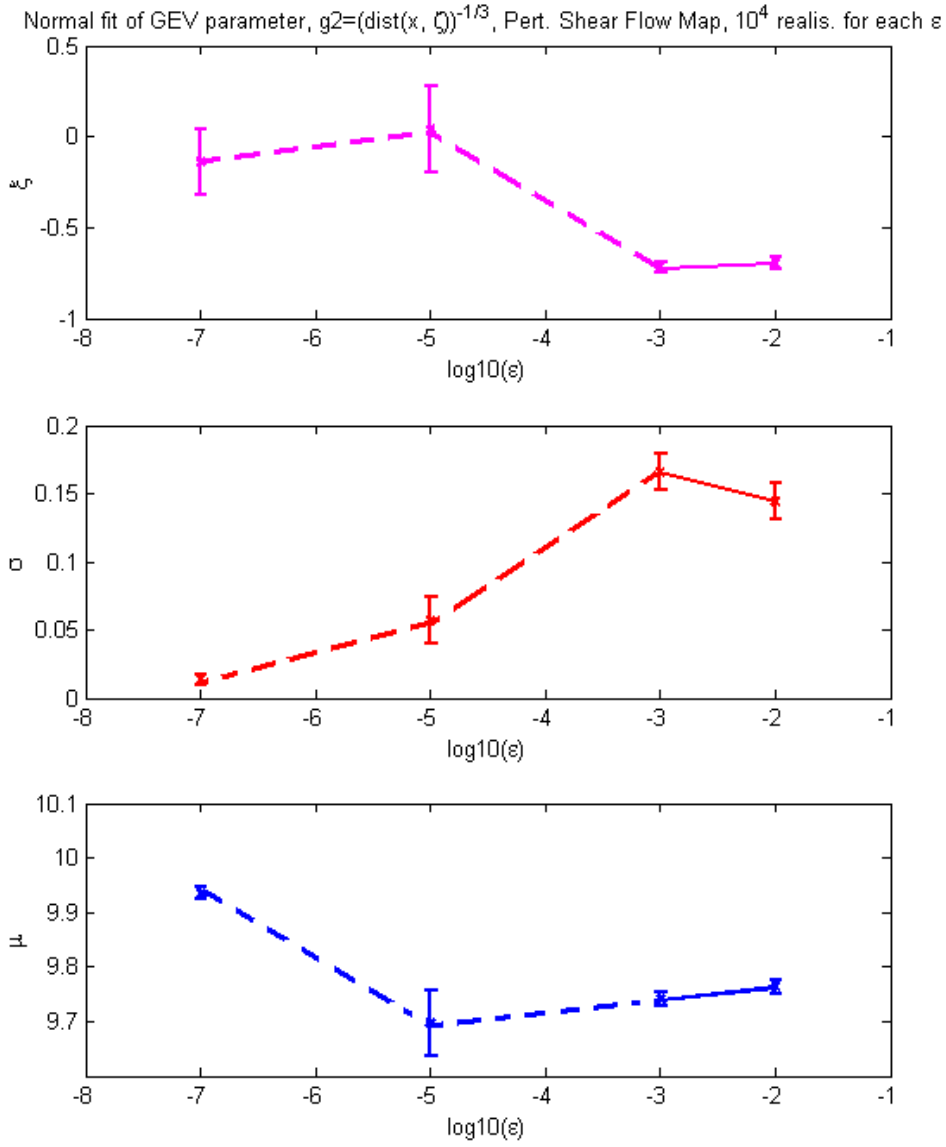

Figure 5.7: Normal fit mean and standard deviation of GEV parameter for 10^4 realisations of Shear Flow Perturbed Map VS (noise on x) VS ϵ; g_2 observable

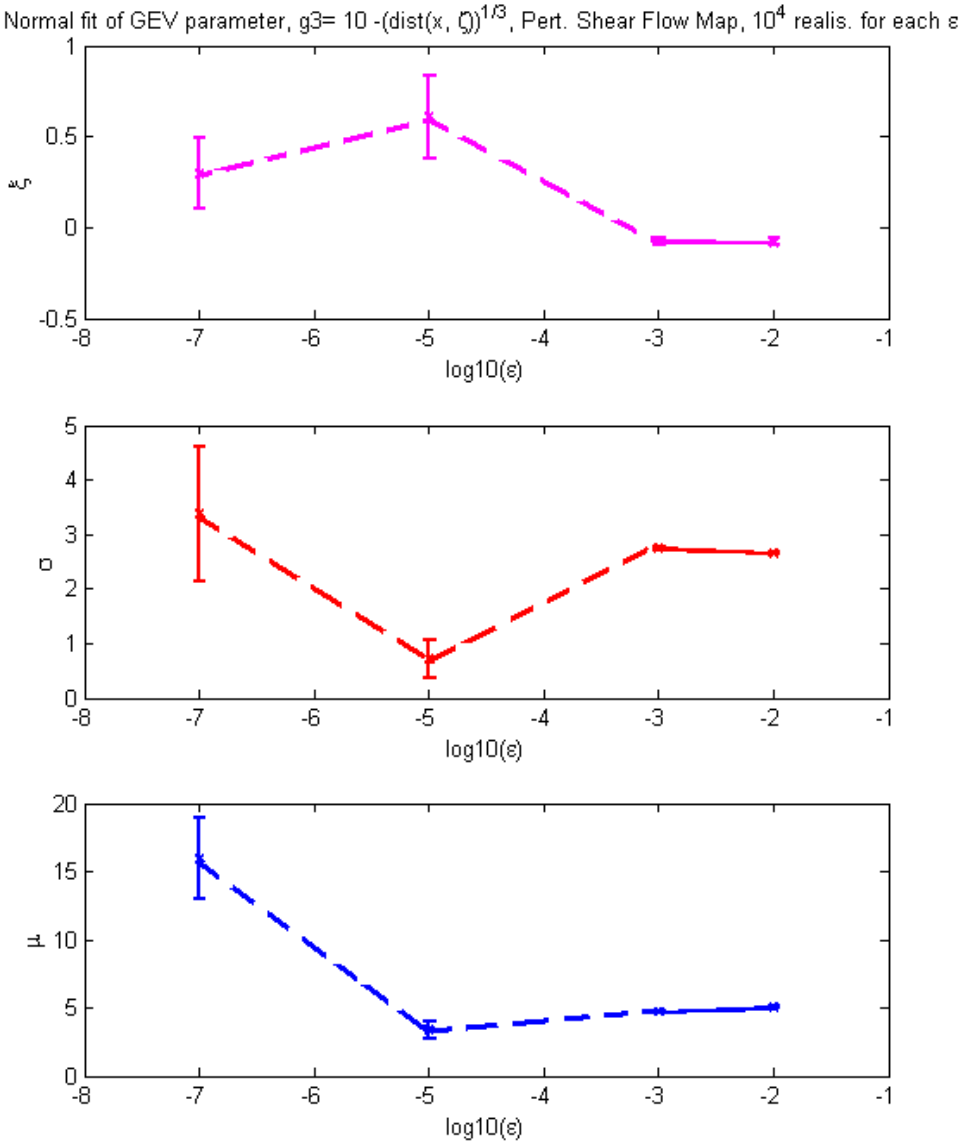

Figure 5.8: Normal fit mean and standard deviation of GEV parameter for 10^4 realisations of Shear Flow Perturbed Map VS (noise on x) VS ϵ; g_3 observable

5.3 Bernoulli Shift map

This map starts with an initial parameter and transforms it like all other discrete maps using the result as input of the next iteration:

$$x_{n+1} = qx_n \mod 1 \qquad q \in \mathbb{N} \tag{5.40}$$

$$x_{n+1} = q^n x_0 \mod 1 \qquad q \in \mathbb{N} \tag{5.41}$$

Despite its simplicity, this map owns three important characteristics of chaotic systems as. It is:

- **Area preserving**: guarantees the the preservation of phase-space volume as the system evolves through time (Louisville's theorem).
- **Bounded**: as it is the result of linear transformations.
- **Deterministic**: It is completely deterministic yet very sensitive to initial conditions.

The concept behind the Bernoulli shift can be better understood looking at a numeric representation of a shift map. The shift map considered in this chapter and used in the subsequent numerical investigations is defined by the equation:

$$x_{n+1} = 2x_n \mod 1 \tag{5.42}$$

This map is also called a shift map because the numbers can be easily manipulated when in binary form. Let us consider a seed number in the mapping represented in the form 0.1010010... To iterate the map we multiply by 2 that, in binary representation, is done by simply shifting all the numbers over to the left such that we get 1.011101... in the example above. To take the modulus we simply drop the integer part so we have 0.011101...

A random seed would have any possible complexity and this is what makes the map chaotic. The output is indistinguishable from noise even though the process is completely deterministic.

5.3.1 Orbit divergence

We derive some analytical results following again the pattern described in section 5.1.1.

- First we consider the unperturbed map:

$$\bar{x}_{n+1} = q^n(x_0 + \delta x_0) \tag{5.43}$$

$$\mathbb{D}x_{n+1} = \bar{x}_{n+1} - x_{n+1} \tag{5.44}$$

$$\mathbb{D}x_{n+1} = q^n \delta x_0 \tag{5.45}$$

  the divergence is proportional to q^n.

- If we introduce a deterministic perturbation η of the map (note that in this case the map is discontinuous):

$$\bar{x}_{n+1} = (q + \eta)^n(x_0 + \delta x_0) \tag{5.46}$$

  if $\eta \simeq \mathcal{O}(\delta x_0)$ then:

$$\mathbb{D}x_{n+1} = q^n \delta x_0 + \eta n q^{n-1} x_0 \tag{5.47}$$

  and again the important term is q^n

- In case of a stochastic perturbation:

$$\bar{x}_{n+1} = q^n x_0 + \sum_{j=1}^{n} q^j \xi_{n-j} \tag{5.48}$$

then:

$$\mathbb{D}x_{n+1} =< (x_{n+1} - < \bar{x}_{n+1} >)^2 >^{1/2} \tag{5.49}$$

$$\mathbb{D}x_{n+1} =< \sum_{j,l=1}^{n} q^j q^l < \xi_{n-l}\xi_{n-j} >^2 >^{1/2} \tag{5.50}$$

that is different from zero if $j = l$:

$$\mathbb{D}x_{n+1} = \sum_{j=1}^{n} q^{2j} \simeq \int_0^n q^{2x} dx \tag{5.51}$$

$$\mathbb{D}x_{n+1} \simeq \int_0^n \exp(2x \log q) dx \tag{5.52}$$

and eventually we obtain an exponential divergence:

$$\mathbb{D}x_{n+1} \simeq \frac{1}{2\log q} \exp(2n \log q) \tag{5.53}$$

5.3.2 Correlations decay

$$c_n = \int_0^1 \phi(q^n x)\psi(x) dx$$

Let us introduce a periodic observable $\phi(x) = \phi(x+1)$. Then, using Fourier theory, we rewrite our correlations:

$$c_n = \sum_{k,k'} \phi_k^* \phi_{k'} \int_0^1 e^{i2\pi kx} e^{i2\pi k q^n x} dx$$

it follows that $k = q^n k'$ is the condition to obtain $c_n \neq 0$. Since:

$$c_n = \phi_0 \phi_0^* + \sum_{k\neq 0} \phi_k \phi_k^* \int_0^1 e^{-i2\pi k q^n} dx$$

$$c_n = \phi_0 \phi_0^* + \sum_{k\neq 0} \phi_k \phi_k^* \frac{e^{i2\pi k q^n} - 1}{i2\pi k q^n}$$

if $|\phi_k| \leq C/|k|$ then:

$$C_\phi(n) = |c_n - \phi_0^2| \leq 2C^2 \sum_{k=1}^{\infty} \frac{\sin 2\pi k q^n}{2\pi k q^n}$$

The correlations decay is shown in figure 5.9 with $\phi(x) = \cos(2\pi x)$ then $\phi_{\pm 1} = 1/2$ and $\phi_k = 0$ otherwise. As stated in chapter 3, this function shows an exponential decay. A Monte Carlo integration is not suitable to obtain the same result since for $C_\phi(n) < 10^{-4}$ the method is unreliable and the noise overcame the signal.

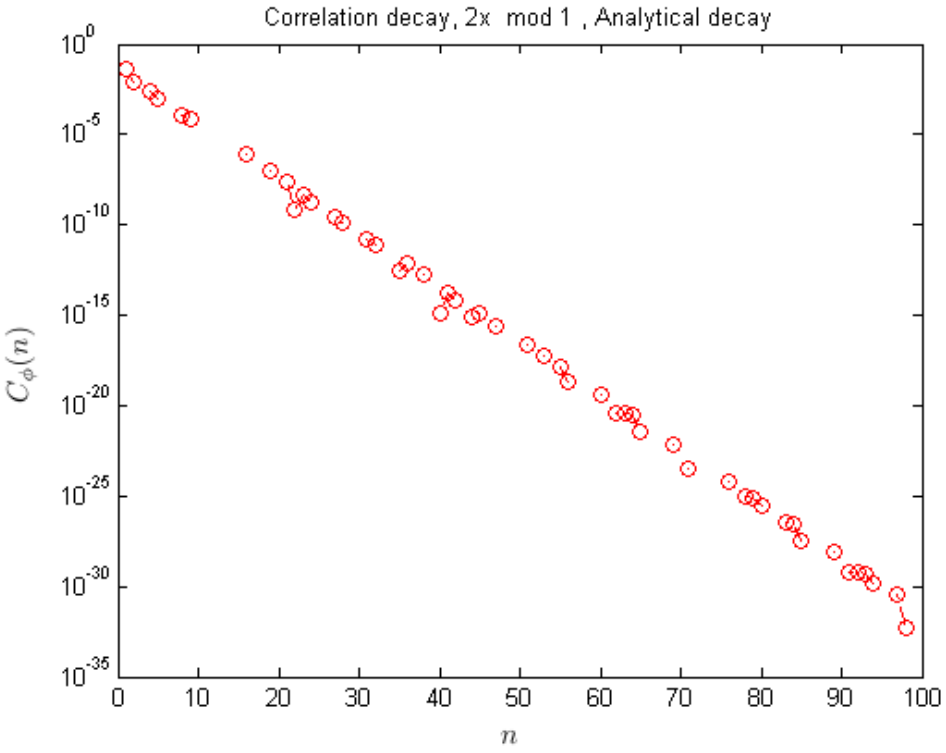

Figure 5.9: Correlation $C_\phi(n)$ for different ϵ, $2x$ mod 1 map

5.3.3 Fidelity decay

Let us analyse the perturbed version of the Bernoulli shift map:

$$x_{n+1} = qx_n + \epsilon \cdot \xi_n \mod 1 \tag{5.54}$$

where ϵ represents the noise amplitude of a stochastic perturbation, and $\xi \in [-1, 1]$ is a random variable with uniform distribution.
Therefore, following the procedure described for correlations decay, the Fidelity is:

$$F^{\epsilon}_{\phi,\psi}(n) = \int_0^1 \left(\int_{-1}^1 \cdots \int_{-1}^1 \phi\left(q^n x\right) \psi\left(q^n x + \epsilon \sum_{j=1}^{n} \xi_j q^{n-j} \right) \frac{d\xi_1}{2} \cdots \frac{d\xi_n}{2} \right) dx$$

Let $\phi(x+1) = \phi(x)$ be periodic of period 1. Using Fourier theory as in the decay of correlations:

$$F^{\epsilon}_{\phi,\phi}(n) = \phi_0^2 + \sum_{k\neq 0} |\phi_k|^2 \int_{-1}^1 \cdots \int_{-1}^1 e^{2\pi i k \epsilon \left(\sum_{j=1}^{n} \xi_j q^{n-j} \right)} \frac{d\xi_1}{2} \cdots \frac{d\xi_n}{2}$$

If we perform the integrals over noise, then:

$$F^{\epsilon}_{\phi,\phi}(n) = \phi_0^2 + \sum_{k\neq 0} |\phi_k|^2 \prod_{j=0}^{n-1} \frac{\sin(2\pi k \epsilon q^j)}{2\pi k \epsilon q^j}$$

As before, let us choose $\phi(x) = \cos(2\pi x)$ then $\phi_{\pm 1} = 1/2$ and $\phi_k = 0$ otherwise. Then:

$$F^{\epsilon}_{\phi,\phi}(n) = \frac{1}{2} \prod_{j=0}^{n-1} \frac{\sin(2\pi k \epsilon q^j)}{2\pi k \epsilon q^j} \tag{5.55}$$

The following relations hold:

$$\lim_{n\to\infty} F^{\epsilon}_{\phi,\phi}(n) = 0 \qquad F^{\epsilon}_{\phi,\phi}(0) = 1/2$$

In figure 5.10 it has been plotted the behaviour of $\delta F^{\epsilon}_{\phi,\phi}(n)$, with $\phi(x) = \cos(2\pi x)$, $q = 2$ and for different ϵ values. The analytical plots of equation 5.55 show an initial plateau of length $\bar{n} \simeq -\ln(\epsilon)$ then a super-exponential decay. The results are confirmed even with a Monte Carlo integration although if $\delta F^{\epsilon}_{\phi,\phi}(n) < 10^{-4}$ noise overcomes signal.

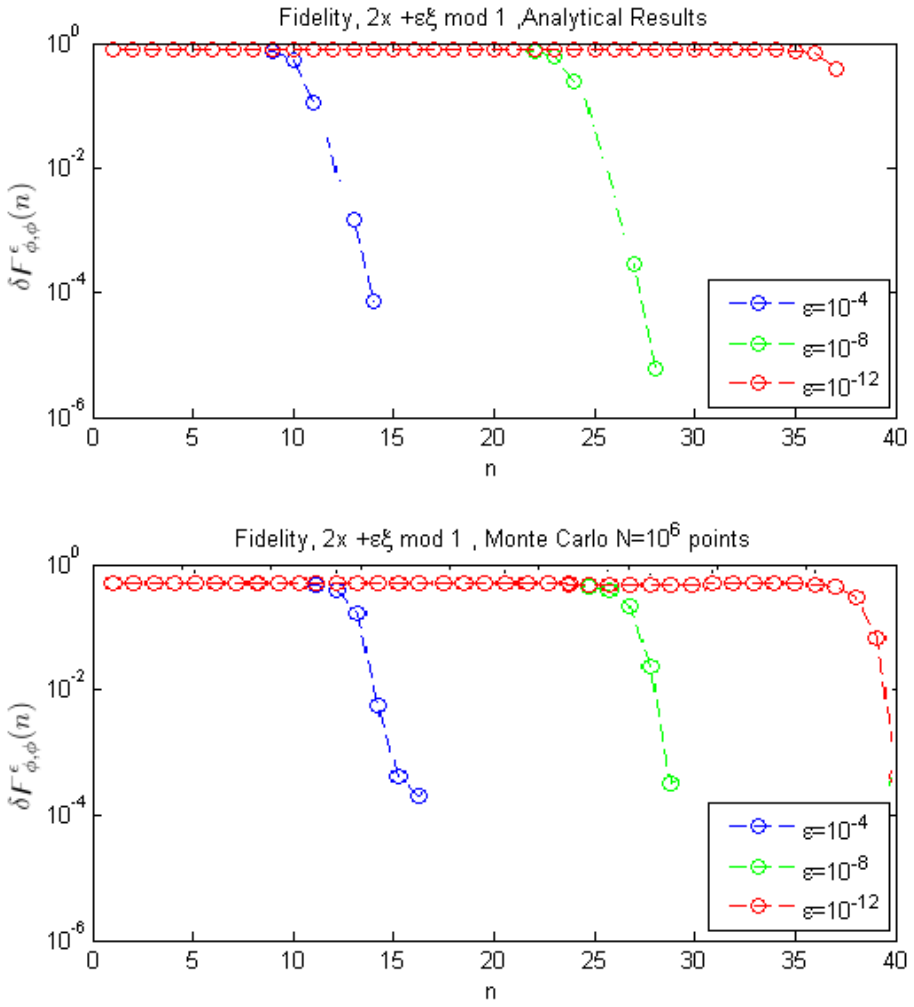

Figure 5.10: Fidelity for different ϵ, $2x$ mod 1 map

5.3.4 Return time Statistics

We have investigated Return time Statistics for the map $2x \mod 1$ even in the perturbed case. Since μ_ϵ is equal to the invariant measure used in the unperturbed case, we expect no difference in spectral decay. The Return time statistics is computed over $2.5 \cdot 10^5$ trajectories with initial point inside a segment ς of width 0.01 using equation:

$$\tilde{F}_\varsigma(t) = \mu_\varsigma \left(x \in \varsigma : \frac{\tau_\varsigma(x)}{\tau_\varsigma} \leq t \right) \tag{5.56}$$

where, if n is the n-th iteration of the map, $t = n \cdot \varsigma$. In figure 5.11 it is possible to observe the same exponential decay for all the ϵ values and no difference with deterministic case.

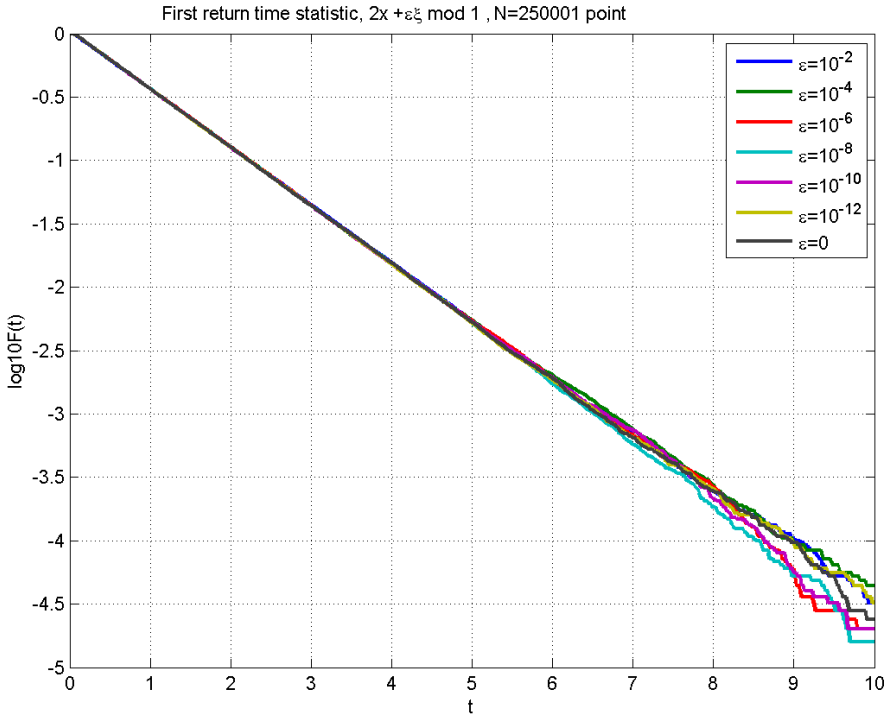

Figure 5.11: Recurrence Statistics for different ϵ, $2x$ mod 1 map

5.3.5 Extreme value distribution

As stated by the Freitas' Theorem in section 4.2.2, Bernoulli Shift Map is suitable to obtain a reliable fit of GEV distribution. For each different ϵ value, we have performed 10^4 realisations of the map in equation 5.54 with $q = 2$, starting from the same initial point $\zeta = 0.3 + \pi/10$. we have used the block of maxima approach in order to obtain a fit to GEV distribution using the following procedure: first we iterate the map for 10^8 steps. For each time step we compute the distance from the initial point as

$$\text{dist}(x_n, \zeta) = \min(|x_n - \zeta|, 1 - |x_n - \zeta|)$$

Then, once divided distance series in 10^4 bin each containing 10^4 iterations of the map, we compute the minimum distance for each bin and then calculate the observable functions g_1, g_2, g_3. Eventually we fit 10^4 g_i data to the GEV distribution using maximum likelihood estimation of parameters. The GEV parameters obtained show a normal distribution (KS test for normal distribution passed at confidence level 0.20). Since in this case, as said, μ_ϵ is equal to the invariant measure used in the unperturbed case we expect no difference in noise distribution for different ϵ value and almost the same expected value of the deterministic case. These results are presented in figures 5.12-5.14 where the deterministic values for the parameter ξ, σ, μ of the GEV distribution have been noted with a dotted black line while the colored bar delimits one standard deviation of the normal distribution fit for each ϵ value. Note that the uncertainty over deterministic parameter estimation is about two times greater than the standard deviation of normal fit. For small ϵ value it is possible to observe a perfect agreement between the deterministic and perturbed case. The standard deviation of normal fit, as expected, remains the same on the whole ϵ value interval . We encounter a small deviation from the determistic parameter value for $\epsilon \geq 10^{-4}$ while the standard deviation does not change magnitude. This behaviour is repeated for the three parameters and for all the observable functions. Since these deviations appear to be randomly directed for different observables and pa-

rameter we consider them as natural effects of increased amplitude of noise.

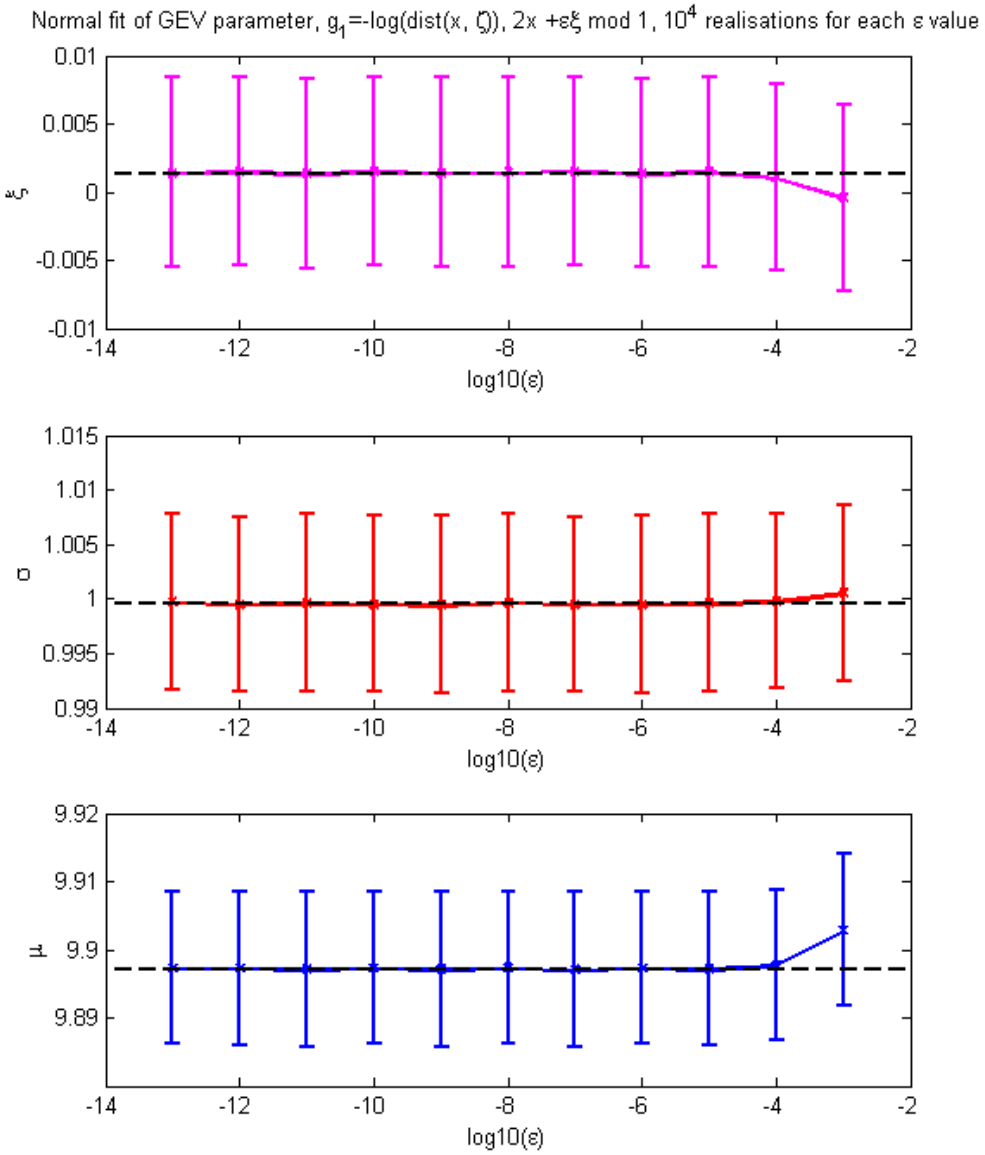

Figure 5.12: Normal fit mean and standard deviation of GEV parameter for 10^4 realisations of Bernoulli Shift Perturbed Map VS ϵ; g_1 observable

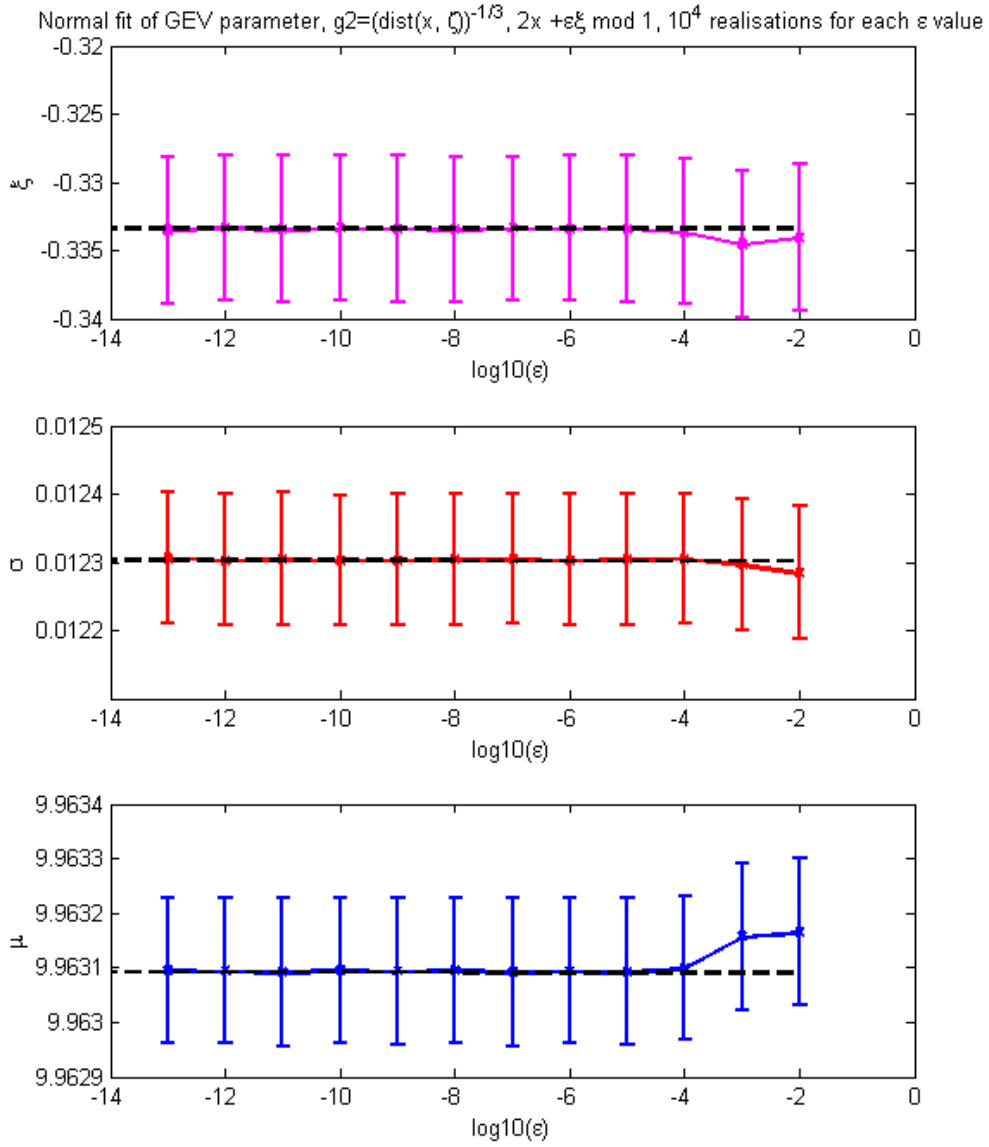

Figure 5.13: Normal fit mean and standard deviation of GEV parameter for 10^4 realisations of Bernoulli Shift Perturbed Map VS ϵ; g_2 observable

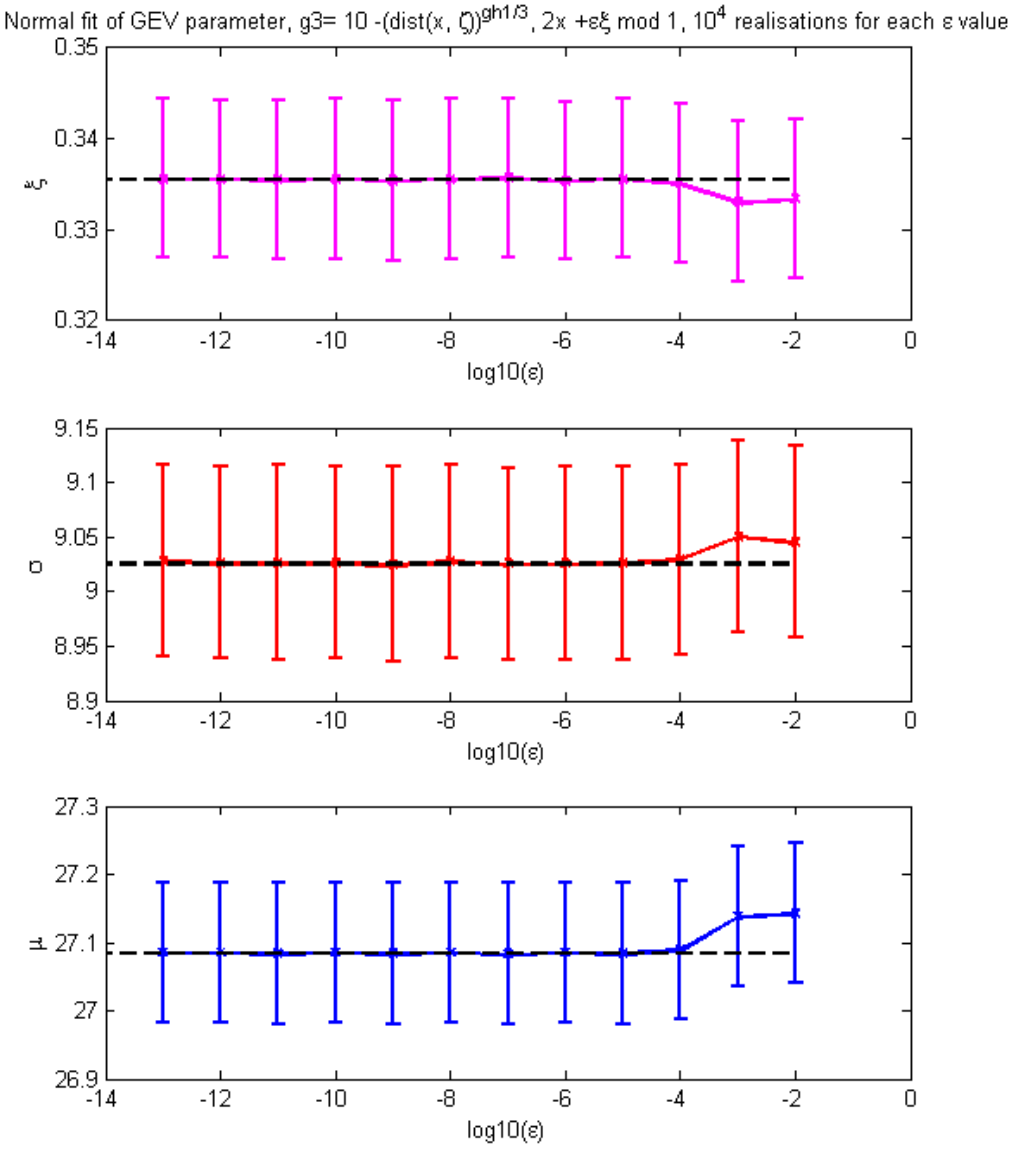

Figure 5.14: Normal fit mean and standard deviation of GEV parameter for 10^4 realisations of Bernoulli Shift Perturbed Map VS ϵ; g_3 observable

5.4 Arnold's cat Map

Arnold's cat map is a chaotic map from the torus into itself. It was named by Vladimir Arnold, who demonstrated its effects in the 1960s using an image of a cat [Arnold and Avez, 1968]. It is given by the transformation:

$$\begin{bmatrix} x_{n+1} \\ y_{n+1} \end{bmatrix} = \begin{bmatrix} 2 & 1 \\ 1 & 1 \end{bmatrix} \begin{bmatrix} x_n \\ y_n \end{bmatrix} \tag{5.57}$$

If we consider all the point of the bi-dimensional torus as an image, the effect of the map is to shear one unit to the right, then one unit up, and all that lies without that unit square is wrapped around on the other respective side to be within it. We can resume the main properties of Arnold's cat Map as follow:

- It is area-preserving since the determinant is 1.

- It is an hyperbolic map: its eigenvalues are real numbers, one greater and the other smaller than 1, so they are associated respectively to an expanding and a contracting eigenspace which are also the stable and unstable manifolds. The eigenspace are orthogonal because the matrix is symmetric.

- The Lyapunov characteristic exponents are given by

$$\begin{bmatrix} 1-\sigma & 1 \\ 1 & 2-\sigma \end{bmatrix} = \sigma^2 - 3\sigma + 1 = 0 \tag{5.58}$$

  so that:

$$\sigma_{\pm} = \frac{1}{2}(3 \pm \sqrt{5}) \tag{5.59}$$

- It is ergodic (equation 2.3) and strong mixing (equation 2.18).

5.4.1 Correlations and Fidelity decay

Since the map is strong mixing it presents an exponential decay of fidelity and correlation functions can be proved, see Casati et al. [1982] for some examples.
It is difficult to use Fourier Theory to prove analytically this results . We have tried to obtain numeric evidence using Monte Carlo method as described in the precedent case. Unfortunately, after few iterations, numerical noise overcomes signal and it is impossible to verify or estimate a trend.

5.4.2 Return time Statistics

Let us consider the following perturbed Arnold's cat map:

$$\begin{cases} x_{n+1} = 2x_n + y_n + \epsilon\xi_n & \mod 1 \\ y_{n+1} = x_n + y_n & \mod 1 \end{cases} \tag{5.60}$$

We have studied the Recurrence following the orbit of 10^4 points starting in a square centred in $x_c = 0.3, y_c = 0.6$ and $l_{side} = 0.01$. For each orbit the number of iterations that causes a return into the initial square have been registered. In this way we have constructed return time statistics that now are reported in figure 5.15. The time on x axis is normalized as: $t = n \cdot l_{side}^2$.

As seen for Bernoulli Shift map, Lebesgue measure is the same of stationary measure. For this reason we expect no difference in Return time spectrum even in the perturbed case. This is what we have verified numerically for various ϵ. There are no difference even with the deterministic case: the curve which represent $\epsilon = 0$ spectrum is superimposed to the others.

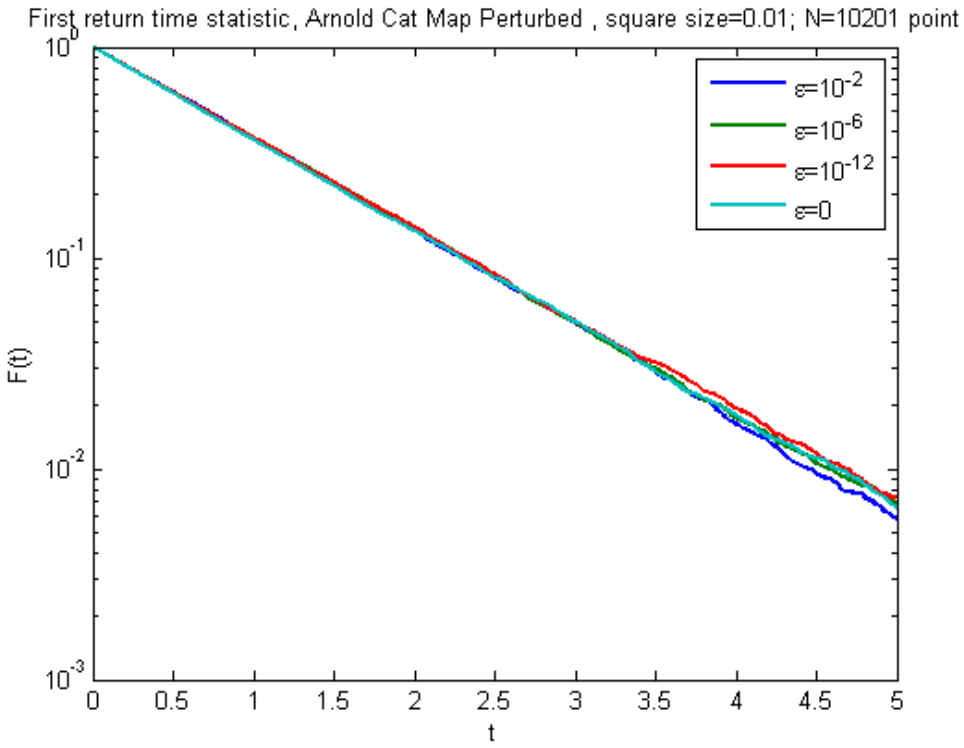

Figure 5.15: Recurrence Statistics for different ϵ, Arnold's cat Map map

5.4.3 Extreme value distribution

As well as Bernoulli Shift map, even Arnold's cat map is suitable to obtain a reliable fit of GEV distribution. We proceed as in the case of $2x \mod 1$ except for the distance which has been computed using the following equation:

$$d((x,y),(\zeta_x,\zeta_y)) = \sqrt{\min\{|x-\zeta_x|, 1-|x-\zeta_x|\}^2 + \min\{|y-\zeta_y|, 1-|y-\zeta_y|\}^2} \tag{5.61}$$

$\zeta_x = \zeta_y = 0.5$. Our results are presented in figures 5.16-5.18 where the deterministic values for the parameter ξ, σ, μ of the GEV distribution have been noted with a dotted black line while the coloured bar delimits one standard deviation of the normal distribution fit for each ϵ value. A perfect

agreement between the deterministic and perturbed case hold in this map even for noise of great amplitude.

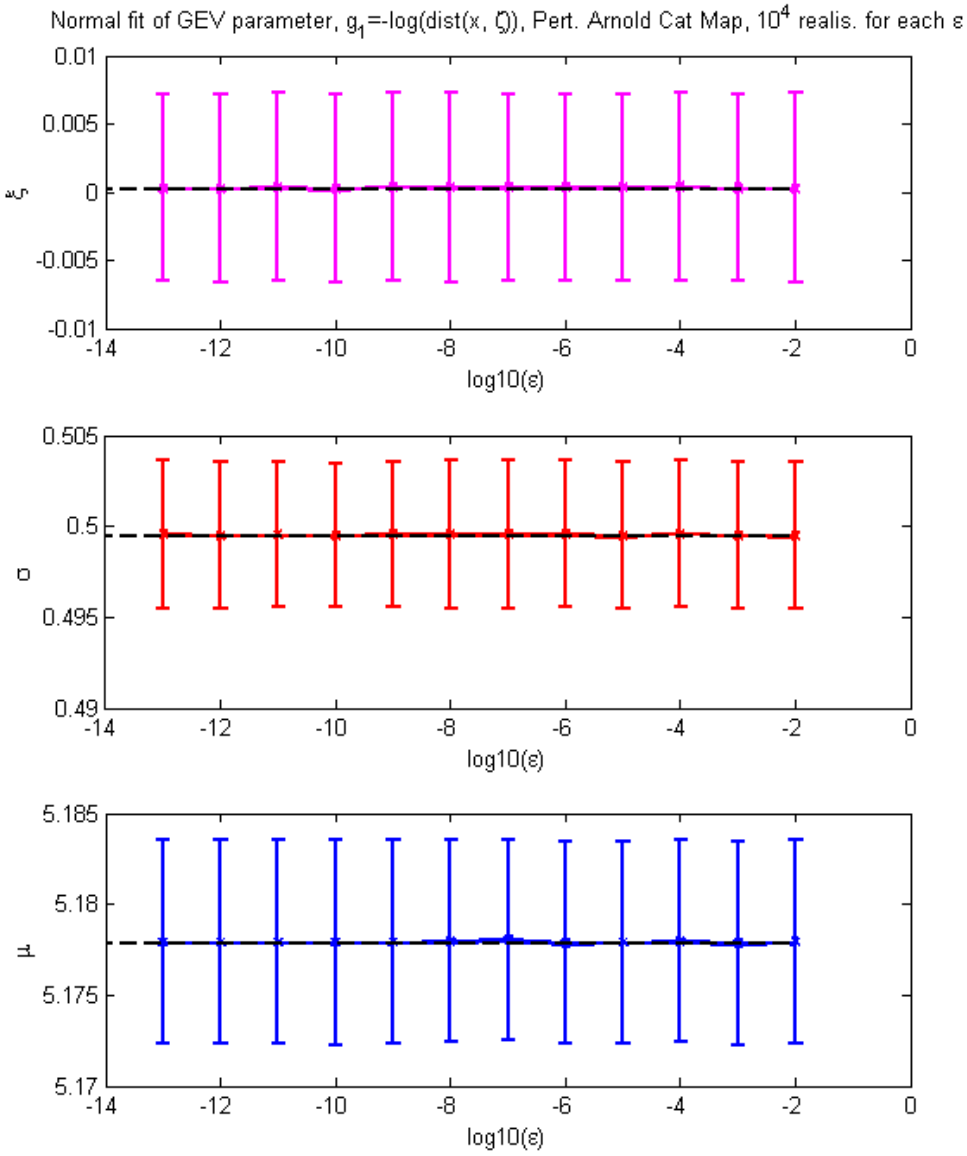

Figure 5.16: Normal fit mean and standard deviation of GEV parameter for 10^4 realisations of Perturbed Arnold's cat Map VS ϵ; g_1 observable

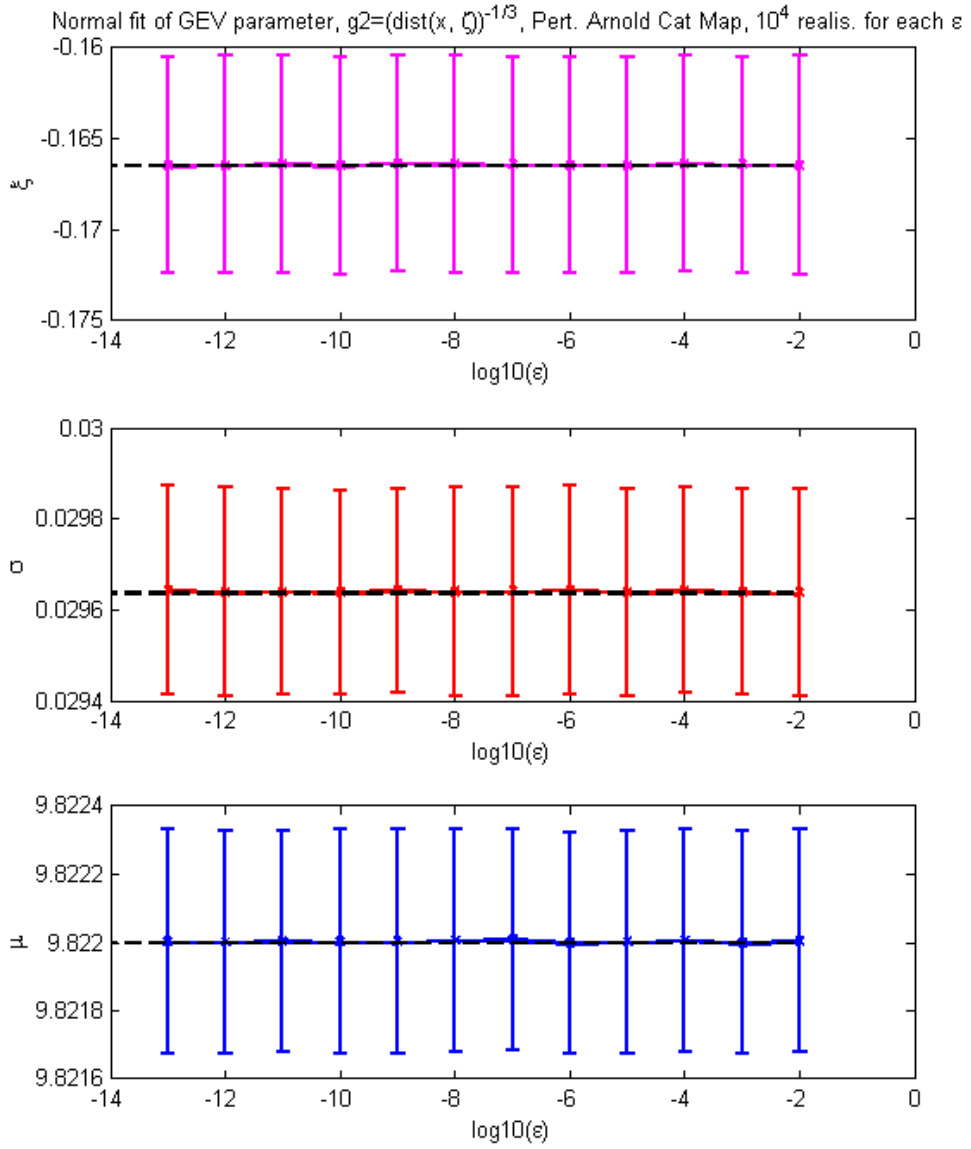

Figure 5.17: Normal fit mean and standard deviation of GEV parameter for 10^4 realisations of Perturbed Arnold's cat Map VS ϵ; g_2 observable

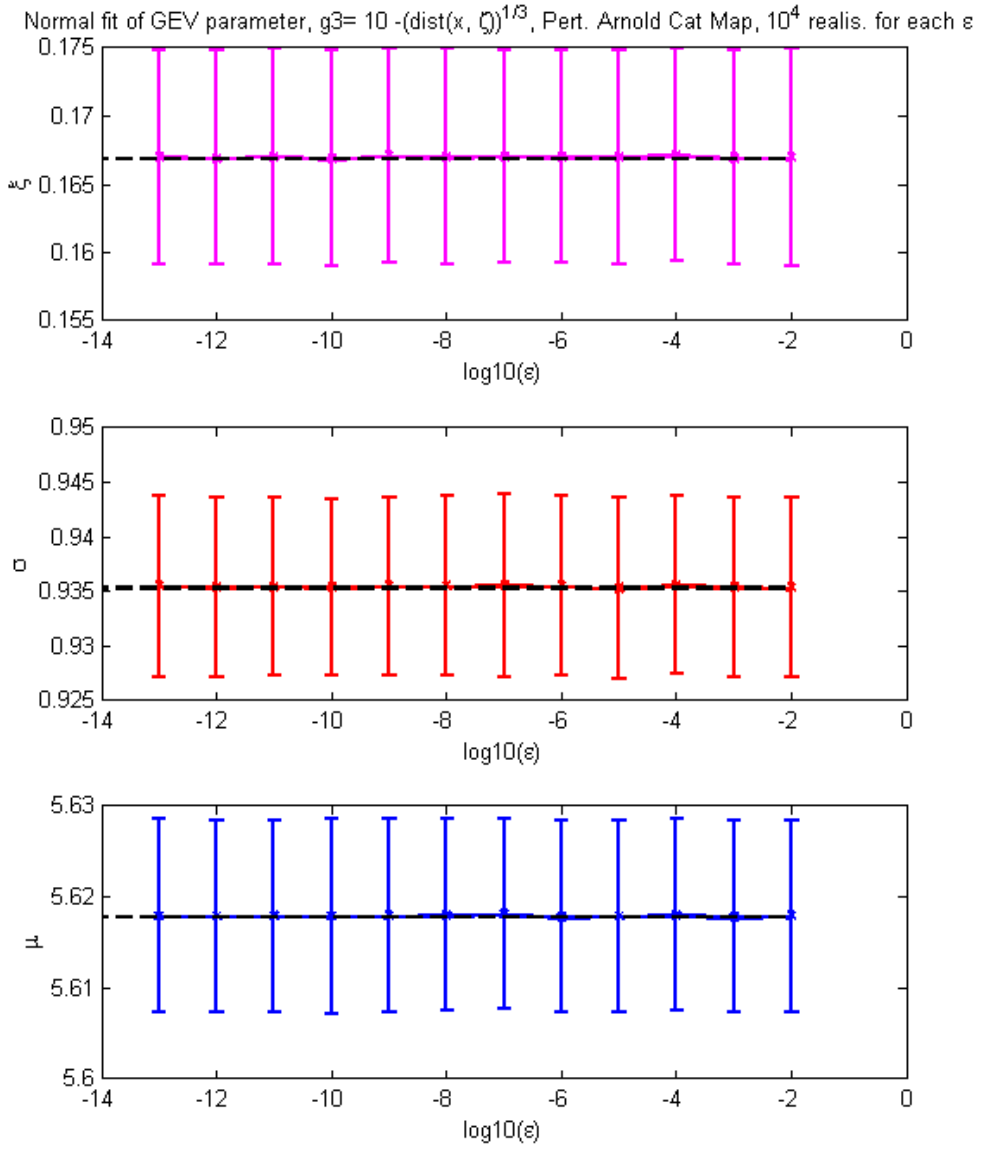

Figure 5.18: Normal fit mean and standard deviation of GEV parameter for 10^4 realisations of Perturbed Arnold's cat Map VS ϵ; g_3 observable

Chapter 6

Physical models

In this chapter we present different physical models which show appealing features such as resonances or exhibit a mixed behaviour with chaotic and regular regions.
It is interesting to investigate which dynamic indicators of stability are suitable to highlight main characteristics of this kind of maps or dynamical systems. In particular we put to the test new indicators strictly connected with Freitas' work: Kolmogorov-Smirnov fit parameter and fit confidence level for GEV distribution of observable functions, widely described in section 4.4.2. Quite surprisingly we discover that this parameter is a good indicator of stability as well as Reversibility Error.
In this chapter only maps with low dimensionality have been considered. This choice is justified by the great computational time required to carry out parametric scans and the number of iteration and bins required to obtain a good fit to GEV distribution.

6.1 Standard Map

The Standard map (also known as Chirikov-Taylor map or Chirikov standard map) is an area-preserving chaotic map from a square with side 1 onto itself. It can be thought as a stick that is free of the gravitational force,

which can rotate frictionless in a plane around an axis located in one of its tips, and which is periodically kicked on the other tip. This mechanical system is usually called a kicked rotator. It is defined by:

$$\begin{cases} y_{n+1} = y_n - \frac{K}{2\pi}\sin(2\pi x) & \mod 1 \\ x_{n+1} = x_n + y_n + 1 & \mod 1 \end{cases} \tag{6.1}$$

Standard map is one of the most widely-studied examples of dynamical chaos in physics. It can be regular or chaotic, depending on the strength of the impulses: stronger kicks lead to chaotic behaviours. The variables y_n and x_n respectively represent the angular position and angular momentum of the stick at the n-th kick. K measures the intensity of the kicks. For $K < 0.971635$ the variation of momentum y is bounded. Which type of orbit is observed depends on the map's initial conditions [Lichtenberg and Lieberman, 1983]. Nonlinearity of the map increases with K, and with it the possibility to observe chaotic dynamics for appropriate initial conditions. The map in equation 6.1 describes a situation present in different physical phenomena. Due to this property various dynamical systems and maps can be locally reduced to the standard map. As example we cite:

- Charged particle confinement in magnetic traps [Chirikov, 1969].
- Particle dynamics in accelerators [Izraelev, 1980].
- Comet dynamics in solar system (a similar map is found for the comet Halley) [Chirikov and Vecheslavov, 1989].

and due to this reason the term standard map was coined by Chirikov [1969].

6.1.1 Stability indicators and Standard Map

In this section we present the results obtained using different indicators in order to show standard map characteristics with different K values. We found that it is possible to depict the map using the stability indicators

presented in previous chapters.
The Reversibility Error at the n-th iteration with n=1000 and the Kolmogorov Smirnov fit parameter have been computed and they are represented respectively in figure 6.1 for K=2 parameter and in figure 6.2 for K=3. The GEV fit has been done considering $2 \cdot 10^3$ bin each containing $1 \cdot 10^3$ iteration of the map. The distance is computed as in equation 5.61. The points unable to be fitted have been excluded by this analysis. Furthermore, the original image obtained using fitted data shows a noisy behaviour like a picture underexposed. To highlight the behaviour of the map, then, it has been applied a Gaussian convolution filter to the image obtained by GEV D fit parameter data. Then, for every pixel of the image it was taken the sum of products. Each product is the value of the current pixel or a neighbour of it, with the corresponding value of the kernel filter matrix that in our case is:

$$\begin{pmatrix} 1/11 & 1/11 & 1/11 \\ 1/11 & 3/11 & 1/11 \\ 1/11 & 1/11 & 1/11 \end{pmatrix} \tag{6.2}$$

Considering Reversibility Error we note that the regions of regular motion are characterized by lower values of Δ_n while the chaotic sea shows higher values. The structure of the map is exactly reproduced as you can see comparing with Chirikov and Shepelyansky [2008]. The same patterns can be found using GEV KS parameter in the successfully fitted regions: in this case the regular region show high D parameter since the KS test is not accomplished by data.
When $K = 2$ intermediate values of both Reversibility Error and KS parameter are found at the border of central island while the highest values of Δ_n match the lower ones of D.
$K = 3$ plots in figure 6.2 show the agreement between the two indicators especially in finding the islands of regular motion at the border and around the centre of the figure.

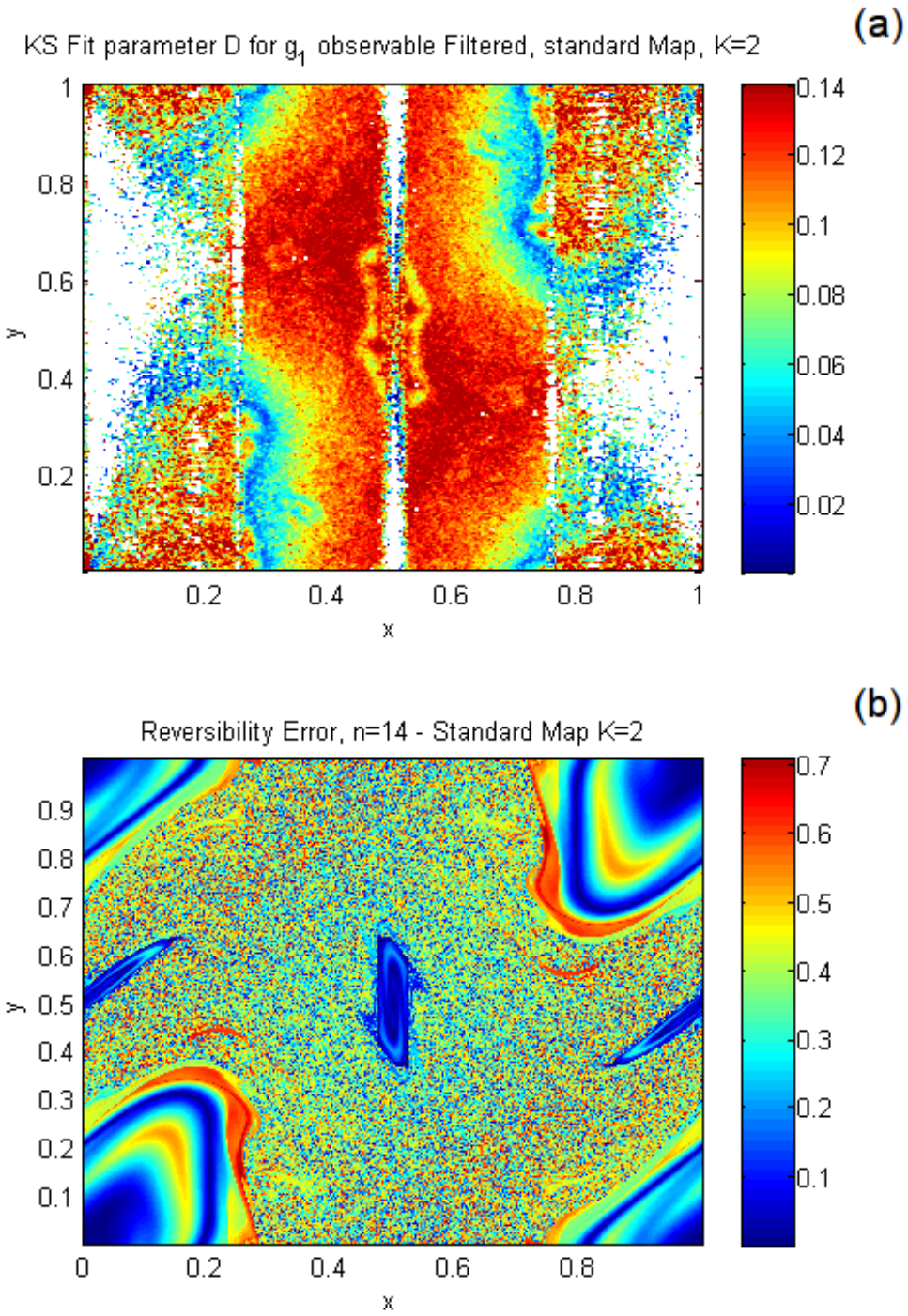

Figure 6.1: Filtered Kolomogorov Smirnov Fit Parameter D (a) and Reversibility Error Δ_n (b), Standard Map, $K = 2$.

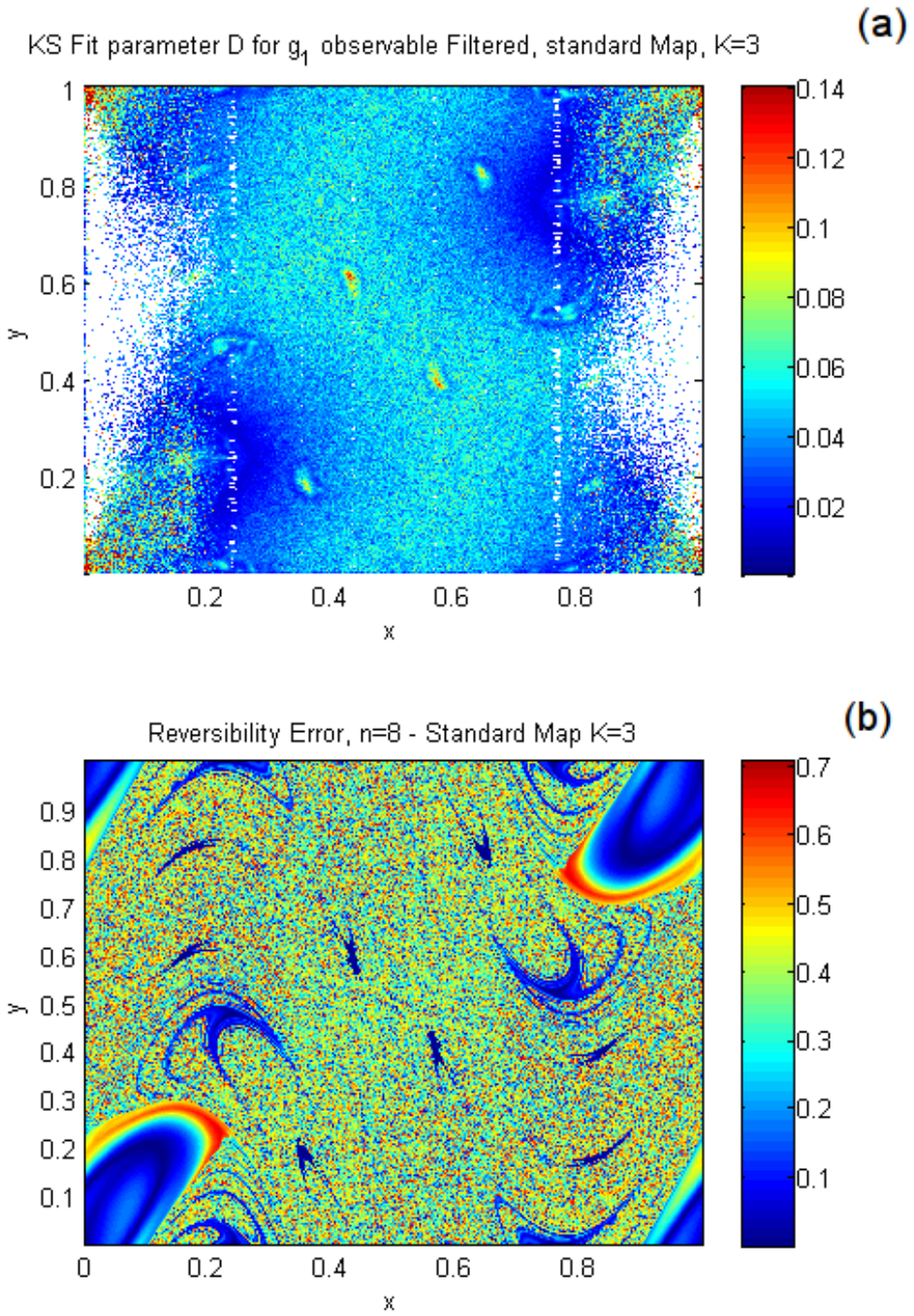

Figure 6.2: Filtered Kolomogorov Smirnov Fit Parameter D (a) and Reversibility Error Δ_n (b), Standard Map, $K = 3$.

6.2 Hill's equation - Parametric Resonance

We now prove our indicators of stability in systems which exhibit parametric resonance briefly recalling the theoretical framework beyond this systems. For a detailed treatment see Turchetti [1998] and Verhulst [2009].

Let us consider the equation:

$$\dot{x} = Ax + \eta B(t)x \tag{6.3}$$

in which $x \in \mathbb{R}^m$, A is a constant m x m-matrix, $B(t)$ is continuous and T periodic m x m-matrix and ϵ is a small parameter. Floquet Theory tells how it is possible to write solutions of equation 6.3:

$$x(t) = \Phi(t, \eta)e^{C(\eta)t} \tag{6.4}$$

with $\Phi(t, \eta)$ a T-periodic m x m-matrix and $C(\epsilon)$ as a constant m x m-matrix. It is the determination of $C(\epsilon)$ which provides us stability behaviour of the solutions.
As particular case of equation 6.3 let us introduce the following equation called Hill's equation:

$$\ddot{x} + (\omega + \eta f(t))x = 0 \tag{6.5}$$

in this case we have no dissipation then it can be useful to introduce canonical transformations such as:

$$\dot{x} = y \qquad \dot{y} = -\frac{\partial H}{\partial x}$$

with Hamiltonian function:

$$\mathcal{H}(x, y, t) = \frac{1}{2}y^2 + \frac{1}{2}(\omega + \eta f(t))x^2 \tag{6.6}$$

A typical problem to study is for which values of ω and η in (ω, η) parameter space the trivial solution $\dot{x} = y = 0$ is stable. Solutions of Hill's equation

can be written in the Floquet form with $\Phi(t,\eta)$ π-periodic. The eigenvalues λ_1, λ_2 of C are ϵ dependent and are called characteristic exponents. Furthermore, we know that:

$$\sum_{i=1}^{n} \lambda_i = \frac{1}{T}\int_0^T Tr(A + \eta B(t))dt \tag{6.7}$$

This leads to:

$$\lambda_1(\epsilon) + \lambda_2(\epsilon) = 0$$

The characteristic exponents, which are complex conjugate, are purely imaginary or real:

- If $\omega^2 \neq n^2, n = 1, 2 \Longrightarrow \lambda_1, \lambda_2 \in \mathbb{C}$ so that $x = 0$ is stable near $\epsilon = 0$.
- If $\omega^2 = n^2$ for some $n \in N \Longrightarrow \lambda_1, \lambda_2 \in \mathbb{R}$ since we can include the imaginary part in $\Phi(t,\eta)$

Assuming $\omega^2 = n^2$ for some $n \in N$ we look for periodic solutions of Hill's equation 6.5 and this solutions define the boundaries between stable and unstable solutions in parametric space. putting:

$$\omega^2 = n^2 - \eta\beta \tag{6.8}$$

with β constant. Applying Poincaré-Lindstedt method to find the solution we find periodic solutions for n=1 if:

$$\omega^2 = 1 \pm \frac{1}{2}\eta + \mathcal{O}(\eta^2) \tag{6.9}$$

for $n = 2$ if:

$$\omega^2 = 4 - \frac{1}{48}\eta^2 + \mathcal{O}(\eta^4)$$

$$\omega^2 = 4 + \frac{5}{48}\eta^2 - \mathcal{O}(\eta^4)$$

the corresponding instability domain called Floquet tongues are shown in figure 6.3

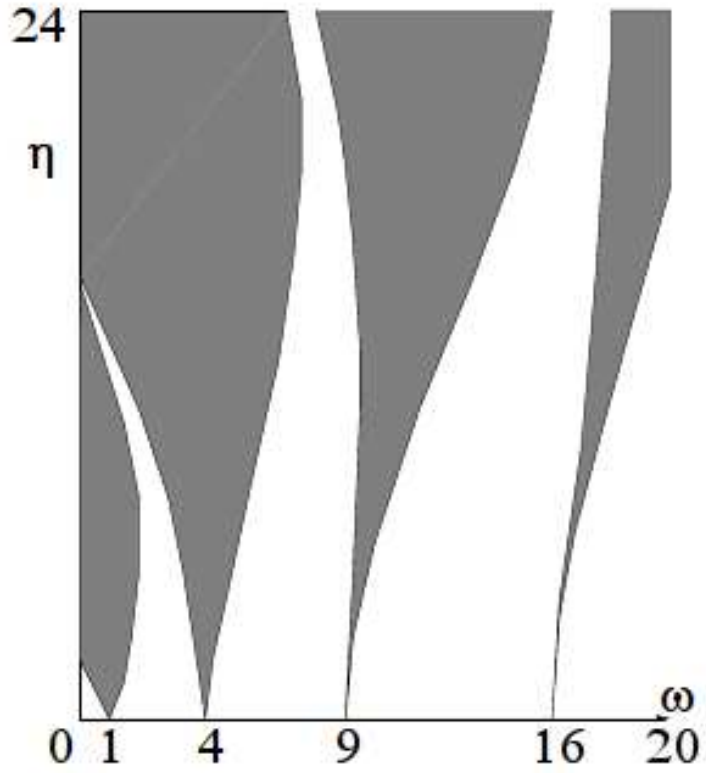

Figure 6.3: Tongues of parametric resonance in parametric space (ω, η). After [Verhulst, 2009]

As a case of study we have analysed a system showing this kind of parametric resonance but similar in structure to a shear-flow forced periodically:

$$\mathcal{H} = \omega j(1 + \epsilon \cos^2 \phi(t)) \tag{6.10}$$

that is the Hamiltonian in equation 6.6 if $f(t) = \cos^2(\phi(t))$, $x^2/2 = j$ and $\eta/\omega^2 = \epsilon$.

This Hamiltonian corresponds to the following system of equation:

$$\begin{cases} \dot{\phi} &= \omega(1 + \epsilon \cos^2 \phi(t)) \\ \dot{j} &= \epsilon\omega j \sin 2\phi(t) \end{cases} \tag{6.11}$$

discretized as:

$$\begin{cases} \phi_{n+1} &= \phi_n + \omega(1 + \epsilon \cos^2 \phi_n) \\ j_{n+1} &= j_n + \epsilon\omega j \sin 2\phi_n \end{cases} \tag{6.12}$$

Whit this structure we expect to find numerical evidence of parametric resonance.
In figures 6.4 and 6.5 we use respectively the Kolomogorov-Smirnov Fit parameter D and the confidence level of fit to Extreme Value Distribution to depict the parametric space in both logarithmic and linear scale. For each pair of (ϵ, ω) the GEV fit has been done over $2 \cdot 10^3$ bins each of containing $1.5 \cdot 10^4$ map iterations. Tongues of parametric resonance are well highlighted using parameter of GEV distribution and represent instability regions of parametric space.

Studying standard map behaviour we have found that fit confidence interval is unreliable to highlight stability features of the map for the presence of embedded islands of stability in unstable regions and *vice versa*.
Working with Hill's equation confidence level seems a good indicator of stability since there is a clear division among different stability regions. The same results is achieved using Reversibility error as represented in figure 6.6. As for the standard map, in this case the regions with higher reversibility error value individuate instability behaviour.

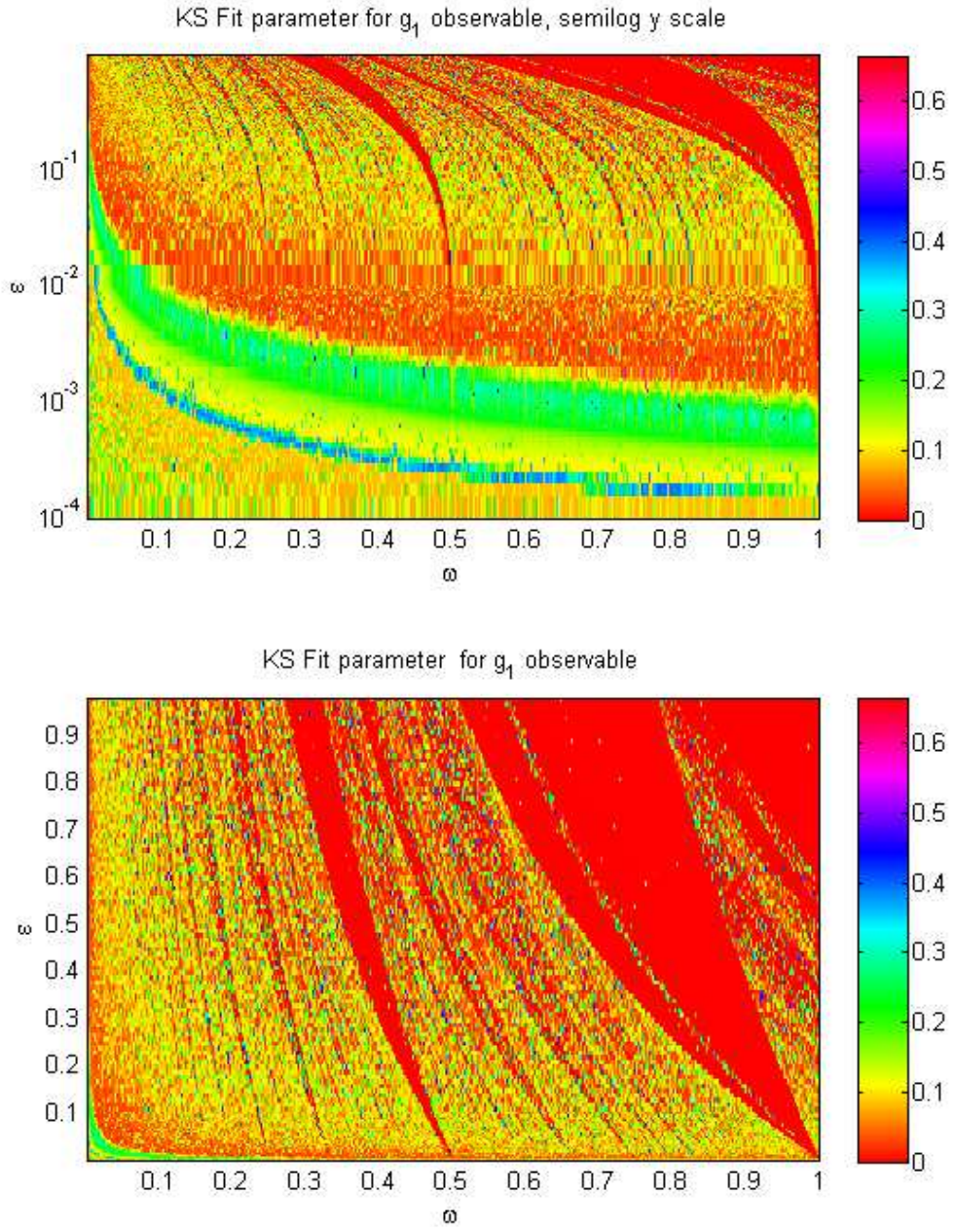

Figure 6.4: Tongues of parametric resonance highlighted using Kolmogorov Smirnov Fit Parameter for GEV distribution, Hill's equation, number of bins: $2 \cdot 10^3$, length of each bin: $1.5 \cdot 10^4$, g_1 observable.

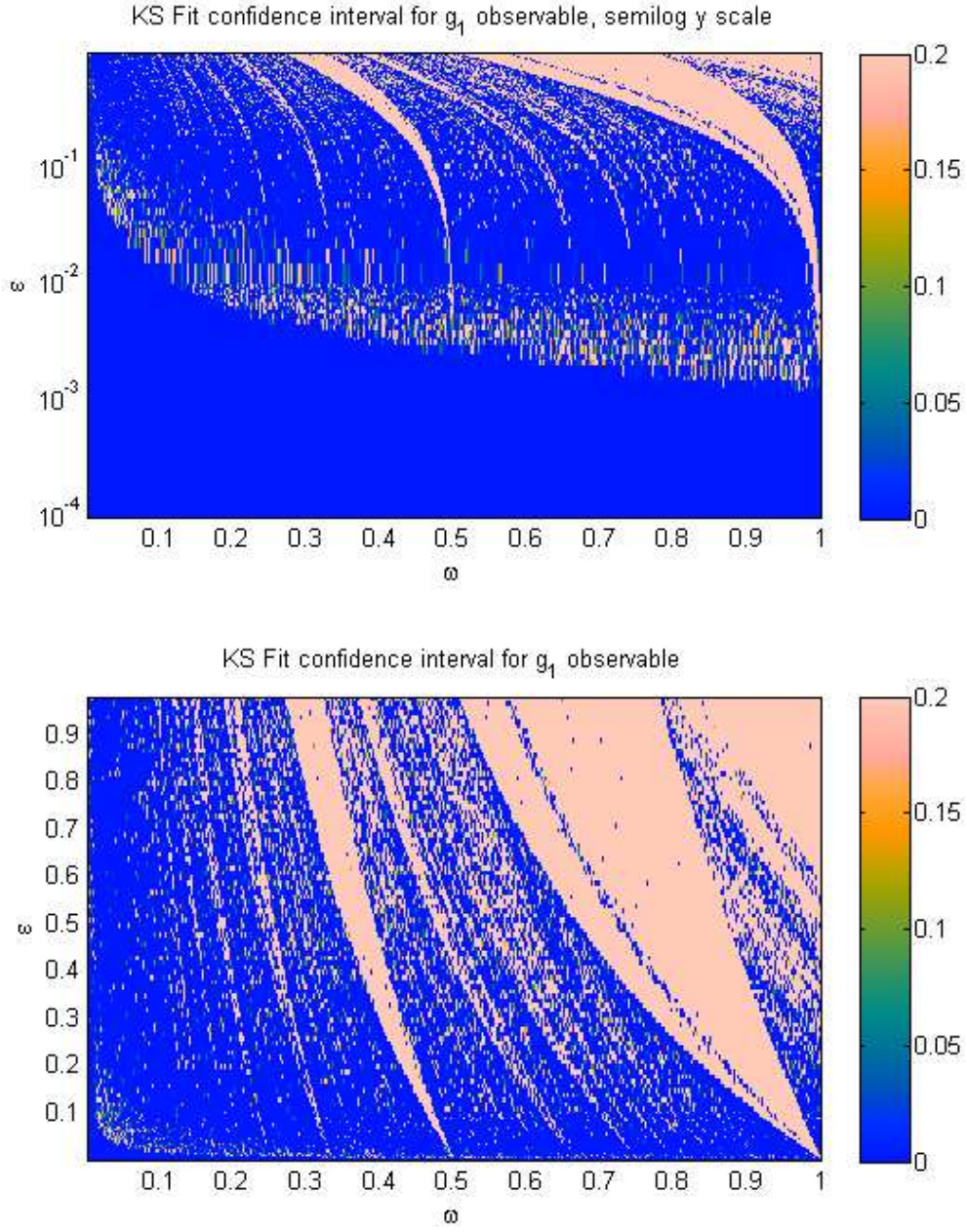

Figure 6.5: Tongues of parametric resonance highlighted using Kolmogorov Smirnov Fit Confidence level for GEV distribution, Hill's equation, number of bins: $2 \cdot 10^3$, length of each bin: $1.5 \cdot 10^4$, g_1 observable.

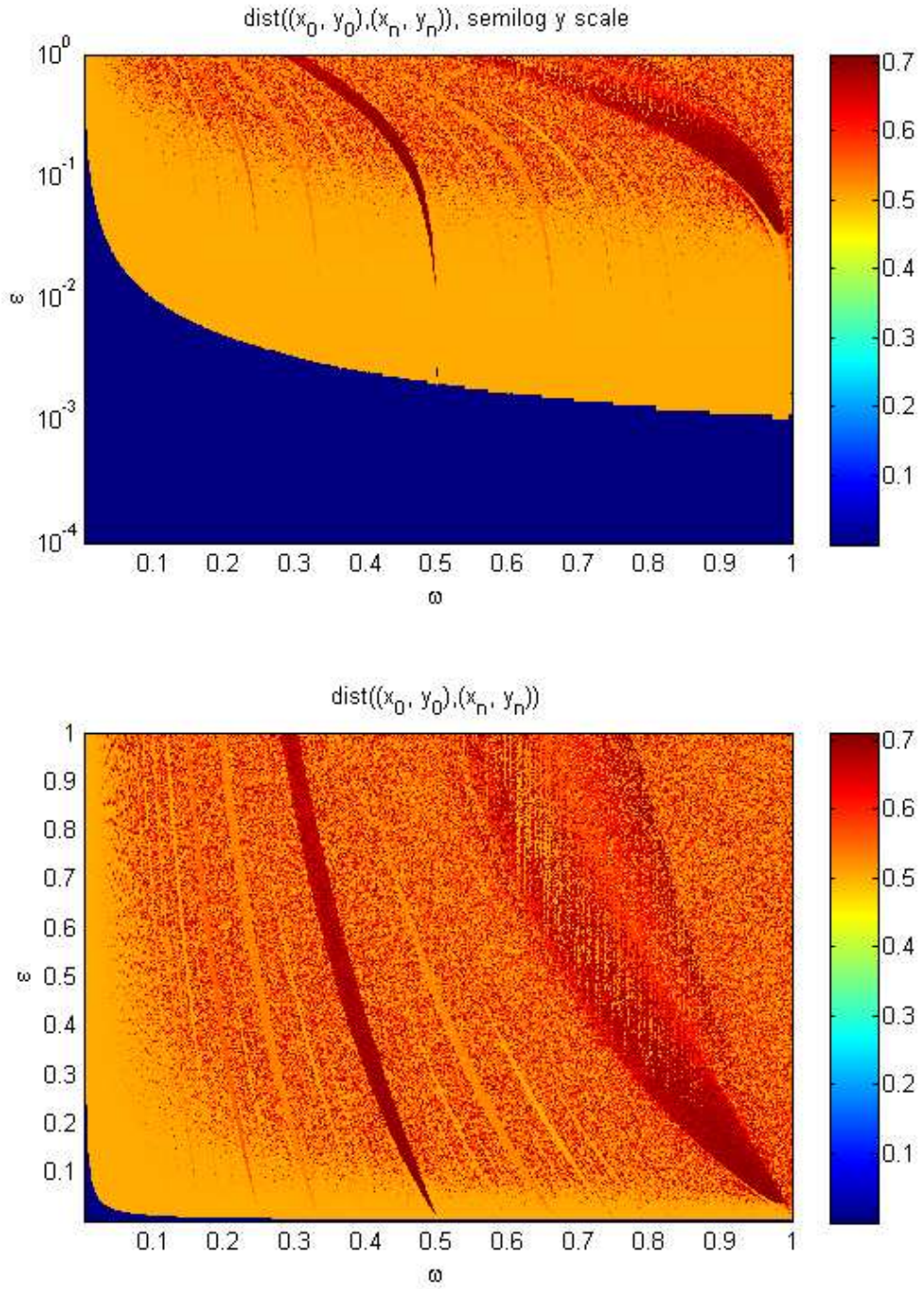

Figure 6.6: Tongues of parametric resonance highlighted using Reversibility Error with $n = 1000$, Hill's equation.

6.3 Hénon Map

The Hénon map is one of the most studied examples of dynamical systems that exhibit chaotic behaviour. The map was constructed by Hénon attempting to modify every point of an oval stretching its form : to accomplish this task the map takes a point (x_n, y_n) in the plane and maps it to a new point:

$$\begin{cases} x_{n+1} &= y_n + 1 - ax_n^2 \\ y_{n+1} &= bx_n \end{cases} \tag{6.13}$$

a and b are two parameters, which for the canonical Hénon map have values of $a = 1.4$ and $b = 0.3$. For the canonical values the Hénon map is chaotic. For other parameter values the map assumes different behaviours: it may be chaotic, intermittent, or converge to a periodic orbit.

The map was introduced by Michel Hénon as a simplified model of the Poincaré section of the Lorenz model. For the canonical map, an initial point of the plane will either approach a set of points known as the Hénon strange attractor, or diverge to infinity. The Hénon attractor is a fractal, smooth in one direction and a Cantor set in another. Numerical estimates yield a correlation dimension of 1.42 ± 0.02[1] and a Hausdorff dimension of 1.261 ± 0.003[2] for the attractor of the canonical map.

Its shape changes drastically as a and b do. In general, suppose we fix a and increase b from 0 on up. For b=0 the Hénon map smashes everything down onto the parabola $y = 1 - ax^2$, and the map on that parabola is essentially the 1D map associated to it. For small non-zero values of b it is known that there is an attractor. As b is raised, a certain critical value will be passed after which a horseshoe appears and the non-wandering set is described by all two-sided binary strings. For $a = 1.4$ this critical value is just above 1.3. In between 0 and the critical value just about nothing is known rigorously. We present our analysis for a=0.2, b=0.9991 and apply our indicators of stability to investigate the behaviour of the map.

Considering Reversibility Error in figure 6.7 we note that the regions of

regular motion are characterized by lower values of Δ_n while values $\Delta_n > 10^2$ have been filled with azure colour . The structure of the attractor is well reproduced with this indicator while the same result can not be achieved using GEV fit parameters: in this case, depending on initial conditions we fall into different situations:

1. The distribution of maxima is a Dirac delta: the value corresponds to the distance between initial point and stable point.

2. The distribution of maxima cannot be calculate because the distance diverges quickly.

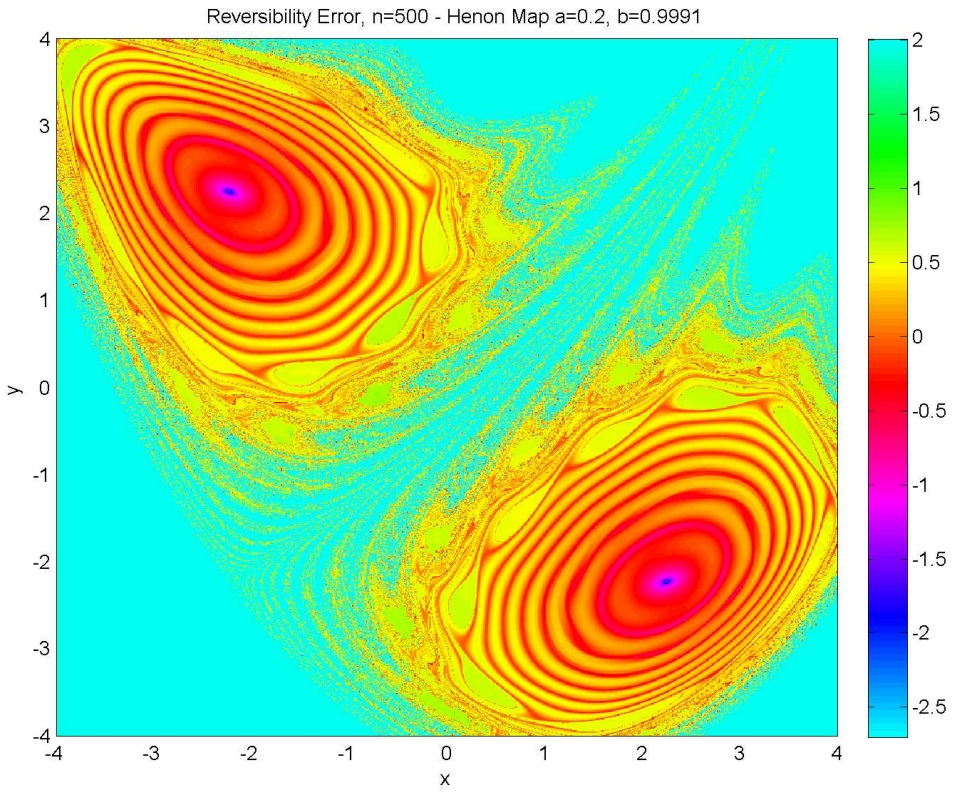

Figure 6.7: Reversibility Error, Henon Map, a=0.2, b=0.9991, n=500

Conclusions

This work of thesis has pointed out the utility of dynamical stability indicators in recognize and highlight properties of discrete maps as well as continuous dynamical systems.
Starting from the intuitive orbit divergence that is quick (exponential) in chaotic or mixing systems, while is not present or follows a power decay in regular maps, we have analysed the role of many indicators:
For Correlation functions we have verified a power law decay in regular map and an exponential decay in chaotic maps. A different behaviour is achieved looking at Fidelity decay: this indicator presents exponential decay in mixing systems and over-exponential decay in regular perturbed maps. All these results have been verified with numerical simulations performed using Monte Carlo methods or directly computing analytical results .

Following the work of Freitas we have proved the validity of their theorem in the stochastic perturbed case. We have also verified empirically that we are able to use Generalized Extreme Value distribution rather than one parameter Extreme Value distribution by substituting normalizing sequences a_n and b_n respectively with μ and $1/\sigma$.
For mixing maps such Arnold's Cat map and Bernoulli Shift map in which the stationary measure μ_ϵ is equal to the Lebesgue measure μ_{LEB}. Considering a perturbed version of Skew Map, that shows a Recurrence Time Spectrum exponential decay only if ϵ, the noise strength, is greater than 10^{-3}, we have observed unreliable fits for small value of ϵ. Increasing noise

strength, Kolmogorov-Smirnov test succeeds and we obtain significant parameters distribution values.

In some physical systems we have proved Kolmogorov-Smirnov fit parameter as indicator of dynamic stability: when it is small, the fit succeeds telling us that we are in a mixing region of our space. On the other hand if the fit is bad, KS parameter increases and the region considered is not mixing.
This indicator has been verified on maps such as Standard Map and Hill's Equation both with Reversibility Error. We satisfactorily find a good agreement between these two indicators.

This wide knowledge of dynamical indicators allow us to plan the study of more involved systems. To enhance our understanding of climate system and weather forecasts we can imagine to use Extreme Value Theory as indicator of stability in a contest in which it is rather meaningful: extreme temperature, large precipitation amount, powerful thunderstorms, high greenhouse gases concentrations are examples that may be interesting to study. We may also try to improve quality forecast by knowing what situations can cause instability: indicators like fidelity or reversibility error may accompany ensamble predictions that are now widely used to ensure and evaluate quality forecast.

In these theoretical and numerical studies we have tried to add a brick to the bearing wall of dynamical systems theory hoping that this work will be followed by further applications especially in geophysical systems.

Bibliography

M. Abadi and A. Galves. Inequalities for the occurrence times of rare events in mixing processes. The state of the art. *Markov Process. Related Fields*, 7(1):97–112, 2001.

E.G. Altmann, S. Hallerberg, and H. Kantz. Reactions to extreme events: Moving threshold model. *Physica A: Statistical Mechanics and its Applications*, 364:435–444, 2006.

V.I. Arnold and A. Avez. *Ergodic problems of classical mechanics*. Benjamin New York, 1968.

R. Artuso. Correlation decay and return time statistics. *Physica D: Nonlinear Phenomena*, 131(1-4):68–77, 1999.

V. Baladi. Decay of correlations. In *Smooth Ergodic Theory and Its Applications: Proceedings of the AMS Summer Research Institute on Smooth Ergodic Theory and Its Applications, July 26-August 13, 1999, University of Washington, Seattle*, volume 69, page 297. Amer Mathematical Society, 1999.

J. Barrow-Green. *Poincaré and the three body problem*. Amer Mathematical Society, 1997.

G. Benenti, G. Casati, and G. Veble. Stability of classical chaotic motion under a system's perturbations. *Physical Review E*, 67(5):55202, 2003.

E. Brodin and C. Kluppelberg. Extreme Value Theory in Finance. *Submitted for publication: Center for Mathematical Sciences, Munich University of Technology*, 2006.

R. Brun, F. Rademakers, et al. ROOT-An object oriented data analysis framework. *Nuclear Instruments and Methods in Physics Research-Section A Only*, 389(1):81–86, 1997.

N. Buric, A. Rampioni, and G. Turchetti. Statistics of Poincaré recurrences for a class of smooth circle maps. *Chaos, Solitons & Fractals*, 23(5):1829–1840, 2005.

G. Casati, G. Comparin, and I. Guarneri. Decay of correlations in certain hyperbolic systems. *Physical Review A*, 26(1):717–719, 1982.

N. Chernov. Decay of correlations. *Scholarpedia*, pages 3(4):4862, Created: 26 August 2007, reviewed: 22 January 2008, accepted: 10 April 2008, 2008.

N. Chernov and R. Markarian. Dispersing billiards with cusps: slow decay of correlations. *Communications in Mathematical Physics*, 270(3):727–758, 2007.

N. Chernov and HK Zhang. Billiards with polynomial mixing rates. *Nonlinearity*, 18:1527, 2005.

B. Chirikov and D. Shepelyansky. Chirikov standard map. *Scholarpedia*, 3 (3):3550, 2008.

BV Chirikov. Research Concerning the Theory of Nonlinear Resonance and Stochasticity Preprint 267. *Institute of Nuclear Physics, Novosibirsk*, 1969.

RV Chirikov and VV Vecheslavov. Chaotic dynamics of comet Halley. *Astronomy and Astrophysics (ISSN*, 221(1):146–154, 1989.

Z. Coelho. Asymptotic laws for symbolic dynamical systems. *Topics in Symbolic Dynamics and Applications*, pages 123–165, 2000.

Z. Coelho and E. De Faria. Limit laws of entrance times for homeomorphisms of the circle. *Israel Journal of Mathematics*, 93(1):93–112, 1996.

L. De Haan and A. Ferreira. *Extreme value theory: an introduction*. Springer Verlag, 2006.

J. Diebolt, A. Guillou, P. Naveau, and P. Ribereau. Improving probability-weighted moment methods for the generalized extreme value distribution. *REVSTAT–Statistical Journal*, 6(1):33–50, 2008.

P. Embrechts, CP Kluppelberg, and T. Mikosh. Modelling Extremal Events, 645 pp, 1997.

M. Felici, V. Lucarini, A. Speranza, and R. Vitolo. Extreme value statistics of the total energy in an intermediate complexity model of the mid-latitude atmospheric jet. Part II: trend detection and assessment. *Arxiv preprint physics/0612042*, 2006.

RA Fisher and LHC Tippett. Limiting forms of the frequency distribution of the largest or smallest member of a sample. In *Proceedings of the Cambridge philosophical society*, volume 24, page 180, 1928.

Roque T. Franceschelli S., Paty M. *Chaos et systemes dynamiques, Elements pour une epistemologie* . Vision des Sciences, Hermann, 2007.

A.C.M. Freitas and J.M. Freitas. On the link between dependence and independence in Extreme Value Theory for Dynamical Systems. *Statistics and Probability Letters*, 78(9):1088–1093, 2008.

A.C.M. Freitas, J.M. Freitas, and M. Todd. Hitting time statistics and extreme value theory. *Probability Theory and Related Fields*, pages 1–36, 2009.

H. Furstenberg. Poincaré recurrence and number theory. *American Mathematical Society*, 5(3), 1981.

B. Gnedenko. Sur la distribution limite du terme maximum d'une série aléatoire. *The Annals of Mathematics*, 44(3):423–453, 1943.

R.F. Green. Partial attraction of maxima. *Journal of Applied Probability*, 13(1):159–163, 1976.

B. Hasselblatt and AB Katok. *A first course in dynamics: with a panorama of recent developments*. Cambridge Univ Pr, 2003.

M. Hirata, B. Saussol, and S. Vaienti. Statistics of Return Times: A General Framework and New Applications. *Communications in Mathematical Physics*, 206(1):33–55, 1999.

H. Hu, A. Rampioni, L. Rossi, G. Turchetti, and S. Vaienti. Statistics of Poincaré recurrences for maps with integrable and ergodic components. *Chaos: An Interdisciplinary Journal of Nonlinear Science*, 14:160, 2004.

FM Izraelev. Nearly linear mappings and their applications. *Physica D: Nonlinear Phenomena*, 1(3):243–266, 1980.

S. Kotz and S. Nadarajah. *Extreme value distributions: theory and applications*. World Scientific Publishing Company, 2000.

M. Kupsa and Y. Lacroix. Asymptotics for hitting times. *Annals of probability*, pages 610–619, 2005.

MR Leadbetter, G. Lindgren, and H. Rootzen. Extremes and related properties of random sequences and processes. 1983.

H. Lebesgue. Sur l'intégration des fonctions discontinues. *AsENS*, 27:361–450, 1910.

AJ Lichtenberg and MA Lieberman. Regular and stochastic motion. *Applied Mathematics*, 38, 1983.

C. Liverani, P. Marie, and S. Vaienti. Random Classical Fidelity. *Journal of Statistical Physics*, 128(4):1079–1091, 2007.

P. Marie. Propriétés statistiques des systèmes dynamiques déterministes et aléatoires. 2009.

P. Marie, G. Turchetti, S. Vaienti, and F. Zanlungo. Error distribution in randomly perturbed orbits. *Chaos: An Interdisciplinary Journal of Nonlinear Science*, 19:043118, 2009.

W.L. Martinez and A.R. Martinez. *Computational statistics handbook with MATLAB*. CRC Press, 2002.

E.S. Martins and J.R. Stedinger. Generalized maximum-likelihood generalized extreme-value quantile estimators for hydrologic data. *Water Resources Research*, 36(3).

M. Matsumoto and T. Nishimura. Mersenne twister: a 623-dimensionally equidistributed uniform pseudo-random number generator. *ACM Transactions on Modeling and Computer Simulation (TOMACS)*, 8(1):3–30, 1998.

F. Pauli and S. Coles. Penalized likelihood inference in extreme value analyses. *Journal of Applied Statistics*, 28(5):547–560, 2001.

J. Pickands III. Moment convergence of sample extremes. *The Annals of Mathematical Statistics*, 39(3):881–889, 1968.

VF Pisarenko and D. Sornette. Characterization of the frequency of extreme earthquake events by the generalized Pareto distribution. *Pure and Applied Geophysics*, 160(12):2343–2364, 2003.

H. Poincaré. Sur le problème des trois corps et les équations de la dynamique. *Acta Mathematica*, 13(1):3–270, 1890.

M. Pollicott and M. Yuri. *Dynamical systems and ergodic theory*. Cambridge Univ Pr, 1998.

L. Rossi, G. Turchetti, and S. Vaienti. Poincaré recurrences as a tool to investigate the statistical properties of dynamical systems with integrable and mixing components. In *Journal of Physics: Conference Series*, volume 7, page 94. IOP Publishing, 2005.

B. Ruggiero, P. Delsing, C. Granata, P. Silvestrini, and Y. Pashkin. *Quantum computing in solid state systems*. Springer Verlag, 2006.

O.G.B. Sveinsson and D.C. Boes. Regional frequency analysis of extreme precipitation in northeastern colorado and fort collins flood of 1997. *Journal of Hydrologic Engineering*, 7:49, 2002.

G. Turchetti. *Dinamica classica dei sistemi fisici*. Zanichelli, 1998.

G. Turchetti, S. Vaienti, and F. Zanlungo. Relaxation to the asymptotic distribution of global errors due to round off. *EPL (Europhysics Letters)*, 89:40006, 2010.

F. Verhulst. Perturbation analysis of parametric resonance. *Encyclopedia of Complexity and Systems Science. Springer-Verlag*, 2009.

L.S. Young. Recurrence times and rates of mixing. *Israel Journal of Mathematics*, 110(1):153–188, 1999.

Ringraziamenti

Qui possiamo ringraziare il mondo intero!!!!!!!!!!
Ovviamente solo se uno vuole, non è obbligatorio.